Application of noble gas tracers to identify the retention mechanisms of CO2 migrated from a deep reservoir into shallow groundwater

Manuscript Details

Manuscript number	JGGC_2019_597_R2
Title	Application of noble gas tracers to identify the retention mechanisms of CO2 migrated from a deep reservoir into shallow groundwater
Article type	Full Length Article

Abstract

Carbon Capture and Storage (CCS) is a valuable climate-mitigation technology, which offers the potential to cost-effectively reduce the emissions associated with the burning of fossil fuels. However, there is a potential risk of a small portion of the stored CO2 unintentionally migrating from a storage site to a shallow groundwater aquifer which is the final retaining zone for any migrated CO2 before it escapes to the atmosphere. Hence, it is imperative to identify the physical retention mechanisms of CO2 within a shallow aquifer. In this study 1.70x102 kg of CO2 and noble gas tracers (He, Ar and Kr) were continuously injected into a groundwater aquifer over 28 days with the aim of identifying the mechanisms and amount of CO2 retention. Among the tracers, Kr was found to be the earliest indicator of CO2 migration. The other tracers – He and Ar – arrived later and exhibited diluted signals. The diluted signals were attributed to degassing of the plume mass (1.6% of CO2) during the early stages of CO2 migration. Diffusion accelerated the dilution of the lighter elements at the plume boundaries. Consequently, the clear relation of the noble gases with the CO2 proved that degassing and mixing primarily control the mass retention of CO2 in shallow groundwater, and the relative importance of these processes varies along the evolving path of migrating CO2.

Keywords	CCS; monitoring; CO2 leakage; noble gas tracing; artificial tracer; geochemical monitoring

Corresponding Author	Kang-Kun Lee
Corresponding Author's Institution	Seoul National University - School of Earth and Environmental Sciences
Order of Authors	YeoJin Ju, Stuart Gilfillan, Seong-Sun Lee, Dugin Kaown, Doshik Hahm, Sanghoon Lee, In-Woo Park, Seung-Wook Ha, Keyhong Park, Hyun-Kwon Do, Seong-Taek Yun, Kang-Kun Lee

Suggested reviewers	Greg Holland, Finlay Stuart, Stephanie Flude, Domokos Gyore

Submission Files Included in this PDF

File Name [File Type]

Cover letter.docx [Cover Letter]

Response to Reviewers.docx [Response to Reviewers]

[1] Ju et al.,_revised.docx [Review Reports]

Highlights_revised.docx [Highlights]

[2] Ju et al.,_revised.docx [Manuscript File]

Figure1.tif [Figure]

Figure2.tif [Figure]

Figure3.tif [Figure]

Figure4_revised.tif [Figure]

Figure5.tif [Figure]

Figure 6_revised.tif [Figure]

Figure7_revised.tif [Figure]

Figure8.tif [Figure]

Figure9.tif [Figure]

Figure10.tif [Figure]

Figure11.tif [Figure]

Figure12.tif [Figure]

declaration-of-competing-interests.docx [Conflict of Interest]

Credit Author Statement.docx [Author Statement]

Supplementary Material.docx [Supplementary Material]

To view all the submission files, including those not included in the PDF, click on the manuscript title on your EVISE Homepage, then click 'Download zip file'.

Research Data Related to this Submission

Data set https://data.mendeley.com/datasets/hrydvx2xgp/1

The dataset associated with the mass balance calculation

You can find all the dataset associated with the mass balance calculation (Figure 8~12).

Seoul National University
College of Natural Sciences

School of Earth and Environmental Sciences, Seoul National University,
Seoul 08826, Republic of Korea

March 27, 2020

Editors-in-chief
International Journal of Greenhouse Gas Control

Dear Editors-in-chief,

RE: Manuscript by Ju, Gilfillan, Lee …. et al. "**Application of noble gas tracers to identify the retention mechanisms of CO_2 migrated from a deep reservoir into shallow groundwater**"

Once again, we would like to thank the associate editor and all the reviewers for very informative and constructive comments for the improvement of our manuscript. We tried to respond to every comment by the reviewers and incorporated the responses into the revised manuscript. You can find all details in the 'Response to Reviewers.docx' file listing all the comments and responses.

I hope the revised manuscript is suitable for publication in the *International Journal of Greenhouse Gas Control*.

Sincerely,

Kang-Kun Lee, Ph.D.
Professor and Chair, School of Earth and Environmental Sciences
Seoul National University
Seoul 08826, Korea
Email: kklee@snu.ac.kr
Phone: +82-2-880-8161
Fax: +82-2-873-3647

[Reviewer 1]

Once again, we thank Reviewer #1 for his/her very detailed reading of our manuscript and associated comments and suggestions. Please see our responses below with the revised version of the manuscript ([1] Ju et al.,_revised).

Specific comments

Introduction

1) Line 40 (Languages)

- RESPONSE: CHANGES MADE.
- It has been modified as below:
- From: "This leaked CO2 could potentially migrate through geological conduits such as permeable faults and/or abandoned wells resulting in the deterioration of fresh water resources above the CO2 reservoir"
- To: "This CO2 could potentially migrate through geological conduits such as permeable faults and/or abandoned wells resulting in the deterioration of fresh water resources above the CO2 reservoir" (Lines 40–42 in [1]).

2) Line 70 (Languages)

- RESPONSE: CHANGES MADE.
- It has been modified as below:
- From: "The degree of solubility trapping has also been determined using noble gases, through identification of the fractionation of naturally present noble gas tracers due to the partitioning of the noble gases into groundwater present within the reservoir formations"
- To: "The degree of solubility trapping has also been determined using noble gases, through identification of the degree of partitioning of the noble gases into groundwater present within the reservoir formations" (Lines 69–71 in [1]).

Materials and methods

3) Line 145 (Languages)

- RESPONSE: CHANGES MADE.
- It has been modified as below:
- From: "The SMWs are located along the created groundwater flow, while PS-04 was upgradient relative to the CO2 injection point."
- To: "The SMWs are located along the created groundwater flow pathway, while PS-04 was up-gradient relative to the CO2 injection point." (Lines 143–144 in [1])

4) Line 147 (Languages)

- RESPONSE: CHANGES MADE.
- It has been modified as below:
- From: "The well BS-09 was intended to capture the preferential movement of a released CO2 along a high connectivity zone between injection well and BS-09, identified in the work of Ju et al. (2019)."
- To: "The well BS-09 was intended to capture the preferential movement of the released CO2 along a high connectivity zone between injection well and BS-09, identified in the work of Ju et al. (2019)." (Lines 144–146 in [1])

5) **Line 229 (Languages)**

- RESPONSE: CHANGES MADE.
- It has been modified as below:
- From: "…before samples injection into the RGA200 mass spectrometer (Stanford Research Systems, California, USA)."
- To: "…before sample injection into the RGA200 mass spectrometer (Stanford Research Systems, California, USA) for analysis." (Lines 229–230 in [1])

Results

6) **Line 376-377 (Languages)**

- RESPONSE: CHANGES MADE.
- It has been modified as below:
- From: "This was attributed to dilution of CO2 plume along a concentration gradient"
- To: "This was attributed to the Kr taking a less distributed pathway through the subsurface than the other tracers, and a result of the dilution of CO2 plume along the concentration gradient" (Lines 370–372 in [1]).

7) **Line 389-391 (Languages)**

- RESPONSE: CHANGES MADE.
- It has been modified as below:
- From: "Note that SMW 4-2 showed a stronger signal at the plateau than SWM 3-2 did (Figure 6), implied a low conductivity zone existing and hindering the SMW 3-2 from capturing a CO2 plume efficiently. This result was consistent with the observations made in alkalinity and pCO2 (Figure 5)."
- To: "It is worth noting that SMW 4-2 exhibited a higher concentration of Kr once the tracers arrived than SWM 3-2 (Figure 6), implying that a low conductivity zone hinders well SMW 3-2 from capturing the full CO2 plume. This result was consistent with the observations made in alkalinity and pCO2 (Figure 5)." (Lines 383–386 in [1])

8) **Line 403 (Languages)**

- RESPONSE: CHANGES MADE.
- It has been modified as below:
- From: "In the final stage of BTCs, the plume tail is recorded in all of the monitoring wells through the decrease of noble gas concentration resulting after the injection at the IW ceased."
- To: "In the final stage of BTCs, the plume tail is recorded in all of the monitoring wells through the decrease of noble gas concentrations after injection at the IW ceased." (Lines 397–399 in [1])

Conclusions

9) **Line 603-604 (Languages)**

- RESPONSE: CHANGES MADE.
- It has been modified as below:
- From: "Around the leak point, CO2 degassing dominantly occurred from a dissolved plume of high gas pressure, suggesting a near-surface monitoring network is necessary for capturing the active "vertical" movement of degassed budget in this area."

- To: "Our findings indicate that around the injection point, CO2 degassing dominantly occurs from the dissolved plume due to the high gas pressure, suggesting a near-surface monitoring network is necessary for capturing the active "vertical" movement of degassed budget in this area." (Lines 595–598 in [1])

[Reviewer 2]

Once again, we thank Reviewer #2 for his/her very detailed reading of our manuscript and associated comments and suggestions. Please see our responses below with the revised version of the manuscript ([1] Ju et al.,_revised).

General observations

The authors have made changes that have improved the manuscript significantly. I have a couple substantial comments however that need attention.

- RESPONSE: CHANGES MADE.
- We sincerely appreciate your thorough review. Please find detailed responses below.

Major comments

Results

1) **Table 1** has several errors. First, the exponents for the values were not fully updated and so the results are non-sensical.

- RESPONSE: CHANGES MADE.
- My apologies for the confusion. The exponents have been fully updated according to your comment (Table 1 in [1]).

Second, the data originally shown for "% lost" were not updated when the column title was changed to "% remaining".

- RESPONSE: CHANGES MADE.
- My apologies for the confusion. The column has been updated according to the changed title (Table 1 in [1]).

2) A major conclusion of this work is that the Kr plume front precedes the CO2 plume front. However, that is difficult to see based on comparisons of Figs. 5 and 6. Perhaps you could add a BTC figure that plots these two gases at the higher time resolution of Fig. 6, to help convince the reader that Kr precedes CO2. It might work to add pCO2 to Fig. 6, but it might also be too difficult to see with all four gases plotted.

- RESPONSE: CHANGES MADE.
- Thank you for the beneficial comment. This has been modified according to your suggestions in the revised version of the manuscript (Figure 6 in [1]).

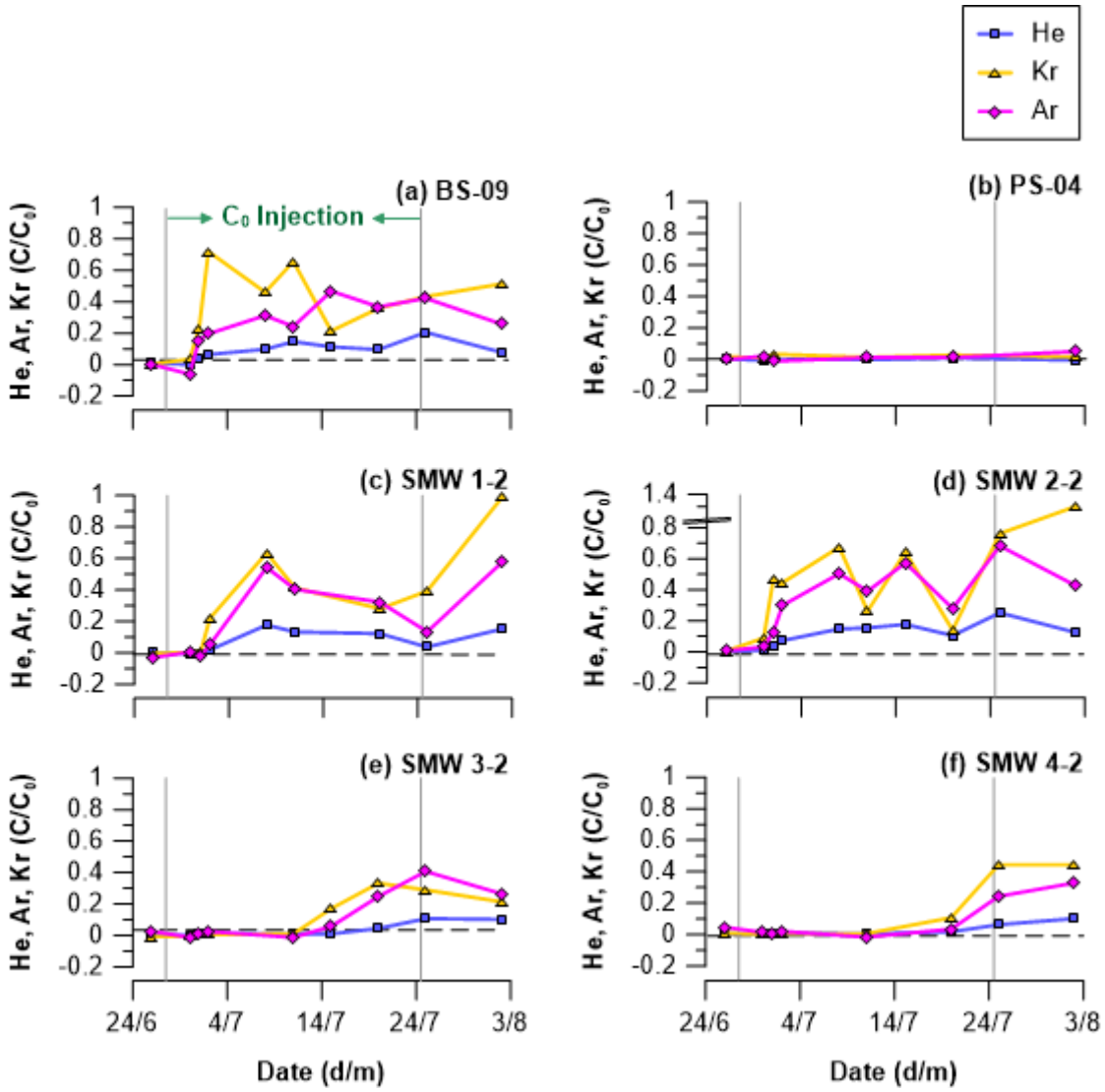

Figure R1 Original version of Figure 6.

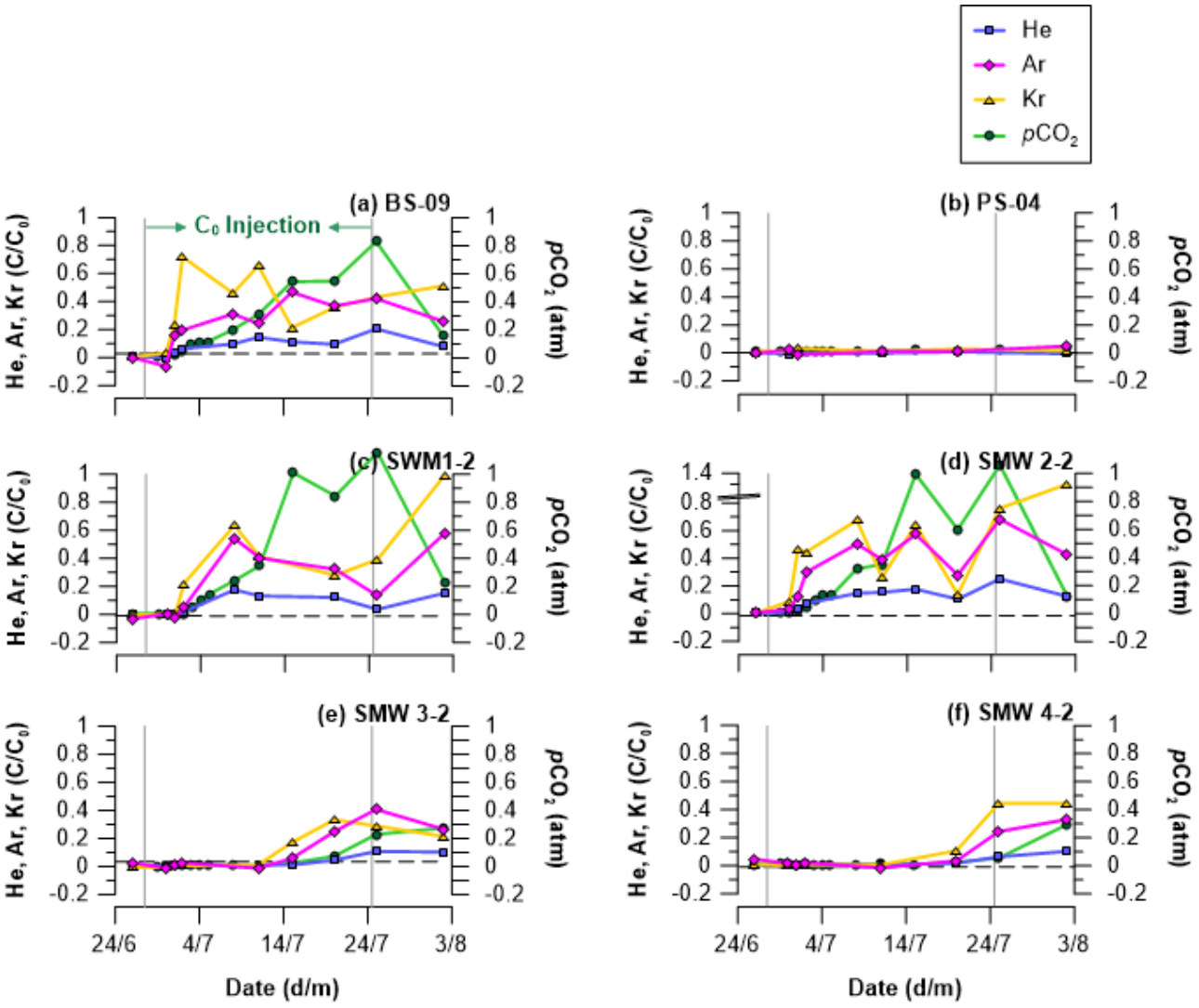

Figure R2 Modified version of Figure 6.

Specific comments

We sincerely appreciate the English corrections. All of your suggestions have been accepted and reflected in the revised version of the manuscript.

Introduction

3) **Line 82-83** change to read " . . . and ASW. Differences in the noble gas contents of these samples stemmed from . . ."

- RESPONSE: CHANGES MADE.
- It has been modified according to your comment (Lines 86–87 in [1]).

4) **Line 98** delete "artificial" (there is no such thing as an artificial noble gas!

- RESPONSE: CHANGES MADE.
- It has been modified according to your comment (Line 102 in [1]).

Materials and methods

5) **Line 152** delete "works".

- RESPONSE: CHANGES MADE.
- It has been modified according to your comment (Line 166 in [1]).

6) **Line 200** change to read "Figure 3. Schedule for water sample collection during the CO2 injection test"

- RESPONSE: CHANGES MADE.
- It has been modified according to your comment (Lines 206–207 in [1]).

7) **Line 222** change to read " . . . before sample injection . . ."

- RESPONSE: CHANGES MADE.
- It has been modified according to your comment (Line 229 in [1]).

Results

8) **Line 246** change to read "However, prior to the experiment the hydrostatic pressure data showed a stable correlation with atmospheric pressure changes and no irregular turbulence . . ."

- RESPONSE: CHANGES MADE.
- It has been modified according to your comment (Lines 254–256 in [1]).

9) **Line 256** delete "to"

- RESPONSE: CHANGES MADE.
- It has been modified according to your comment (Line 264 in [1]).

10) **Line 257** change to read "In contrast, wells SMW 3-2 . . ."

- RESPONSE: CHANGES MADE.
- It has been modified according to your comment (Lines 264–265 in [1]).

11) **Line 344** change to read "The pH also decreased noticeably, . . ."

- RESPONSE: CHANGES MADE.
- It has been modified according to your comment (Line 352 in [1]).

12) **Figure 6** Still need to change the order of the noble gases in the figure legend so that they align with atomic mass (i.e., He, Ar, Kr).

- RESPONSE: CHANGES MADE.
- The legend has been modified according to your suggestion (Figure 6 in [1]).

Discussion

13) **Figure 8, 9, 10 and 11** Vertical axis title is only partly shown.

- RESPONSE: EXPLAINED.
- They look okay in both word and pdf format. In case, the figures were also uploaded to the website as a separate file.

Conclusions

14) **Line 562** change to read: ". . . plume and the other . . ."

- RESPONSE: CHANGES MADE.
- It has been modified according to your comment (Line 580 in [1]).

15) **Line 592** change to read " . . . just a few meters from the leak point . . ."

- RESPONSE: CHANGES MADE.
- It has been modified according to your comment (Line 611 in [1]).

16) **Line 596** spelling of "gaseous"

- RESPONSE: CHANGES MADE.
- It has been modified according to your comment (Line 615 in [1]).

17) **Line 596-597** change to read " . . . pathways in the vadose zone depending on the . . ."

- RESPONSE: CHANGES MADE.
- It has been modified according to your comment (Lines 615–616 in [1]).

Application of noble gas tracers to identify the retention mechanisms of CO_2 migrated from a deep reservoir into shallow groundwater

YeoJin Ju[1], Stuart M. V. Gilfillan [2], Seong-Sun Lee[1], Dugin Kaown[1], Doshik Hahm[3], Sanghoon Lee[1], In-Woo Park[1], Seung-Wook Ha[1], Keyhong Park[4], Hyun-Kwon Do[5], Seong-Taek Yun[5], Kang-Kun Lee[1],*

[1]School of Earth and Environmental Sciences, Seoul National University, 1 Gwanak-ro, Gwanak-gu, Seoul, 08826, South Korea.

[2]School of GeoSciences, The University of Edinburgh, Grant Institute, James Hutton Road, Edinburgh EH9 3FE, UK.

[3]Department of Oceanography, Pusan National University, Busan, South Korea.

[4]Korea Polar Research Institute, Incheon, South Korea.

[5]Department of Earth and Environmental Sciences, Korea University, Seoul 02841, South Korea.

Email: jinee18@snu.ac.kr, stuart.gilfillan@ed.ac.uk, soon3311@snu.ac.kr, dugin1@snu.ac.kr, hahm@pusan.ac.kr, lshlsh2311@snu.ac.kr, inwoo0415@snu.ac.kr, hasabana@snu.ac.kr, keyhongpark@kopri.re.kr, iq1pc@korea.ac.kr, styun@korea.ac.kr.

*Corresponding author. Tel.: +82 2 873 3647. E-mail address: kklee@snu.ac.kr.

Abstract

Carbon Capture and Storage (CCS) is a valuable climate-mitigation technology, which offers the potential to cost-effectively reduce the emissions associated with the burning of fossil fuels. However, there is a potential risk of a small portion of the stored CO_2 unintentionally migrating from a storage site to a shallow groundwater aquifer. The shallow groundwater which is the final retaining zone for any migrated CO_2 before it escapes into the atmosphere. Hence, it is imperative toTo identify the physical retention mechanisms of CO_2 within a shallow aquifer. , In this study $1.70x10^2$ kg of CO_2 and noble gas tracers (He, Ar and Kr) were continuously injected into a groundwater aquifer over 28 days with the aim of identifying the mechanisms and amount of CO_2 retention. Among the tracers, Kr was found to be the earliest indicator of CO_2 migration. The other tracers – He and Ar – arrived later and exhibited diluted signals. The diluted signals were attributed to degassing of the plume mass (1.6% of CO_2) during the early stages of CO_2 migration. Diffusion accelerated the dilution of the lighter elements at the plume boundaries. Consequently, the clear relation of the noble gases with the CO_2 proved that degassing and mixing primarily control the mass retention of CO_2 in shallow groundwater, and the relative importance of these processes is differentiatedvaries along the evolving path of migrating CO_2.

Keywords: CCS; monitoring; CO_2 leakage; noble gas tracing; artificial tracer; geochemical monitoring

1. Introduction

Carbon Capture and Storage (CCS) is a climate change mitigation technology that comprises the capture of CO_2 from an industrial point source, such as a power plant or refinery, transport of the captured CO_2 to a storage site followed by the injection of the captured CO_2 into deep geological strata for permanent disposal (IPCC, 2005). However, there is a potential risk that a small portion of the mobile CO_2 in a storage site could accidently migrate out of the subsurface reservoir and inadvertently reach shallower levels of the subsurface (Alcalde et al., 2018). This ~~leaked~~ CO_2 could potentially migrate through geological conduits such as permeable faults and/or abandoned wells resulting in the deterioration of fresh water resources above the CO_2 reservoir (Harvey et al., 2012; IEAGHG, 2011; Lemieux, 2011; Lion et al., 2014) and ~~in the~~ leakage of a small portion of the CO_2 into the atmosphere (Ide et al., 2006; IPCC, 2005). Recently, the Weyburn-Midale (Canada) CO_2 monitoring and storage project faced allegations that leakage of CO_2 injected into the Weyburn-Midale oil field for Enhanced Oil Recovery (EOR) and storage was causing a deterioration of the groundwater quality on a farm located above the field (Beaubien et al., 2013; Gilfillan et al., 2017).

A variety of geochemical tools have been used to verify CO_2 storage security and track the fate of CO_2 injected for storage. These include CO_2 soil gas and groundwater concentrations, stable C and O isotopes within the CO_2, on-site monitoring parameters (pH, alkalinity, ORP, EC, temperature and DO), inert gas tracers, major and trace ions and radiocarbon (^{14}C) (Flude et al., 2016; Lee et al., 2016). Soil gas and dissolved CO_2 concentrations in groundwater can provide a direct tracer of CO_2 migration, allowing discrimination of different CO_2 origins and providing a means to establish the mass balance of CO_2 present in the groundwater system (Ballentine et al., 2001; Beaubien et al., 2014; Gilfillan et al., 2011; Lollar et al., 1997; Sathaye et al., 2016). Recent developments in on-site monitoring technologies now allow the continuous measurement of a number of parameters (e.g. alkalinity, T, EC, pH) which can be used to establish the overall distribution and temporal evolution of a small CO_2 plume within a shallow groundwater aquifer (Lee et al., 2016). Noble gases are characterized by their- inert behavior, which makes them ideal tracers within a subsurface system. This inertness means that noble gases are

conservative tracers and do not partake in the chemical reactions that dilute the CO_2 leakage signals and hence are capable of providing a robust means to distinguish between natural and stored CO_2 (Risk et al., 2015).

Noble gas tracing techniques have been used to track both the fate and migration pathways of injected CO_2 in reservoirs. Within a typical porous CO_2 storage reservoir, CO_2 is retained by a combination of structural, residual and solubility trapping mechanisms (Alcalde et al., 2018; Holland and Gilfillan, 2013; IPCC, 2005). Recent experiments at the CO2CRC Otway Demonstration site for CO_2 storage in Australia have used Kr and Xe as conservative tracers to determine the degree of residual trapping within a porous saline formation, using a numerical mass balance approach (LaForce et al., 2014). The degree of solubility trapping has also been determined using noble gases, through identification of the degree of ~~fractionation of naturally present noble gas tracers due to the~~ partitioning of the noble gases into groundwater present within the reservoir formations (Ballentine et al., 1991; Brennwald et al., 2005; Gilfillan et al., 2008, 2009; 2014; Pinti and Marty, 1995; Zhou et al., 2005).

Noble gas tracers are also suitable for monitoring the vertical migration of the reservoir CO_2, thanks to the compositional difference of natural noble gas tracers between storage reservoir and the near surface environment (Mackintosh and Ballentine, 2012). Gilfillan et al. (2011) applied noble gas tracing tools to constrain the nature of CO_2 leakage into shallow groundwater and surface water bodies. ~~The~~ Further work by Gilfillan et al., (2017) used inherent tracers residing in ~~a~~ the Weyburn-Midale injection and storage project reservoir ~~CO_2 reservoir provided a means~~ to show that CO_2 ~~-~~ migration from ~~a~~ the deep reservoir into the shallow aquifer system had not occurred ~~near an artificial CO_2 injection site at the Weyburn-Midale Storage and Monitoring project~~. This work found that ~~as~~the noble gas composition in the groundwater samples above the CO_2 injection and storage project did not vary over a typical background level of a shallow aquifer, ~~that is, the~~of Air Saturated Water (ASW) with an excess air component of up to 45% (Gilfillan et al., 2017). Recent work by Flude et al. (2016) and Flude et al. (2017) evaluated the inherent tracing ability of noble gases focusing on the compositional difference of them between captured CO_2, the subsurface storage reservoir, air and ASW. ~~The~~

distinguished _composition ofDifferences in the noble gases contents of these samplesbetween the sampled gases stemmed from the different CO_2 capturing processes and what controls the composition of noble gas tracer in a stored fluid (e.g. gas stripping of reservoir water and/or interaction with radiogenic components).

The concept of inert tracers was extended to artificial enhancement studies, involving the addition of inert gas tracers such as SF_6 and noble gases to the injected CO_2 in CCS storage. This aimed to provide a much clearer distinction between the injected CO_2 and that naturally present in the subsurface and so improving the monitoring efficiency (Myers et al., 2013; Nimz and Hudson, 2005). For example, noble gases have been previously used as artificial tracers to indicate CO_2 leakage pathways in the vadose zone (Cohen et al., 2013; Rillard et al., 2015) and in the aquifer system (Lu et al., 2012; Nimz and Hudson, 2005; Stalker et al., 2009). In the CO_2-Vadose project, undertaken at a test CO_2 release site in France, the lighter noble gases (He and Ne) were found to have the fastest arrival time in monitoring wells due to their higher diffusion coefficient and low solubility within the soil water compared to the CO_2 and other tracers (Cohen et al., 2013). In contrast, the heavier noble gas tracers (Kr and Xe) exhibited the fastest arrival in the aquifer system due to their solubility in groundwater compared to other noble gases following the artificial injection into a deep reservoir (~2 km) (Stalker et al., 2015). In a recent test, a small amount of CO_2 (16.9 kg) spiked with artificial noble gas was released into a shallow aquifer at Korea CO_2 Storage Environmental Management (K-COSEM) study site, in order to understand the behavior of the leaked plume in the shallow groundwater system. This study identified that the mass distribution of the leaked CO_2 is predominantly controlled by the solubility of the individual noble gases and mixing processes during the limited time of monitoring work (i.e. 4 months) (Ju et al., 2019).

The shallow groundwater is the final zone encountered by migrating CO_2 before it is lost into the vadose zone and atmosphere. Furthermore, this reservoir is directly linked into the human activity, hence, should be protected from a potential leakage of stored CO_2 (Lee et al., 2016). While noble gas tracers have proven useful to monitor leaked CO_2 plume in shallow aquifer systems (Flude et al., 2016;

2017), this has only been demonstrated on a few occasions, for example, in a natural CO_2 production site using inherent noble gases (Gilfillan et al., 2011), in a CO_2 injection test site using artificially enhanced noble gases (Ju et al., 2019) and to rule out CO_2 migration in a shallow aquifer above an actual CO_2 storage reservoir using inherent noble gases (Gilfillan et al., 2017), as described above. In this study, we present~~s~~ the results of applying noble gases to a CO_2 injection test into a near-surface aquifer. This artificial CO_2 migration test aims to mimic a situation where a measurable amount of CO_2 ($1.70x10^2$ kg) has migrated from a deep CO_2 storage reservoir into a shallow groundwater aquifer. This study ~~aims~~ focuses on~~to~~ determining~~e~~ the amount of CO_2 retained in the groundwater and the mechanisms controlling the migration of the CO_2 plume using noble gas tracers. A mass balance model was constructed based on the partitioning coefficients of noble gas tracers in a gas-water system, to understand and to quantify the final retention of the injected CO_2 within the shallow aquifer system.

2. Materials and methods

2.1 Site description

The Korea CO_2 Storage Environmental Management (K-COSEM) Research Center has installed a controlled CO_2 release experiment at Eumseong gun (county) of South Korea (Figure 1). The geology at the field experimental site includes three different subsurface media, firstly consisting of a weathered soil layer composed of medium to coarse grained silty sand (0–30 m below ground surface (bgs)), followed by weathered biotite granite (30–70 m bgs), and finally consolidated biotite granite (starting at 70 m bgs) (Lee et al., 2017; Ju et al., 2018a). The water level was located at the 16.0–18.4 m bgs and the hydraulic conductivity of the aquifer was estimated from pumping tests, ranging from 1.7×10^{-5} cm/s for the consolidated bedrock to 2.0×10^{-4} cm/s for the weathered layer. Prior to the commencement of the experiment, the groundwater was flowing from the northwest toward the southeast following a hydraulic gradient of 0.003 (i.e., the regional flow in Figure 1a).

At the K-COSEM site, a total of 24 monitoring wells had been installed in the shallow aquifer (i.e. < 15 m below the water table) including the injection well (IW), partially screened (PS), boreholes (BH), borehole screened (BS) and saturated zone monitoring wells (SMWs) (Figure 1a). Each saturated

zone monitoring well (SMW) contained several screened multi-depth monitoring wells for groundwater monitoring at different depths (Figure 1f). In this CO_2 injection study, the IW and six monitoring wells (PS-04, SMW1 to 4, BS-04, -09 and -10) were employed for the CO_2 injection experiment (Figure 1b). The wells BS-04 and BS-10 located at both ends of the monitoring range were used to create an induced pressure gradient field by pumping out groundwater at a down-gradient location (BS-10) and successive injection in at an up-gradient location (BS-4) (Figure 1c). The SMWs are located along the created groundwater flow pathway, while PS-04 was up-gradient relative to the CO_2 injection point. The well BS-09 was intended to capture the preferential movement of ~~a~~ the released CO_2 along a high connectivity zone between injection well and BS-09, identified in the work of Ju et al. (2019). Details on the study site and monitoring network can also be found in previous works (Lee et al., 2017; Lee et al., 2018; Ju et al., 2018b; Ju et al., 2019).

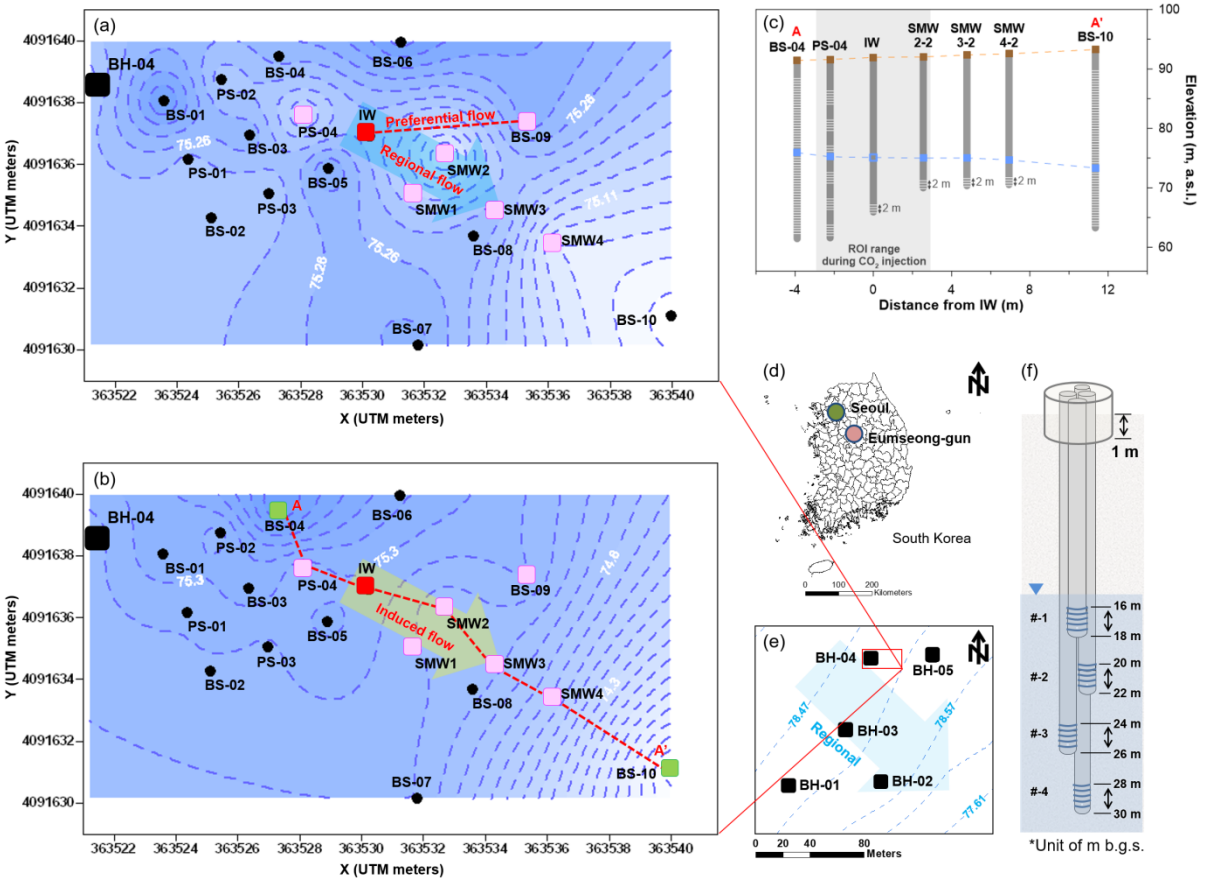

150

151 **Figure 1**. Maps of the study site. Figures on the left show (a) natural ~~pressure gradient~~regional
152 groundwater flow ~~field~~ (shown as a blue-colored arrow) before enhanced groundwater circulation using
153 the wells BS-04 and BS-10, where a preferential path exists in this field due to local hydrogeological
154 heterogeneity (16 May 2016), (b) induced pressure gradient field (shown as a green-colored arrow) after
155 the pumping out and pumping in using the two wells (see green squares) (4 July 2016). Note that the
156 induced flow was intended to speed up the plume migration along the groundwater flow (i.e., regional
157 flow in [a]). Pink squares represent the wells used for monitoring ~~works~~; a red square represents the
158 injection well (IW). Figures on the right show (c) a cross-section view along the induced pressure
159 gradient (4 July 2016), (d) the location map of the study area, (e) the contours of groundwater levels
160 obtained by kriging using 17 wells surrounding the study site (7 March 2015), and (f) the structure of
161 each saturated zone monitoring well (SMW) containing a bundle of four screened pipes with different
162 lengths.

2.2 Artificial injection

2.2.1 Induced pressure gradient field

The CO_2 injection was undertaken in the induced pressure gradient field to reinforce the groundwater flow, therefore, to speed up the CO_2 plume migration (Figure 2c). The hydraulic pressure gradient was achieved by enhancing groundwater circulation ~~work~~, consisting of water production and reinjection using the BS-04 and BS-10 wells located at both ends of the monitoring network (Figure 2c). A total of 24.0 m^3/d of groundwater was pumped from BS-10 and reinjected into BS-04 (Figure 2c). A period of 1 month was required to stabilize the pressure gradient (22 May 2017 to 27 June 2017). The pressure gradient was steeper near the injection site and production points (i.e. the BS-04 and BS-10), with the average gradient being 0.18 (Figure 2c). The circulation was maintained until 17 September 2017.

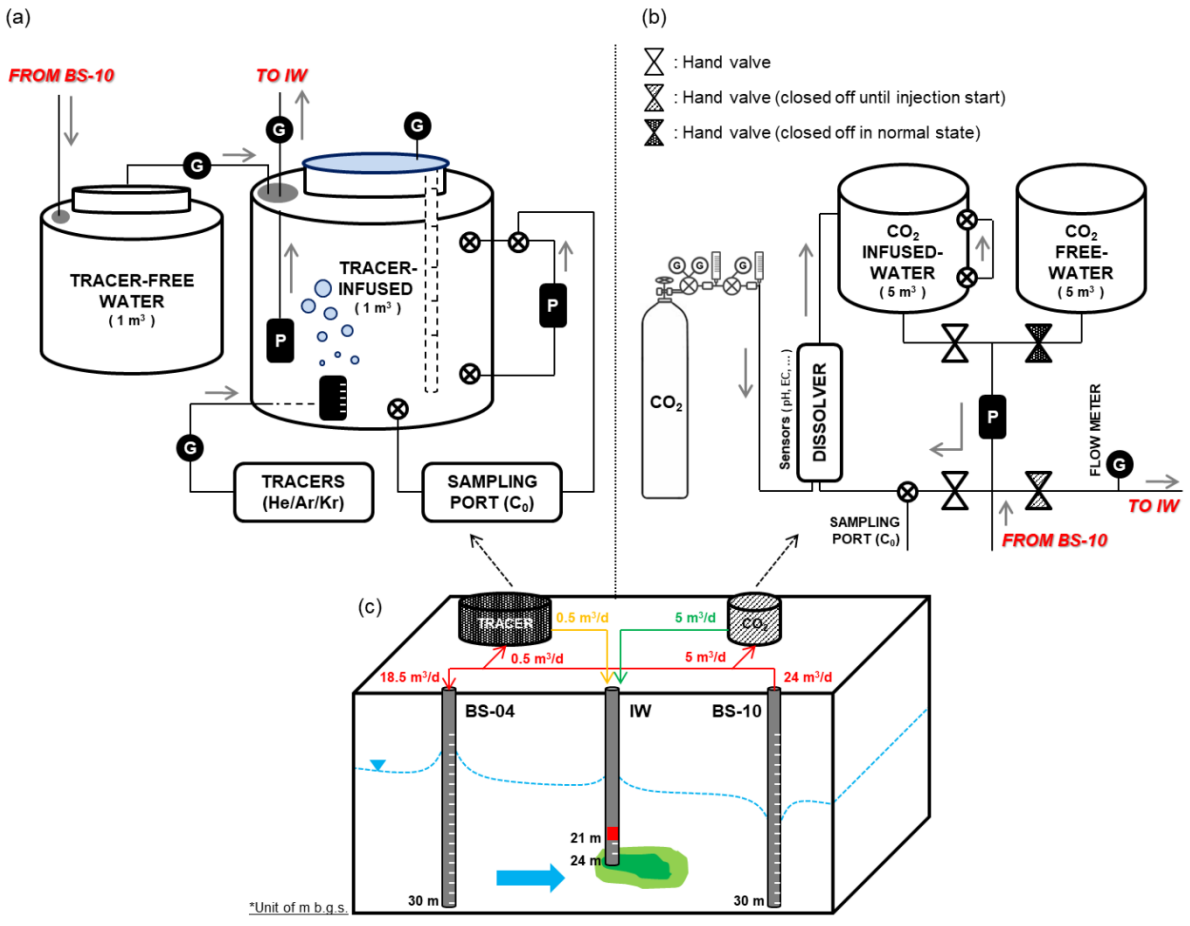

Figure 2. Injection systems for the artificial CO_2 release experiment. (a) tracer-infused groundwater

was prepared in a 1 m^3 tank and (b) CO_2-infused groundwater was prepared in a 5 m^3 tank. (c) gas-charged groundwater was continuously released into the induced pressure gradient field through the IW.

2.2.2 Injection

To prepare the injection water, the water flux sent to BS-04 (24.0 m^3/d) was reduced to 18.5 m^3/d and 5.5 m^3/d of groundwater was sent into the injection tank (Figure 2c). 5.0 m^3/d of groundwater was sent into the CO_2 dissolver tank (Figure 2b) and 0.5 m^3/d of tracer–enhanced water was prepared in the other tank (Figure 2a). The CO_2-infused groundwater was prepared in the 5 m^3 tank equipped with the circulation pump, CO_2 dissolver, water sampling port and flow meter (Figure 2b). Injection was initiated when the CO_2 concentration reached the equilibrium state (termed C_0). To ensure that the equilibrium concentration was maintained, alkalinity, pH, EC, DO, ORP, temperature, salinity, TDS was continuously monitored with real time measurement devices such as YSI (YSI Inc./Xylem Inc., USA), LTC Levelogger Junior (Solinist, Canada) and SH-300-DS (SOHA TECH, Inc., Korea) while circulating water within the tank using a pump (Figure 2b). These measurements showed that it took approximately 24 hours to achieve the equilibrium state. The noble gas infused groundwater was also prepared one day ahead of the injection test. Approximately 0.5 m^3/d of groundwater was pumped into the 1 m^3 of closed tank equipped with the circulation pump, tracer tank, water sampling port and flow meter (Figure 2a). ~~Tracers~~ The injected tracers were a mixture of He (0.2 vol. %), Ar (99.4 vol. %), and Kr (0.4 vol. %) and were injected through a flowmeter and diffuser (AS-10 3/8) into the 1 m^3 dissolver tank. The infused liquids were first injected into the subsurface on 27 June 2017 and continued to be injected for 27 days until 24 July 2017. Samples for initial concentration analyses (i.e. C_0) were collected during the injection event and through the sampling ports (Figures 2a and b). Injection took place at 4.5–7.5 m below the water table (corresponding to 21–24 m bgs) in an isolated zone below a packer (Figure 2c). The ambient surface weather conditions during the injection event were 20.4–26.9^{o}C without precipitation. The injection rate was controlled by a submersible and controllable quantitative pump (model MP1, Grundfos, Denmark) at a constant rate of 5.5 m^3/d (Figure 2c).

2.3 Real-time monitoring

Real-time monitoring data was collected from 17 May 2017 to 13 October 2017 (Figure 3). Over this period, hydraulic pressure (P), temperature (T) and electrical conductivity (EC) were measured in-situ using the LTC Levelogger Junior (Solinist, Canada) and the barometric state was monitored at the same time using the Barologger Edge (Solinist, Canada) at 10 minute intervals.

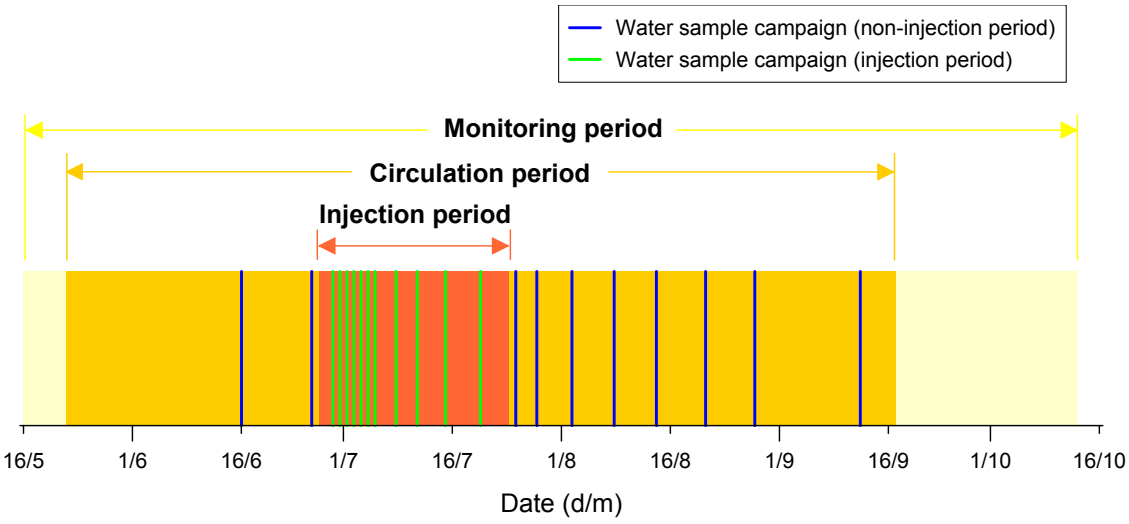

Figure 3. ~~Record for monitoring works~~Schedule for water sample collection during the ~~artificial~~ CO_2 injection test.

2.4 Water sampling campaign

2.4.1 Baseline survey period

Water samples were collected using a Waterra Inertial Pump with PowerPack PP-1 (Wattera, Canada) to obtain baseline data before the CO_2 injection. The local baseline of the pCO_2 was obtained on two occasions through water sampling between 16 June 2017 and 26 June 2017 (Figure 3). The baseline for the noble gas tracers was determined by a single water-sampling operation on 26 June 2017 (Figure 3). Alkalinity was determined in the field site by acid titration method with 0.05 N HNO_3. The pH and temperature were also measured in-situ using a portable water quality meter (YSI ProDSS, YSI Inc./Xylem Inc., USA). The noble gas samples were collected using a standard copper tube of 28 cm^3 and a pinch-off clamp set.

2.4.2 Injection and post-injection period

Data acquisition after the CO_2 injection was conducted in the same manner as the baseline data collection. Water samples were collected on 19 occasions following the injection event, over 76 days from 27 June 2017 to 12 September 2017 (Figure 3).

2.5 Laboratory analyses

2.5.1 Noble gas

The noble gas samples were analyzed in the noble gas analysis laboratory at the Korea Polar Research Institute (KOPRI) using an automated system as outlined in Stanley et al. (2009) and Kim et al. (2016). Gases were first extracted from a groundwater sample under high vacuum condition (~10^{-7} mbar) and stored in an aluminosilicate glass ampoule (Lott and Jenkins, 1998). Excessive water vapor, active gases, and condensable gases were then removed using cryogenic traps and a series of hot and cold Zr-Al alloy getters (St 101, SAES Getters S.p.A., Italy) before sample~~s~~ injection into the RGA200 mass spectrometer (Stanford Research Systems, California, USA) for analysis. The noble gases, He, Ne, Ar, and Kr were calibrated against air standards of 0.9 and 2.7 cm^3 STP, to cover the wide range of the tracer enhanced injection water. The discrepancy between duplicate samples was less than 5% (Ju et al., 2019).

2.6 Analytical methods

2.6.1 pCO_2 calculation

pCO_2 values for the sampled waters were calculated using the monitored parameters of alkalinity, pH, and temperature. Alkalinity, pH and temperature were measured in-situ. Using these data a robust calculation for pCO_2 value was made using the program PHREEQC Version 3 (Parkhurst and Appelo, 2013).

2.6.2 Mass balance model

At the early stage of the CO_2 injection, the CO_2 plume is unstable with a high partial pressure, resulting in a degree of CO_2 degassing. Hence, CO_2 bubbles rise freely from the brine with a proportion of the CO_2 remaining in the dissolved phase. During the degassing period, the free-phase CO_2 strips out

the dissolved, relatively insoluble noble gases, especially the lighter elements (He and Ne), leaving the system relatively enriched in the heavier noble gases (Ar, Kr, Xe) (Ballentine et al., 2002; Holland and Gilfillan, 2013). Based on the degree of this enrichment, we can inversely constrain the mass balance of the CO_2 plume in terms of the degassing process (see the Appendix A ~~Mass~~ mass balance model for detailed explanation).

3 Results

3.1 Prior to CO_2 injection

Pressure and temperature changes result in the degassing of insoluble substances from the groundwater system. At the K-COSEM test site, the groundwater level shows a clear decreasing trend due to large-scale water consumption from nearby industrial complexes (Figure 4) (Ju et al., 2019). However, prior to the experiment the hydrostatic pressure data ~~does not record any irregular turbulence prior to the experiment and maintained~~showed a stable correlation with ~~the~~ atmospheric pressure changes and no irregular turbulence (Supplementary Figure S1). Groundwater temperatures corresponded to normal seasonal values ranging between 12.7 to 13.6°C (Figure 4).

The induced pressure gradient commenced on the 22 May 2017 as a result of the onset of water circulation (Figure 3c). Perturbations were detected in the water level (WL), temperature (T), and electrical conductivity (EC) values during the initiation of water circulation (see the start points of dark grey zone in Figure 4). The pressure turbulence was most noticeable within the monitoring wells located inside the radius of influence (ROI) area both of the pumping (BS-10) and injection wells (BS-04). For example, PS-04, SMW 1 series and SMW 2 series wells showed an instant pressure increase after the circulation commenced, as they are located near ~~to~~ the injection well (BS-04) (Figure 4d–j). In ~~Contrastingly~~contrast, wells SMW 3-2 and 4-3 showed an abrupt decrease in pressure, as a result of their location near to well BS-10 where water was extracted (Figure 4k and l). Well BS-09 also displayed a modest increase in pressure 9 days after water circulation commenced (specifically on 31 May 2017) (Figure 4c). Temperature within all monitoring wells showed an overall increase after the water circulation regime started (see the start points of dark grey zone in Figure 4). This is most likely

linked to the groundwater for injection having resided in the surface tank at temperatures warmer (i.e., 17.1 to 28.6^{o}C) than those of the subsurface groundwaters (i.e., 13.3^{o}C) for the day prior to re-injection into the subsurface. The EC showed the overall decreasing trend in the initial circulation period as the re-injected water (BS-10) has a relatively low EC background compared to the other wells, with the exception of well SMW 2-1 (Figure 4).

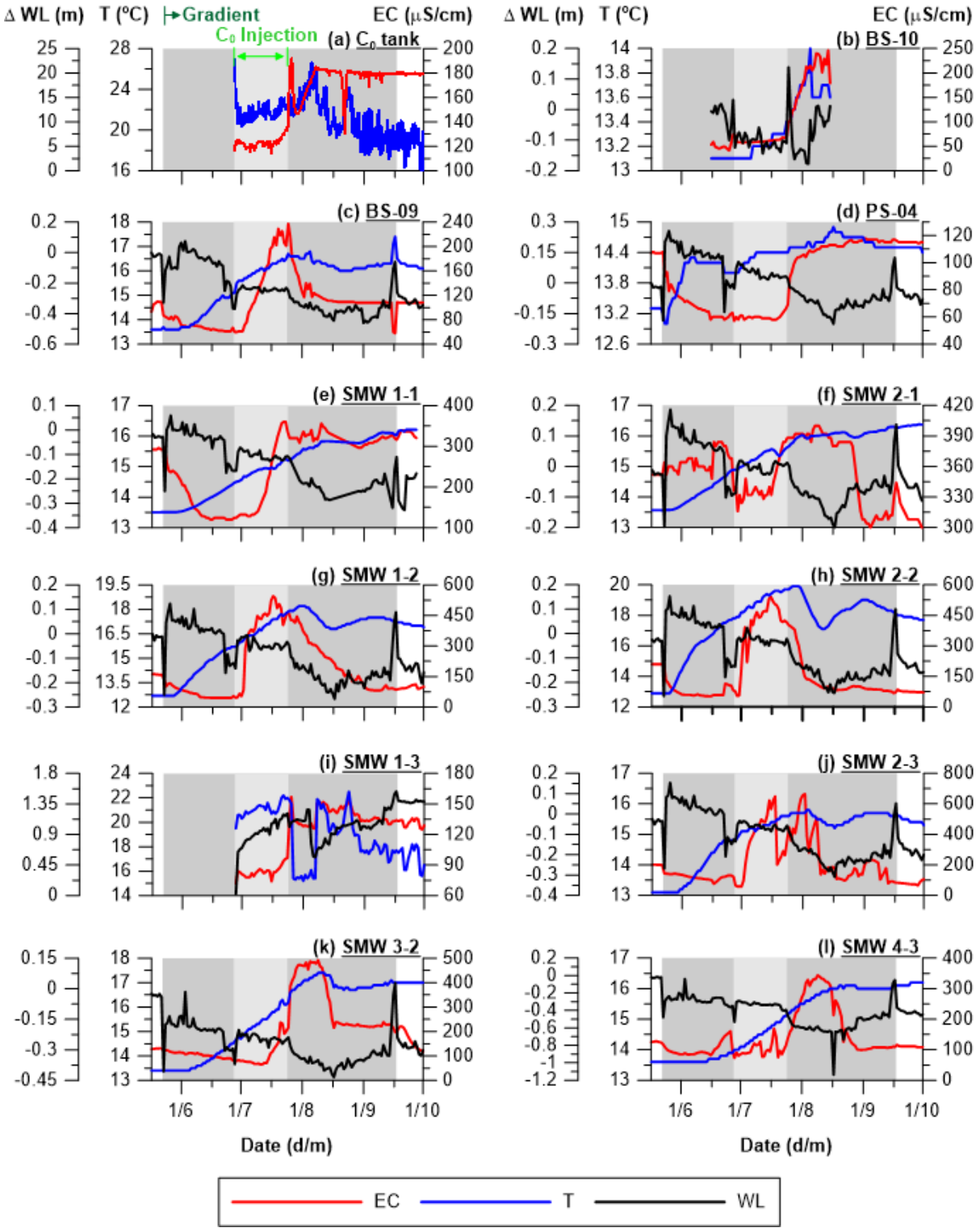

277

278 **Figure 4.** Water level (WL), temperature (T) and electrical conductivity (EC) data. Measurements were
279 completed in the monitoring wells continuously using a LTC data logger. The groundwater circulation
280 was initiated at 22 May 2017 (dark grey shaded zone) and the CO_2 injection started at 27 June 2017 and
281 kept going till 24 July 2017 (light grey shaded zone).

As outlined previously, two water sampling campaigns were conducted during the circulation period and prior to CO_2 injection commenced, in order to establish the groundwater baseline composition (16 June 2017 and 26 June 2017) (Figure 3). The baseline alkalinity values were relatively low (27.5–64.1 mg/L), DO exhibited a wide variation (3.6–8.0), pH was weakly acidic (6.5–7.1) and pCO_2 was relatively low (0.0–0.01 atm) prior to CO_2 injection (Figure 5). All of the parameters were close to the baseline values of low carbonate levels in the biotite granite protolith (Ju et al., 2019).

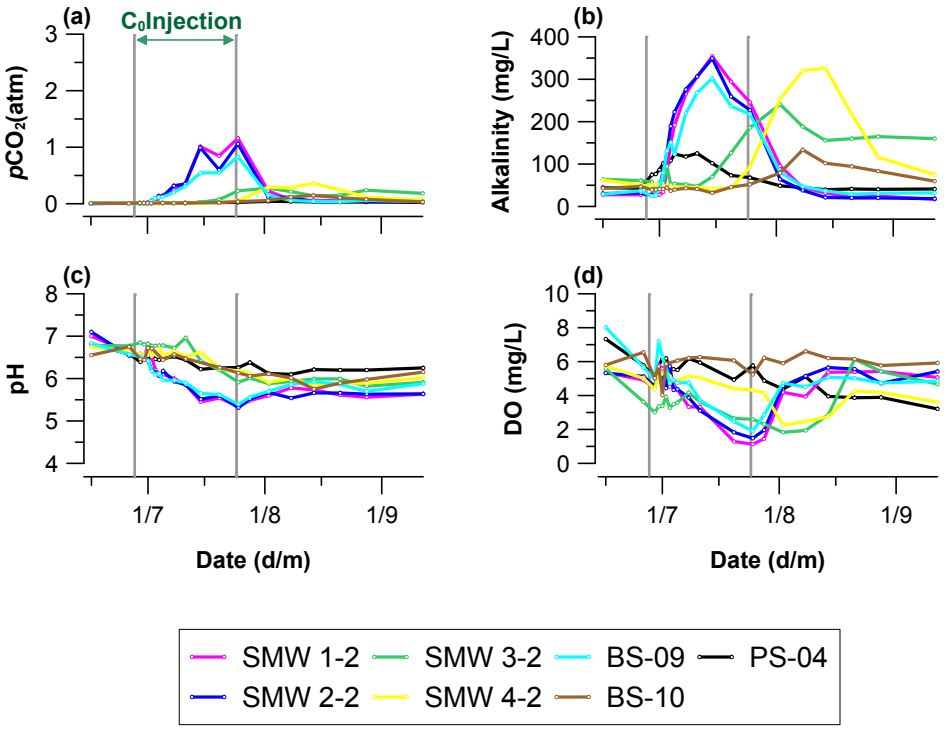

Figure 5. pCO_2, pH, alkalinity and DO values. The grey vertical lines represent the injection period.

During the water circulation period, pH exhibited an overall decreasing trend as the low-pH water was pumped out from the down-gradient well (BS-10) and reinjected into the up-gradient well (BS-04) (Figure 5c). DO also exhibited a decreasing trend as groundwater was re-equilibrated in the warm surface temperature (17.1–28.6°C) before being injected into the well BS-04 (Figure 4d). pCO_2 and alkalinity showed minor variation across the monitored region depending on the groundwater flow direction and the initial C parameter distributions (Figure 4a and b).

296 Mean He, Ar and Kr concentrations measured before the injection commenced were 5.43×10^{-8}
297 cm^3 STP/g_{H2O}, 3.72×10^{-4} cm^3 STP/g_{H2O} and 9.80×10^{-8} cm^3 STP/g_{H2O}, respectively. These are close
298 to the Air Saturated Water (ASW) value at the temperature condition (i.e. 13.3°C) of study site—such
299 as 4.58×10^{-8} cm^3 STP/g_{H2O}, 3.58×10^{-4} cm^3 STP/g_{H2O} and 8.30×10^{-8} cm^3 STP/g_{H2O} for He, Ar and
300 Kr values, respectively (Kipfer et al., 2002).

301 **3.2 Injection fluid**

302 The gas-infused groundwater was released into the IW from 27 June 2017 to 24 July 2017
303 (Figure 3). The CO_2–infused groundwater (C_0) collected from the 5 m^3 tank (Figure 2b) was initially
304 below the saturation point (0.40 atm) for 11 days after the injection (29 June 2017 to 8 July 2017), and
305 reached to the over-saturation state (> 2.3 atm) about 18 days after the injection on 15 July 2017 (Figure
306 5a). This CO_2 variation can be attributed to an accidentally reduced water flux going into the CO_2 tank,
307 causing a decrease of the water level, resulting in altering of the C system balance in CO_2 tank. For the
308 same reason, the pH and DO initially maintained 5.0 and 3.9 mg/L but showed a sudden decrease to 4.2
309 and 0.5 mg/L on the 15 July 2017. Water samples collected from the 1 m^3 tank (C_0) (Figure 2a) were
310 analyzed for their He, Ar and Kr concentrations, and reported at 2.92×10^{-5} cm^3 STP/g_{H2O}, 2.26×10^{-2}
311 cm^3 STP/g_{H2O} and 4.95×10^{-5} cm^3 STP/g_{H2O}, respectively. The noble gas concentrations lie between
312 fully saturated and Air Saturated Water (ASW) levels, and thus they will remain dissolved in the
313 groundwater system unless being exposed to low partial pressure conditions such as air bubbles or the
314 vadose zone interface (i.e. water table) (Ju et al., 2019).

315 **3.3 Post injection**

316 **3.3.1 P, T and EC**

317 Pressure turbulence was observed in all monitoring wells prior to the initiation of CO_2 injection
318 (Figure 4), which can be attributed to the change in water volume from 24.0 m^3/d to 18.5 m^3/d for
319 preparing the gas-infused water of 5.5 m^3 (C_0) before CO_2 injection within the circulation system (see
320 the section 2.2.2 Injection for detailed explanation). Minor changes in temperature were observed inside
321 the Radius of Influence (ROI) zone of IW such as PS-04, BS-09, SMW 1 and SMW 2 (Figure 4c~j).

The temperature showed a gradual increase since the groundwater circulation initiated in which the SMW 2-2 showed the highest increase of up to +7.0°C and followed by SMW1-2 (+5.5°C), SMW 3-2 (+4.0°C), BS-09 (+3.8°C) and the others (< +2.8°C) (Figure 4). The higher increase in the temperature of BS-09 indicates a preferential flow gradient still exists in the study site even after the formation of the induced pressure gradient (Figure 1a). In EC data, the most prominent signals were recorded at SMW 1-2 (+464 µS/cm, +472%), SMW 2-2 (+447 µS/cm, +368%), SMW 2-3 (+531 µS/cm , +301%), SMW 3-2 (+383 µS/cm, +250%) with the others showing a less pronounced change (< +129%). These observations were consistent with temperature data, exhibiting the greatest change in the SMW #-2 wells. This indicated that the CO_2 plume moved horizontally from the injection depth of 21–24 m to the screen depth of SMW #-2 (i.e., 20–22 m) (Figure 1c). The response in EC is clearly different to that of temperature as a notable increase in EC was only observed after CO_2 injection occurred. This is because EC is the function of geochemical interaction between the CO_2 water and the rock materials (Vialle et al., 2014). In the groundwater flow regime, the SMW series wells, BS-09 and BS-10 are located ahead of the migration direction of the IW, which is illustrated by the clearly increasing EC trend (Figure 1b). Alternatively, well PS-04 is located upgradient from the CO_2 injection point, resulting in a gradual lowering of the EC trend after the CO_2 injection was initiated as there is no communication between this well and the CO_2 rich-water (Figure 1b).

3.3.2 *p*CO_2, pH, alkalinity and DO

As expected, the chemical elements exhibited strong signals correlating with the CO_2 plume arrival. The parameters are presented as breakthrough curves (BTCs) (Figure 5). Note that for the SMWs, the parameters represent the data from the injection depth (i.e., SMW #-2) only, as this generated the largest signals among all depths. The *p*CO_2 produced the strongest signal at SMW 1-2 (+1.15 atm, +25,385%) which was followed by SMW 2-2 (+1.05 atm, +18,067%), BS-09 (+0.82 atm, +12,631%), SWM 4-2 (+0.35 atm, +3,746%) and the others wells (< +2,923%) (Figure 5a). The pronounced response of *p*CO_2 compared to other parameters is attributed to its low baseline concentration (0.0–0.01 atm) (Risk et al., 2015). Alkalinity also showed significant increases with the arrival of the injected CO_2, particularly in wells SMW 1-2 (+326.4 mg/L, +1,189%), SMW 2-2 (+318.0

mg/L, +1,017%), BS-09 (+269.2 mg/L, +821%), SMW 4-2 (+270.0 mg/L, +478%) with other wells showing smaller, but measureable changes (< +286%) (Figure 5b). Alkalinity gradually increases with the chemical interactions between the CO_2 plume and the aquifer materials similar to the EC. The small differences in response to CO_2 injection between EC and alkalinity can be attributed to the geochemical variation of the study site resulting in different CO_2 related buffering capacities (Sechriest, 1960).

The pH also ~~showed~~ decreased noticeably, changing by -1.5 units at SMW 2-2, which was followed by -1.5 units at SMW 1-2, -1.4 units at SMW 2-3, -1.3 units at BS-09 and > -0.96 units at the others (Figure 5c). The DO showed relatively modest change by up to -4.0 mg/L (-78%) at SMW 1-2 which was followed by BS-09 (-4.9 mg/L, -72%), SMW 2-2 (-3.7 mg/L, -72%), SMW 3-2 (-2.8 mg/L, -60%) and the others (< -58%) (Figure 5d). In this experimental setting, the DO evolves with the three-component groundwater mixing between low-DO water volumes (re-injection water at BS-04 and injection water at IW) and high-DO water volume (local groundwater) (Figure 2).

3.3.3 Noble gas tracers

The measured concentrations of He, Ar and Kr tracers are presented in BTCs (Figure 6). The concentration was normalized to the injection amount (C_0) after the background portion (i.e. atmospheric origin) was subtracted from both monitored (C) and initial concentration (C_0), to simply define the CO_2 arrival as a positive signal. Note that for the SMWs, the parameters present the data from the injection depth (i.e., SMW #-2) only, as this exhibited the largest signals of all depths. As a result, the tracers successfully produced the strong positive signals with the CO_2 plume arrival in the BTCs (Figure 6). The tracer concentrations exhibited variable arrival times and concentrations due to the CO_2 plume following different flow paths within the heterogeneous groundwater system at the site, similar to ~~what was~~the findings of ~~described by~~ Kilgallon et al. (2018), Lee et al. (2017), Lu et al. (2012) and Stalker et al. (2015). Most importantly, Kr showed the earliest arrivals through all monitoring wells compared to the He and Ar tracer. This was attributed to the Kr taking a less distributed pathway through the subsurface than the other tracers, and a result of the dilution of CO_2 plume along ~~a~~ the concentration gradient (see the discussion section 4.1.2 Diffusion process controlling the efficiency of noble gas

tracing).

The tracers associated with the CO_2 plume were firstly detected in SMW 2-2 (+4 d) followed by BS-09 (+4 d), SMW 1-2 (+5 d), SMW 3-2 (+18 d) and SMW 4-2 (+23 d) (Figure 6a, c, d, e and f). The strongest signal was recorded at SMW 2-2 (+1,430% for He, +322% for Ar and +6,904% for Kr) suggesting the majority of the CO_2 plume moved along the induced groundwater pressure gradient (Figure 6). A portion of the tracers also moved toward BS-09 and produced a strong signal in spite of ~~its longer~~being a greater ~~moving~~ distance away from the injection point (5.2 m) than that of SWM 1-1 and SMW 2-2 (2.6 m). This can be~~,~~ attributed to the preferential flow pathway present in the study site (Figure 1a) (Ju et al., 2019; Lu et al., 2012). Well PS-04 did not record the presence of any tracers during the injection period due to its location behind the IW in the groundwater flow direction (Figure 1b). ~~Note~~ It is worth noting that SMW 4-2 ~~showed~~ exhibited ~~a stronger signal~~a higher concentration of Kr once the tracers arrived ~~at the plateau~~ than SWM 3-2 ~~did~~ (Figure 6), ~~implied~~ implying that a low conductivity zone ~~existing and hindering~~ hinders well~~the~~ SMW 3-2 from capturing ~~a~~ the full CO_2 plume ~~efficiently~~. This result was consistent with the observations made in alkalinity and pCO_2 (Figure 5).

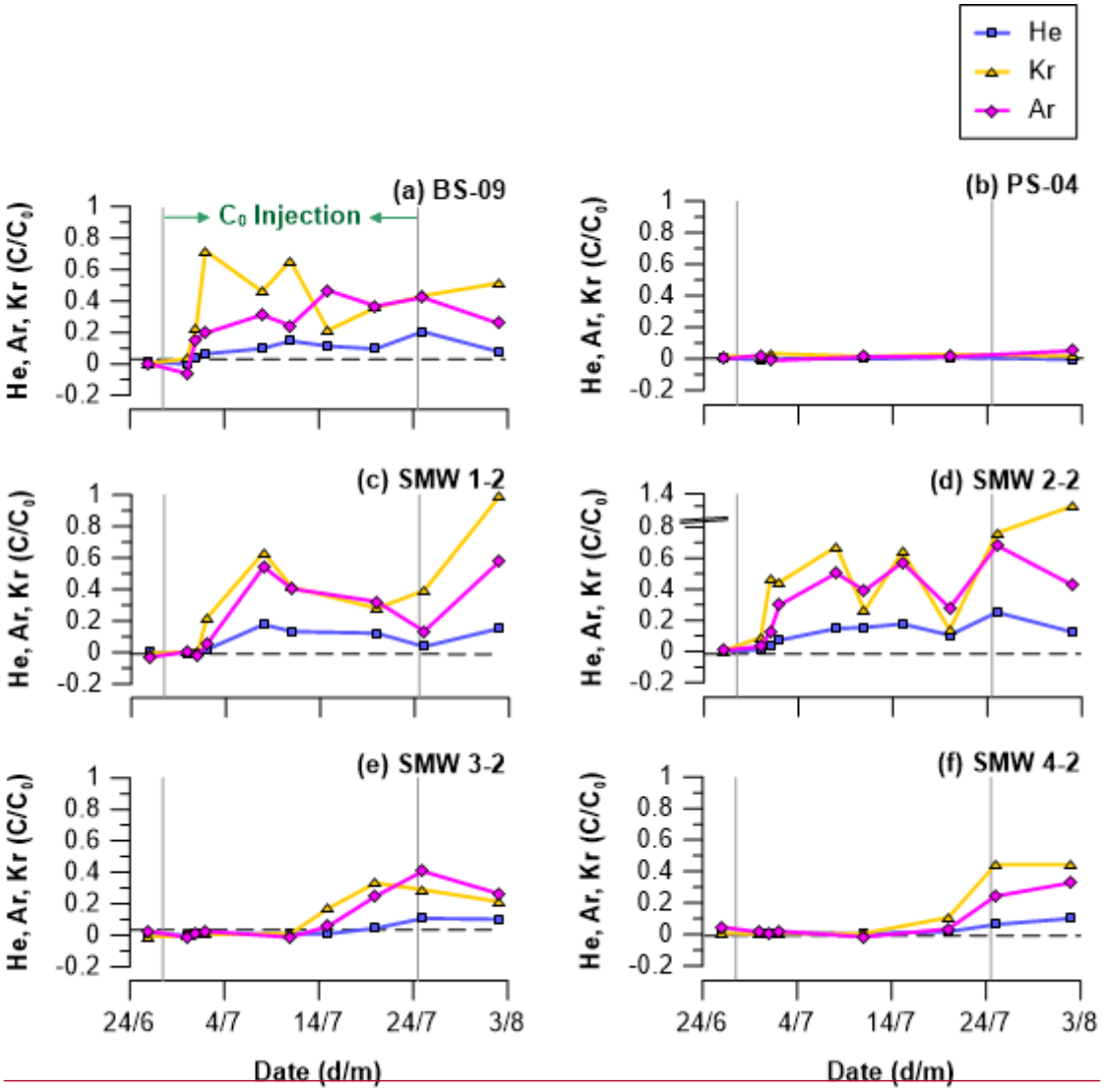
He
Kr
Ar
(a) BS-09
C₀ Injection
(b) PS-04
(c) SMW 1-2
(d) SMW 2-2
(e) SMW 3-2
(f) SMW 4-2
He, Ar, Kr (C/C₀)
24/6
4/7
14/7
24/7
3/8
Date (d/m)

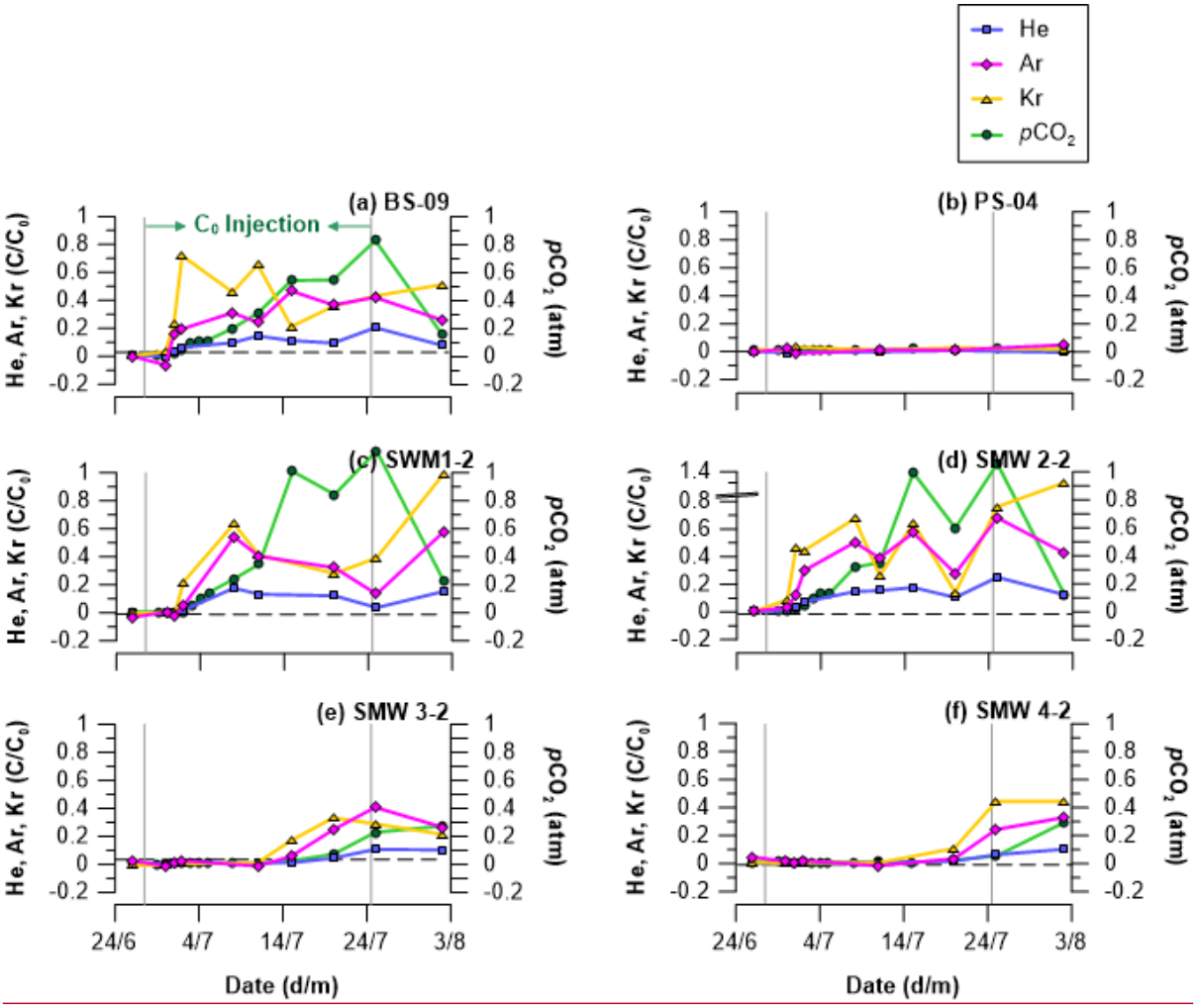

Figure 6. ~~Noble g~~Gas tracer concentration during the experiment. Noble gas was presented as C/C_0 (see the text for details) with pCO_2. The grey vertical lines show the start and end of the injection period. The Air Saturated Water (ASW, black dotted horizontal line) was calculated according to Kipfer et al. (2002) to indicate the local background level of noble gas tracers.

As the injection water gradually approached the monitoring network, the observation wells captured the temporal evolution of the CO_2 plume. In the early stage of BTCs, Kr showed the fastest arrival time compared to the other tracers for all monitoring wells (Figure 6). This was followed by an increase in Ar and He concentrations, with both parameters soon reaching their peak concentration within a few days (Figure 6). In the final stage of BTCs, the plume tail is recorded in all of the monitoring wells through the decrease of noble gas concentrations ~~resulting~~ after ~~the~~ injection at the IW ceased. However, it can be observed that the concentration increased in the last stage of the BTCs for monitoring wells adjacent to IW (Figure 6c and d). This can be attributed to the circulation injection

system of this experiment. In the final stage of the injection period (4 days before the end of injection), the tracer-charged plume had reached BS-10 (Figure 4b). As water was still being produced for the reinjection at the IW, a portion of the CO_2 plume was returned back into the injection tank containing the artificial noble gas tracers. Note that heavier components such as Ar and Kr acted as an early warning tracer for CO_2 arrival in every monitoring well during the monitoring period. This was attributed to physical mechanisms affecting the distribution of the dissolved gases (see the section 4.1.2 Diffusion process controlling the efficiency of noble gas tracing).

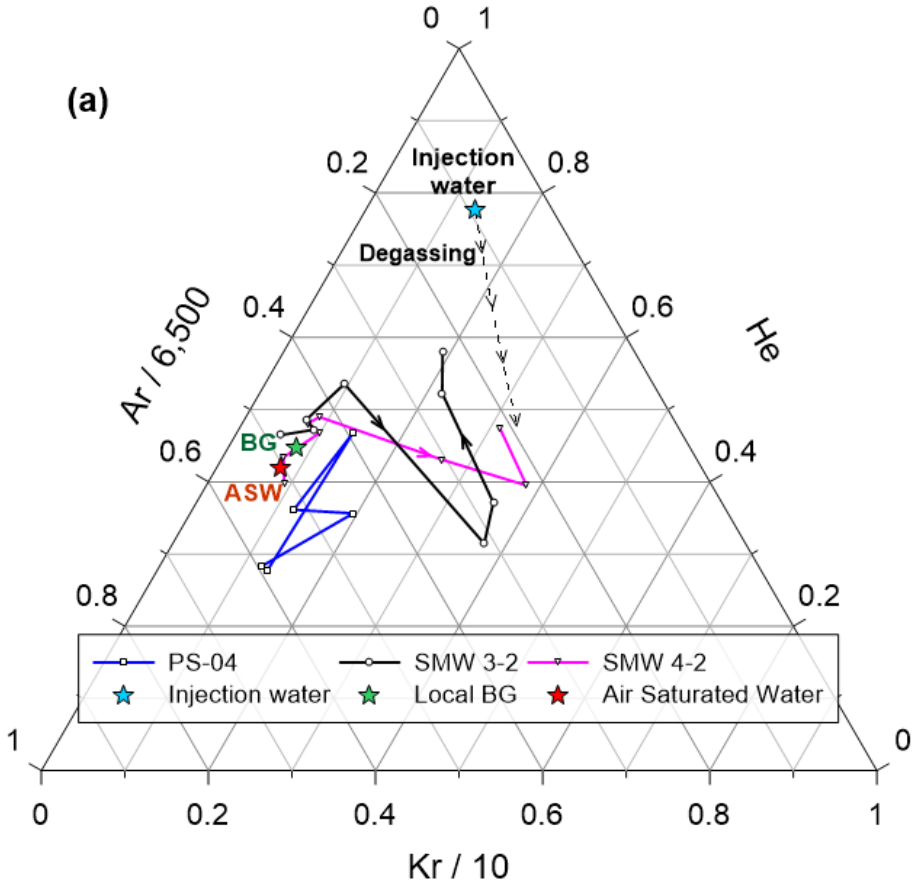
(a)
Injection water
Degassing
BG
ASW
Ar / 6,500
He
Kr / 10
PS-04
SMW 3-2
SMW 4-2
Injection water
Local BG
Air Saturated Water

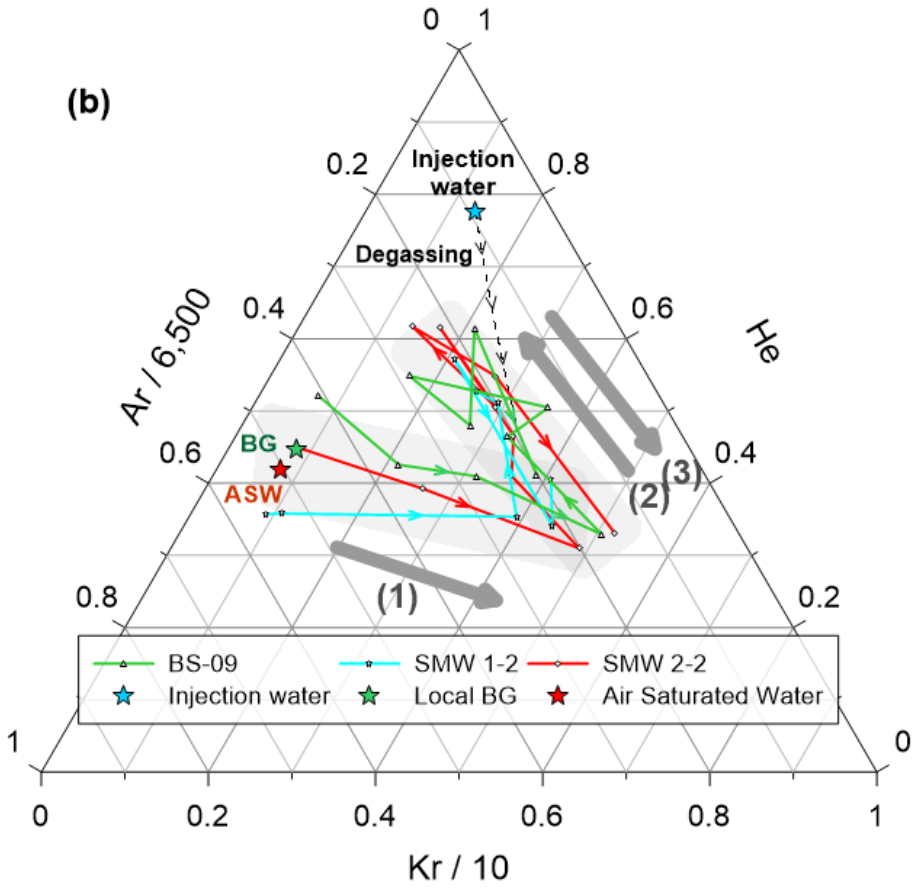
(b)
Injection water
Degassing
BG
ASW
(1)
(2)
(3)
Ar / 6,500
He
Kr / 10
BS-09
SMW 1-2
SMW 2-2
Injection water
Local BG
Air Saturated Water

410

Figure 7. Noble gas ternary diagram showing the two groups of wells categorized by their response. (a) monitoring wells which showed no concentration change from background level (i.e., PS-04) or only an early-stage evolution (i.e., SMW 3-2 and SMW 4-2). (b) monitoring wells that showed a three-step evolution as located close to the injection point (i.e., SMW 1-2 and SMW 2-2) and located in a preferential migration path (i.e., BS-09). The early-stage CO_2 plume is characterized by high Kr concentration (Arrow 1), the plume then gradually increases in He and Ar concentrations (Arrow 2). In the final stage, it becomes rich in Kr again, following the cessation of injection (Arrow 3). The peak composition was different from that of injection water due to initial degassing loss.

The consistent temporal evolution of the recorded noble gas concentrations within the six monitoring wells is depicted in the ternary diagram of Figure 7. The local BG (i.e., green star) represents the average of background level of individual monitoring wells. Prior to the CO_2 plume arrival, each monitoring well plots near to the Air Saturated Water (ASW) level. The initial arrival of the CO_2 plume was marked by a significant increase in Kr in all monitoring wells (see the arrow 1 in Figure 7) which corresponds to the early stage evolution in the BTCs (Figure 6). Note that PS-04 did not exhibit a response after injection. Following the arrival of the Kr tracer, the He and Ar concentrations within the monitoring wells increase as the plume center approached, converging at a single point (Figure 7). However, the concentrations of noble gas tracers at the peak concentrations were lower than those at the time of injection. They were 73.6–88.3% (He), 26.2–55.5% (Ar), and 0–65.5% (Kr) of the initial concentrations. The lower concentrations can be attributed to the degassing loss of the injection fluid (Sathaye et al., 2016), explained in more detail in the section 4.1.1. This degassing process controls the overall retention amount of the injected CO_2. The composition of the plume tail captured in the monitoring wells was similar to the composition of the plume front, characterized by a high Kr concentration (Figure 7).

3.4 Following injection

~~The C_0~~CO_2 injection ceased~~stopped~~ after 28 days ~~of injection~~ (27 June 2017 to 24 July 2017) (Figure 3). This corresponds to the point where the monitoring parameters start to change at the BS-10

(Figure 4b and 5). In this moment, the slight increase of EC was also observable in the CO_2 tank as CO_2 water re-entered the injection tank (Figure 4a). ~~Accordingly~~Additionally, ~~-~~PS-04 also showed a minor increase in EC at the termination period due to the re-circulation of CO_2 injected water (Figure 4d). From this point (24 July 2017), the groundwater circulation system was modified to avoid the re-enhancement of the CO_2 plume. Another local groundwater from BH-03 was prepared and from then onwards substituted the circulation portion going to the BS-04 (Figure 1e and 2c).

3.5 Following groundwater circulation

The groundwater circulation ended on 17 September 2017, 56 days after CO_2 injection stopped and 118 days after groundwater circulation commencement (Figure 3). The pressure turbulence was observable in all monitoring wells (Figure 4) and also EC turbulence was detected in some of the monitoring wells (Figure 4c, f and k), but the groundwater quickly recovered to its previous state (Figure 4).

4 Discussion

4.1 Mass retention mechanisms

4.1.1 Degassing process controlling the overall retention amount of released CO_2

If an inert tracer is continuously released into the groundwater system, the concentration will gradually increase in monitoring wells and eventually become similar to the composition of injection fluid. In this study, as the tracer-charged water was continuously released into the groundwater system, the monitored concentration was expected to resemble the injection fluid's concentration by the final stage. However, a notable difference in CO_2 and noble gas concentrations was observed between the injection fluid and the plateau points (Figure 7). This phenomenon indicates that tracer mass was not conserved in the groundwater system and suffered from mass-reducing processes. As the noble gas tracer is biochemically inert in the groundwater system, the decrease is likely to be the result of physical processes (Holland and Gilfillan, 2013). For instance, a similar noble gas deficit has been observed in a natural CO_2-rich system, where CO_2 and CH_4 bubbles also stripped out the insoluble gases from the groundwater system (Gilfillan et al., 2008, 2017; Brennwald et al., 2005; Zhou et al., 2005) and in

artificial CO_2 injection sites (Nimz and Hudson, 2005; Stalker et al., 2015). Hence, this deficit could be explained by the degassing of unstable CO_2-rich plume.

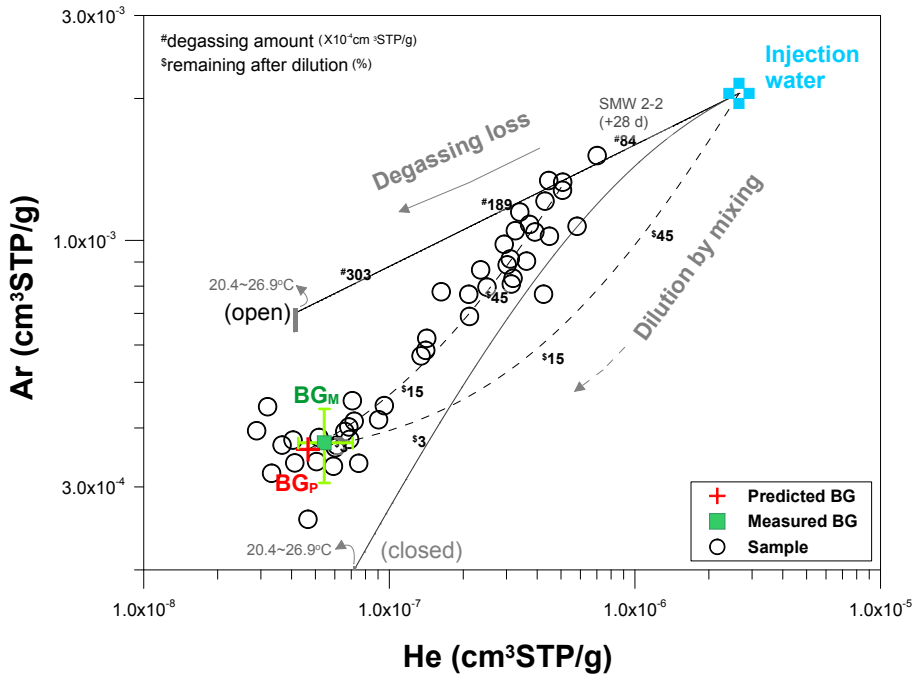

Figure 8. Mass balance of the CO_2 plume depicted with He and Ar tracer. The plume was expected to follow the mixing line between the injection water (blue cross symbol) and the measured background concentration (BG_M, green square symbol). Degassing loss of ~~the~~ CO_2 from the dissolved CO_2 plume, ~~however,~~would result~~ed~~ in a new mixing line starting from the SMW 2-2 (+28 days) toward the background concentration (BG_P, red cross symbol). The BG_P was estimated based on the optimization process of the degassing model (see the Appendix B Model optimization for detailed explanation). The shaded zone on the degassing models indicates the uncertainty arising from the injection water temperature (20.4–26.9°C).

A diagram was constructed using noble gas tracers to determine the major processes influencing the CO_2 plume migration (Figure 8). In Figure 8, the concentrations of He and Ar at the well SMW 2-2 (on 25 July 2017) decreased gradually to their background concentration (BG_p), indicating mixing of the plume with the local groundwater. The mass distribution of observed samples was the function of two distinct processes over the testing period: mass reduction of the CO_2 plume occurred through the degassing process (black line), followed by the dilution of the plume by the local

480 groundwater (black dotted line). The observed data clearly indicated the mixing process was preceded
481 by the degassing process.

482 **Table 1** Mass balance of the leaked CO_2 plume in shallow aquifer system.

Open system	Injection		After degassing loss			Solubility † (mM/atm)
	Amount (kg)	partial pressure (atm)	ΔAmount (kg)	Δpartial pressure (atm)	Remaining (%)	
He	7.04×10^{-5}	3.07×10^{-0}	5.64×10^{-0}	2.46×10^{-0}	~~80.1~~19.9	0.386
Ar	5.43×10^{-0}	6.11×10^{-0}	1.85×10^{-0}	2.08×10^{-0}	~~34.0~~66.0	1.50
Kr	2.50×10^{-0}	7.41×10^{-0}	5.13×10^{-0}	1.52×10^{-0}	~~20.5~~79.5	2.71
$CO_{2\,p.}$ ‡	1.70×10^{2}	6.62×10^{-0}	2.72×10^{0}	1.07×10^{-0}	~~1.6~~98.4	38.7

483 †NIST chemistry webbook of Sander (2017) at temperature of 21.8°C.

484 ‡~~the~~ The predicted value from model optimization (see the Appendix B Model optimization for detailed
485 explanation).

486 Elemental fractionation of noble gases is controlled by their differing solubilities and the
487 ambient reservoir conditions (Figure 8) (Ballentine et al., 2002; Ma et al., 2009). In a closed system,
488 the dissolved air remains in the groundwater, and equilibrium is achieved between the bubbles and the
489 surrounding groundwater. In an open system, the air bubbles are mobile after the phase transition and
490 escape from the aquifer system continuously until the end of the degassing process. In Figure 8, the
491 mixing line (black dotted line) intersects a degassing line (black line) explaining the loss of air bubbles
492 by 1.40×10^{-2} cm^3/g_{H2O} through the degassing process in an open system. The analytical technique for
493 this calculation is shown in Appendix A Mass balance model. In the experiment, CO_2 degassing was
494 detected just above the water table at the IW reconfirming the initial loss happened into the vadose zone
495 (Supplementary Figure S2).

496 Unlike noble gases, CO_2 is involved in diverse chemical and biological processes in the
497 groundwater. To identify the major controls on the CO_2 distribution, the pCO_2 was plotted against
498 measured noble gas tracer concentrations in Figure 9. As expected, the total mass of CO_2 in the plume

was decreased by degassing and mixing processes. Our data designate a clear mixing line stretching from SMW 1-2 (25 July 2017) to BGp, indicating that mixing process mainly controlled the mass distribution of CO_2 in the plume after the initial degassing event. The minor variations from the mixing trend mostly fall in the ranges of the initial composition of injected CO_2-infused water (Figure 9). The solubility-controlled process is shown as the black arrow stretching from the blue-cross symbol to red-cross symbol (Figure 9). The abrupt change in He/Ar ratio stands in strong contrast to the minimal change observed in the pCO_2 during the degassing event (ca. 1.6% overall loss of CO_2). Losses of noble gases (20.5% for Kr, 34.0% for Ar, and 80.1% for He) are much greater than for CO_2 (Table 1).

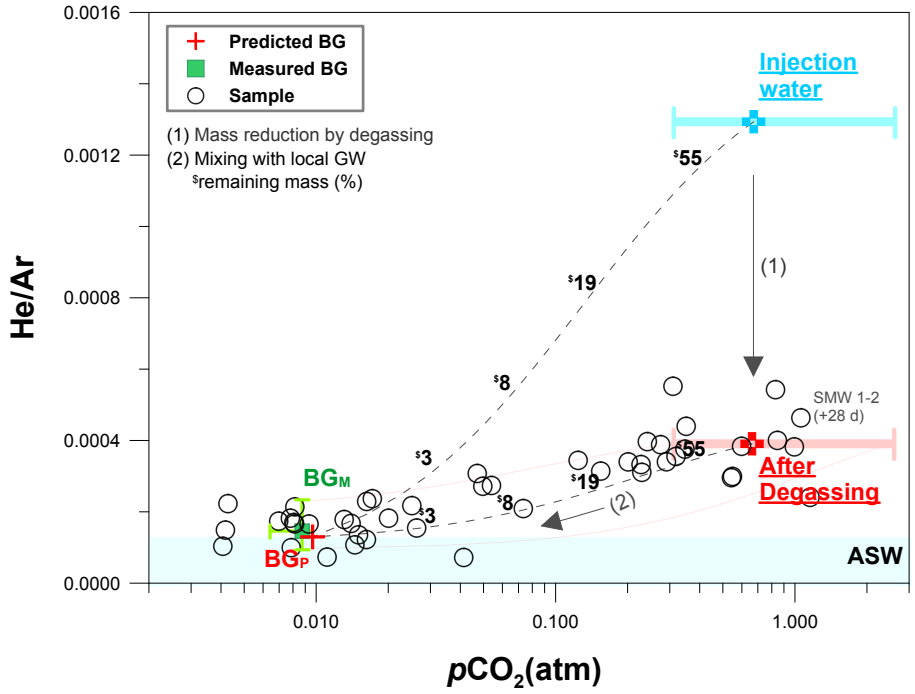

Figure 9. Plot of pCO_2 against He/Ar showing the concentration changes of CO_2 and noble gas tracers during CO_2 plume evolution. The BG_M (green square symbol) is the measured background level, and the BG_P (red cross symbol) is an estimated value from the optimization process of the degassing model (see the Appendix B Model optimization for detailed explanation). The CO_2 plume firstly reduces total mass by the degassing process (Arrow 1) and then gradually gets diluted by mixing with local groundwater (Arrow 2).

4.1.2 Diffusion process controlling the efficiency of noble gas tracing

The different noble gas species cover a wide mass range and thus may provide a chance to constrain the mass-dependent processes occurring in the groundwater system. A comparison was made to scrutinize the behavioral difference for noble gases, as observed from the He/Ar (Figure. 8) and He/Kr (Figure 10) relationships. The mixing line in Figure 10, represented by a black dotted line stretching from the degassing line to BGp, corresponds to the mixing line estimated in Figure 8. However, it is noteworthy that the He and Kr pair did not exhibit a singular trend with many variations scattering from the estimated mixing line. It is also noteworthy that samples from the plume's center tend to converge on the estimated mixing line, while the samples from both the plume's front and tail display a large scatter pattern over the estimated line (Figure 10). Such discordance was also observable in the pCO_2 versus He/Kr diagram (Figure 11) in which many samples, especially those from the plume's front and tail had significantly lower He/Kr ratios (around 0.10) than the ratio describing the estimated mixing line (0.24). This difference indicates that another mass-dependent process was affecting the tracer distribution in addition to the solubility-controlled process.

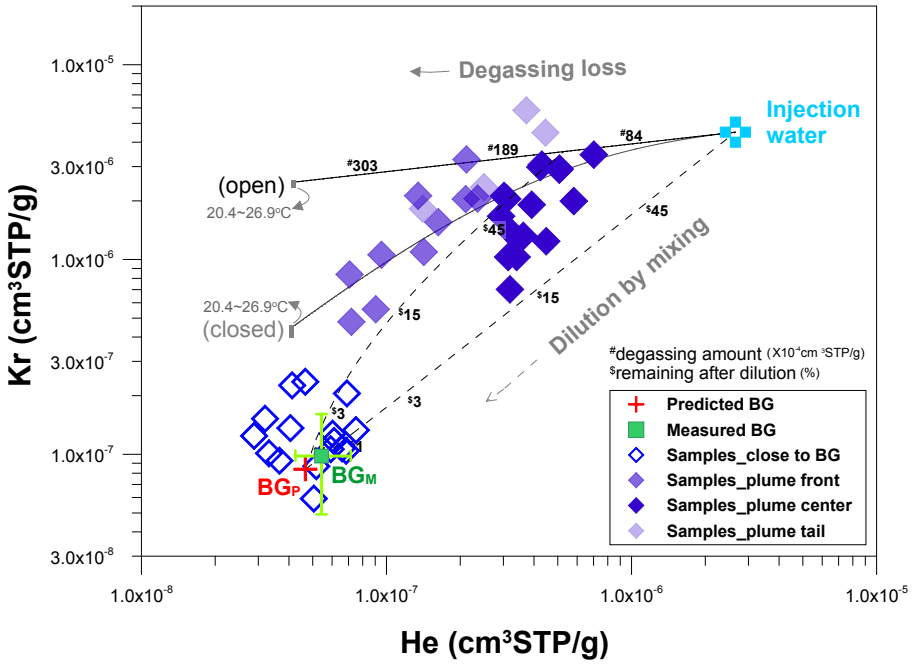

Figure 10. Mass balance of the CO_2 plume depicted with He and Kr tracers. To see the plume evolution in detail, the samples were sorted by the breakthrough positions. Note that many samples, especially on the plume front and tail, are scattered over the estimated mixing line, contrary to the He–Ar pair mixing

trend in Figure 8.

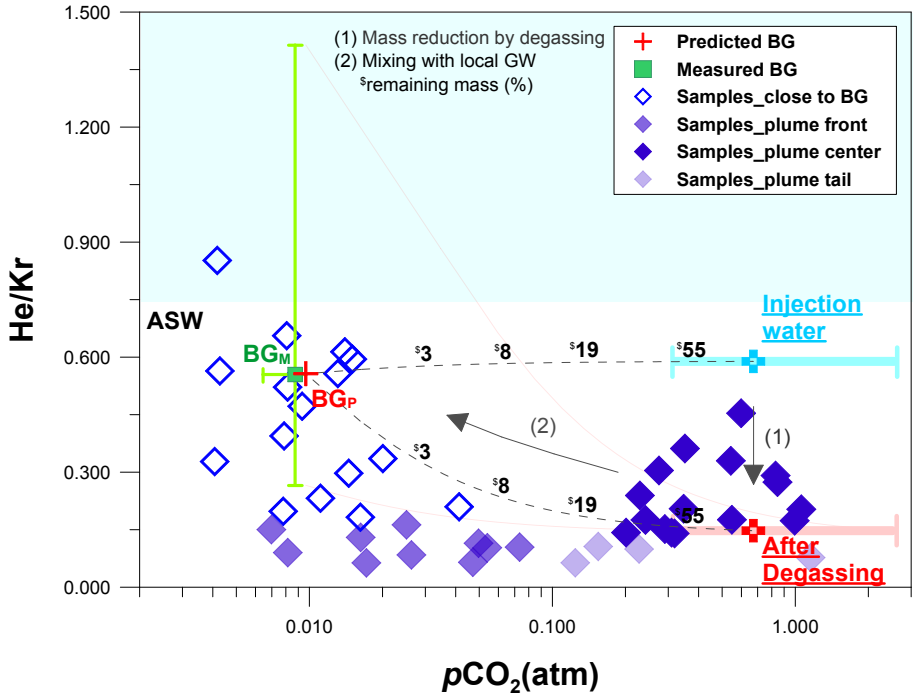

Figure 11. Diagrams showing the concentration changes of CO_2 and noble gas tracers during CO_2 plume evolution. To see the plume evolution in detail, the samples were sorted by the breakthrough positions. Note that, many samples, especially on the plume's front and tail, are scattered from the estimated mixing line, as compared to the observations in the pCO_2 versus He/Ar relationship in Figure 9.

To further examine the temporal progression of the CO_2 plume, ternary plots ~~among~~ of pCO_2 He, and Ar or Kr were composed according to the locations of samples in the plume (i.e., front, center, and tail) (Figure 12). In the He/Ar/pCO_2 diagram, the samples have a small variation near BG_P in the initial period, while as the plume center approached the monitoring points, it showed an upward shift toward the degassing point in the Figure 12a. In the He/Kr/pCO_2 diagram, the samples show a much wider variation during the initial stage of the CO_2 plume arrival than the observed change in the He/Ar/pCO_2 diagram (Figure 12b). This difference indicated that another physical process was involved in the mass distribution at the CO_2 plume's front. Note that the initial composition of the plume was characterized by the high concentration of Kr as it appeared firstly in the observation wells (see also

548 Figure 7).

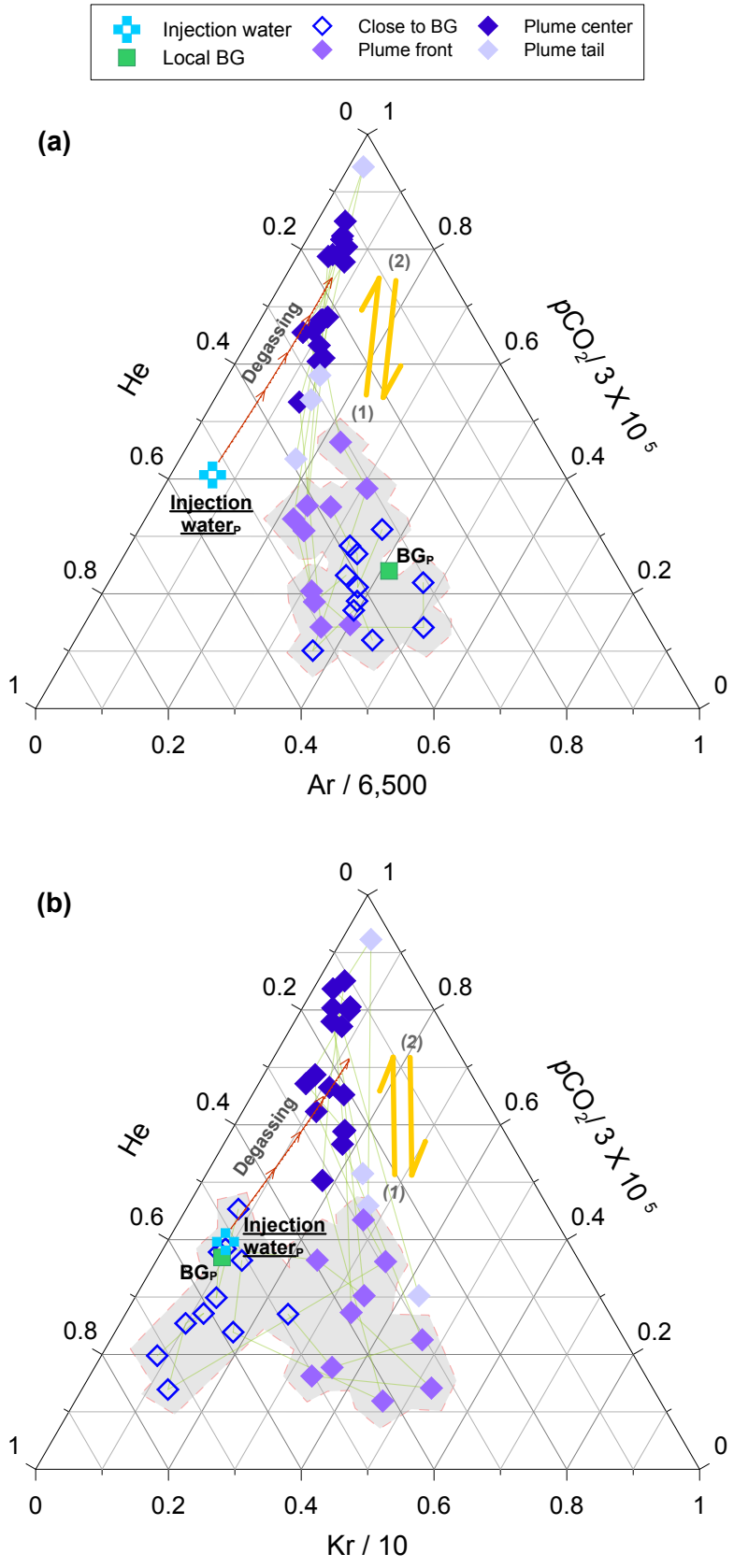
Injection water
Local BG
Close to BG
Plume front
Plume center
Plume tail
(a)
He
pCO2 / 3 X 10 5
Ar / 6,500
Degassing
(1)
(2)
Injection waterP
BGP
(b)
He
pCO2 / 3 X 10 5
Kr / 10
Degassing
(1)
(2)
Injection waterP
BGP

Figure 12. Ternary diagram showing the compositions of pCO_2, He, and Ar (a) or Kr (b) tracers. To scrutinize the plume evolution, the samples were sorted according to the breakthrough positions. In the initial period of plume evolution, the relative compositional change among pCO_2, He and Kr (b) showed a much wider variation near the background levels (BG_P, green square symbol) than that observed among pCO_2, He and Ar (a), which attributed to the diffusion process (see the text for details). This diffusion-dominant movement was followed by the upward shift toward the degassing point (see Arrow 1), as also shown by the intersection point in Figure 8. In the final stage, the samples return to the composition similar to the plume~~'s~~ front (see Arrow 2), after cessation of injection ~~cessation~~.

In open water, diffusion is capable of elemental fractionation depending on the molecular mass (Zheng and Bennett, 2002). According to Fick's law, the mass distribution of a solute in a groundwater system is restricted by molecular diffusion along the concentration gradient. In our experimental design, the artificial injection formed a CO_2- and tracer-rich plume in the groundwater system, setting a steep concentration gradient at the plume boundary. Consequently, the plume boundary was actively subjected to the diffusion process facing with the local groundwater of low concentration level of noble gases. As the diffusion rate is inversely proportional to the elemental mass of the solute, the tracer composition at the plume boundary was regulated by the mass-dependent fractionation. This phenomenon also has been observed in a coal bed methane field, where the free CO_2 and CH_4 gases stripped off the insoluble noble gases from groundwater and this action set the concentration gradient at interfaces with the un-degassed local groundwater, at which diffusion process resulting in a mass dependent fractionation of noble gas tracers (Zhou et al., 2005). Overall, the fact that the diffusion allocates the mass distribution at plume boundary (i.e., plume's front and tail) suggests that the early detection of the migrated CO_2~~leaked~~ plume is dependent on this process. This further implies that the early-stage degassing loss is of primary importance in terms of the noble gas tracing efficiency because the degassing process is associated with the overall plume composition including the feature of the concentration gradient at plume front.

5 Conclusions

A portion of CO_2 stored within the deep subsurface may unintentionally migrate upward to reach overlying shallow aquifers. Whilst noble gas tracers have proved to be useful in monitoring CO_2 leakage, they have been rarely adopted for monitoring purposes in the shallow aquifer system. This study utilized the noble gas tracers to indicate the CO_2 leakage and also to elucidate the mass balance of the leaked plume after injection of 1.70×10^2 kg of CO_2 into a shallow aquifer system. The CO_2- and tracer-enhanced groundwater was released into the induced gradient field and subsequent monitoring works have been conducted. The noble gas tracers produced a strong signal ~~with~~of the ~~the~~migrated CO_2 ~~leakage~~, with Kr consistently exhibiting the first arrival time, ahead of the ~~CO_2~~ plume and ~~than~~ the other noble gas tracers throughout all of the monitoring points.

The mass distribution of the CO_2 plume was controlled by three different physical processes~~;~~, solubility-controlled (degassing), physical groundwater mixing and diffusion. The degassing process reduced the overall mass of the CO_2 plume and caused noble gas tracers to be mass-dependently fractionated, which occurred at the initial stage of CO_2 leakage before plume migration. The diffusion process was also involved during the plume migration, but only influenced the noble gas distributions in the leaked plume and did not act as a primary control for the CO_2 distribution within the monitoring period. This phenomenon, however, can accelerate the dilution of artificial tracers at the plume front, especially for the lighter elements, suggesting this process has an important control on the monitoring efficiency of the artificial tracers in terms of early detection of CO_2 leakage. Most importantly, as the noble gas tracers display more apparent changes according to the retention mechanisms than CO_2 itself, ~~noble gas tracers~~they can provide a robust system for precisely monitoring both the fate and pathway taken by the migrating CO_2.

Noble gas tracers were used to ~~explain~~ constrain the physical retention mechanisms of the injected CO_2 ~~of~~ within a shallow aquifer ~~for the leaked CO_2~~. Our findings indicate that ~~A~~around the injection~~leak~~ point, CO_2 degassing dominantly ~~occurred~~ occurs from ~~a~~ the dissolved plume ~~of~~due to ~~the high~~the high gas pressure, suggesting a near-surface monitoring network is necessary for capturing the active "vertical" movement of degassed budget in this area. This can be accomplished by performing a

602 continuous monitoring of CO_2 at the vadose zone, for example by a soil flux measure, soil gas sampling
603 and borehole head space sampling around a potential leak point. The monitoring regime can be
604 performed cost-effectively with limiting a "degassing boundary" around a suspected leak point. In this
605 study, only a few meters away from the leak point (>2.6 m), the degassing behavior was greatly
606 diminished as a gas pressure of CO_2 plume reduced significantly. From this point, the CO_2 plume was
607 stabilized as a dissolved phase and dominantly diluted by mixing with a local groundwater along a flow
608 direction. Therefore, from this stage, sparse monitoring of saturated zone is recommended for tracing
609 down a horizontal migration of a dissolved CO_2 plume, rather than an intensive gas monitoring for a
610 degassed component. Hence, the key aspect to establish an effective monitoring network is how well
611 constrained the "CO_2 degassing boundary" around a potential leak point is, and how well the
612 groundwater flow regime is understood.

613 Monitoring of degassed CO_2 might not be easily achieved in a real CCS field using direct
614 measurements. In this study, the degassing boundary was just a few meters ~~apart~~ from ~~a~~ the leak point
615 (< 2.6 m), whilst a strong artificial gradient (~0.18) was enforced for the plume migration. This suggests
616 that a degassing boundary would be even narrower in a natural gradient system, making a direct
617 detection of this extremely difficult. Furthermore, heterogeneity in the vadose zone can put an additional
618 uncertainty in monitoring of the vertical flux, as ~~gasesous~~gaseous CO_2 can take various pathways in the
619 vadose zone depending on ~~a~~ the soil permeability distribution (Cohen et al., 2013). Hence, identification
620 of a point source of CO_2 leakage using a direct measurement technique in the vadose zone would be
621 very difficult, unless an intensive monitoring is undertaken around the exact point source. However,
622 noble gas monitoring of groundwater is able to record the migration of a CO_2 plume from the leak point
623 along the groundwater flow pathway, as highlighted in this study. Our findings are similar to previous
624 work (Mackintosh and Ballentine, 2012) that showed monitoring of noble gases in groundwater is an
625 order of magnitude more sensitive for detecting migrated gases than vadose zone gas monitoring.
626 Therefore, we recommend that monitoring of noble gases in groundwaters should be used in addition
627 to direct vadose zone methods, in order to increase the sensitivity of the monitoring regime and improve
628 the protection of the shallow groundwater aquifer above a storage site.

Acknowledgements

This research was supported by a Korea Environmental Industry & Technology Institute (KEITI) grant entitled "R&D Project on Environmental Management of Geologic CO2 Storage" (Project Number: 2018001810002), by a Korea Polar Research Institute grant (PE19060) and by a National Research Foundation of Korea (NRF) grant funded by the Korean government (MSIT) (No. 0409-20190119). We thank all the members of the K-COSEM team and, appreciate Intae Kim and Minjung Kim for their efforts and support on noble gas analysis. Also, we appreciate the help of Dr. Stan E. Beaubien in interpreting the noble gas data. Finally, the authors would like to thank two anonymous reviewers for their detailed comments and observations which greatly improved the present paper.

Appendix A. Mass balance model

At least, two noble gases of different solubility are necessary to determine the degassed mass as outlined in Ju et al. (2019). The closed system is a one-step phase-partitioning process, and therefore, the degassed amount can be determined just by repeatedly adjusting the gas/liquid ratio until the result ($(\frac{A}{B})_{(l)}$) fits into the measured data:

$$(\frac{A}{B})_{(g)} = (\frac{A}{B})_{(l)} \times \alpha$$

$$\alpha = \frac{\frac{r_A}{\emptyset_A}K_A}{\frac{r_B}{\emptyset_B}K_B}$$

Here:

$(\frac{A}{B})_{(g)}$ = A and B ratio in exsolved bubbles, where A and B are different noble gases

$(\frac{A}{B})_{(l)}$ = the composition of A and B remaining in the dissolved phase

α = partitioning coefficient for gas/liquid system

K_A, K_B = Henry's constant for A and B, from Sander et al., (2017)

r_A, r_B = dissolved-phase activity coefficients for A and B and

$\emptyset_A$, $\emptyset_B$ = gas-phase fugacity coefficients for A and B.

In open system, the CO_2 bubble ($V_{(g)}$) is continuously lost into vadose zone carrying the noble gas tracers with it from the groundwater system until the plume is stabilized. An iteration calculation can be undertaken to account for the continuous loss and which terminates when the resultant mass ($m^{i}_{(l)}$) fits the observed noble gas data:

$$m_A{}^{i}_{(l)} = m_A^{i-1}{}_{(l)} - m_A^{i-1}{}_{(g)}$$

$$m_B{}^{i}_{(l)} = m_B^{i-1}{}_{(l)} - m_B^{i-1}{}_{(g)}$$

Here:

i = Iteration step

$m^{i-1}{}_{(l)}$ = mass in dissolved phase before $i-1^{th}$ degassing loss (g)

$m^{i}{}_{(l)}$ = mass in dissolved phase after $i-1^{th}$ degassing loss (g)

$m^{i-1}{}_{(g)}$ = degassed mass during $i-1^{th}$ degassing process (g)

and degassed mass was determined from the degassed volume, such that:

$$m^{i-1}{}_{(g)} = C(V_{(g)} \times p^{i-1})$$

$$C = M/R \cdot T$$

$$p^{i-1} = \gamma\, K\, x^{i-1}/\Phi$$

$$x^{i-1} = 18\,[NG]^{i-1}\,(\rho_{(l)}\, V_{(l)})^{-1}$$

Here:

$V_{(g)}$ = degassed volume during $i-1^{th}$ degassing process (cc)

C = conversion factor from volume to mass

M = molar mass ($\mathrm{g/mol}$)

R = gas constant ($8.314\ \mathrm{cc \cdot atm/K/mol}$)

T = temperature (K)

p^{i-1} = partial pressure of removed noble gas during $i-1^{th}$ degassing process

K = Henry's constant in units of pressure (atm)

γ = liquid-phase activity coefficient

Φ = gas-phase fugacity coefficient

679 x^{i-1} = molar fraction of noble gas in dissolved phase at $i-1^{th}$ degassing moment ($mol_{NG}/mol_{(l)}$)

680 $[NG]^{i-1}$ = number of moles in dissolved phase at $i-1^{th}$ degassing moment (mol)

681 $\rho_{(l)}$ = density of dissolved phase (g/cm^3)

682 $V_{(l)}$ = volume of dissolved phase (cm^3)

683 For an open system, an iterative model was used with a fixed $V_{(g)}$ value which should be small enough
684 to finally achieve convergence with the measured noble gas composition. The noble gas concentration
685 in the groundwater was gradually decreased in iterative steps. In the final stage ($i = n$), $\frac{m_A{}^n_{(l)}}{m_B{}^n_{(l)}}$ was
686 matched against the monitored composition, and then the total degassed volume was calculated by
687 multiplication of the bubble size ($V_{(g)}$) and the number of iteration steps (i) in the open system model.

688 **Appendix B. Model optimization**

689 Model optimization can be achieved in a similar manner to that used by Ballentine (1997) and
690 Castro et al. (2009). The optimization aims to replicate the monitored noble gas data into a calculated
691 mixing line with the smallest misfit to the observed data. As the monitored concentration is defined by
692 mixing between two end-members, therefore, to achieve the minimum misfit, the end-members
693 constituting the predicted mixing line were repeatedly updated. There are two end-members for the
694 mixing line such as: 1) the noble gas concentration after the degassing event; and 2) the noble gas
695 concentration of the background concentration (Supplementary Figure S3). The first end-member is the
696 function of the initial amount and total degassed budget ($V_{(g)}$) of a species as discussed in the previous
697 section. The second end-member is the function of excess air intrusion level (A) to the Air Saturated
698 Water (ASW) (Mazor and Bosch, 1987; Kipfer et al., 2002). Hence, this optimization process allows
699 quantification of the degassing amount and the background level of leaked plume within the
700 groundwater system. The optimization process is given by:

701

$$\chi^2 = \sum_{i=1}^{N}\left[\left(\frac{NG1_i^m - NG1_i^p}{\sigma_{NG_{1,i}}}\right)^2 + \left(\frac{NG2_i^m - NG2_i^p}{\sigma_{NG_{2,i}}}\right)^2\right]$$

Here:

$i = i^{\text{th}}$ sample

N = the number of sample

σ = error of the observed data

$NG1^m$= measured value of noble gas sample

$NG1^p$= predicted value of noble gas sample from the arbitrary mixing line

This optimization process was conducted using a code compatible with the Matlab program.

References

Alcalde, J., Flude, S., Wilkinson, M., Johnson, G., Edlmann, K., Bond, C.E., Scott, V., Gilfillan, S.M.V., Ogaya, X., Haszeldine, R.S., 2018. Estimating geological CO_2 storage security to deliver on climate mitigation. Nat. Commun. 9(1), 2201. https://doi.org/10.1038/s41467-018-04423-1.

Ballentine, C.J., 1997. Resolving the mantle He/Ne and crustal $^{21}Ne/^{22}Ne$ in well gases. Earth Planet Sci. Lett. 152(1-4), 233–249. https://doi.org/10.1016/S0012-821X(97)00142-8.

Ballentine, C.J., Burgess, R., Marty, B., 2002. Tracing fluid origin, transport and interaction in the crust. Rev. Mineral. Geochem. 47(1), 539–614.

Ballentine, C.J., O'nions, R.K., Oxburgh, E.R., Horvath, F., Deak, J., 1991. Rare gas constraints on hydrocarbon accumulation, crustal degassing and groundwater flow in the Pannonian Basin. Earth Planet Sci. Lett. 105(1-3), 229–246. https://doi.org/10.1016/0012-821X(91)90133-3.

Ballentine, C.J., Schoell, M., Coleman, D., Cain, B.A., 2001. 300-Myr-old magmatic CO_2 in natural gas reservoirs of the west Texas Permian basin. Nature 409(6818), 327. https://doi.org/10.1038/35053046.

Beaubien, S.E., Bigi, S., Lombardi, S., Sacco, P., and Tartarello, M.C., 2014. Groundwater changes caused by flow through naturally occurring gas (±water) leakage points. 4th EAGE CO_2 Geological Storage Workshop 2014; Stavanger; Norway; April 22–24, 2014.

Beaubien, S.E., Jones, D.G., Gal, F., Barkwith, A.K.A.P., Braibant, G., Baubron, J.C., Ciotoli, G., Graziani, S., Lister, T.R., Lombardi, S., Michel, K., Quattrocchi, F., Michel, K., 2013. Monitoring of near-surface gas geochemistry at the Weyburn, Canada, CO_2-EOR site, 2001–2011. Int. J. Greenh. Gas Control 16, 236–262. https://doi.org/10.1016/j.ijggc.2013.01.013.

Brennwald, M.S., Kipfer, R., Imboden, D.M., 2005. Release of gas bubbles from lake sediment traced by noble gas isotopes in the sediment pore water. Earth Planet Sci. Lett. 235(1–2), 31–44. https://doi.org/10.1016/j.epsl.2005.03.004.

735 Castro, M.C., Ma, L., Hall, C.M., 2009. A primordial, solar He–Ne signature in crustal fluids
736 of a stable continental region. Earth Planet Sci. Lett. 279(3–4), 174–184.
737 https://doi.org/10.1016/j.epsl.2008.12.042.

738 Cohen, G., Loisy, C., Laveuf, C., Le Roux, O., Delaplace, P., Magnier, C., Rouchon, V., Garcia,
739 B., Cerepi, A., 2013. The CO_2-Vadose project: Experimental study and modelling of CO_2 induced
740 leakage and tracers associated in the carbonate vadose zone. Int. J. Greenh. Gas Control 14, 128–140.
741 https://doi.org/10.1016/j.ijggc.2013.01.008.

742 Flude, S., Györe, D., Stuart, F.M., Zurakowska, M., Boyce, A.J., Haszeldine, R.S.,
743 Chalaturnyk, R., Gilfillan, S.M.V., 2017. The inherent tracer fingerprint of captured CO_2. Int. J. Greenh.
744 Gas Control 65, 40–54. https://doi.org/10.1016/j.ijggc.2017.08.010.

745 Flude, S., Johnson, G., Gilfillan, S.M., Haszeldine, R.S., 2016. Inherent tracers for carbon
746 capture and storage in sedimentary formations: composition and applications. Environ. Sci. Technol.
747 50(15), 7939–7955. https://doi.org/10.1021/acs.est.6b01548.

748 Gilfillan, S.M.V., Ballentine, C.J., Holland, G., Blagburn, D., Sherwood Lollar, B., Scott, S.,
749 Schoell, M., Cassidy, M., 2008. The noble gas geochemistry of natural CO_2 gas reservoirs from the
750 Colorado Plateau and Rocky Mountain provinces, USA. Geochim. Cosmochim. Acta 72, 1174–1198.
751 https://doi.org/10.1016/j.gca.2007.10.009.

752 Gilfillan, S.M.V., Haszeldine, S., Stuart, F., Gyore, D., Kilgallon, R., Wilkinson, M., 2014.
753 The application of noble gases and carbon stable isotopes in tracing the fate, migration and storage of
754 CO_2. Energy Procedia 63, 4123–4133. https://doi.org/10.1016/j.egypro.2014.11.443.

755 Gilfillan, S.M.V., Lollar, B.S., Holland, G., Blagburn, D., Stevens, S., Schoell, M., Cassidy,
756 M., Ding, Z., Zhou, Z., Lacrampe-Couloume, G., Ballentine, C.J., 2009. Solubility trapping in
757 formation water as dominant CO_2 sink in natural gas fields. Nature 458(7238), 614.
758 https://doi.org/10.1016/j.gca.2007.10.009.

759 Gilfillan, S.M.V., Sherk, G.W., Poreda, R.J., Haszeldine, R.S., 2017. Using noble gas

760 fingerprints at the Kerr Farm to assess CO_2 leakage allegations linked to the Weyburn-Midale CO_2
761 monitoring and storage project. Int. J. Greenh. Gas Control 63, 215–225.
762 https://doi.org/10.1016/j.ijggc.2017.05.015.

763 Gilfillan, S.M.V., Wilkinson, M., Haszeldine, R.S., Shipton, Z.K., Nelson, S.T., Poreda, R.J.,
764 2011. He and Ne as tracers of natural CO_2 migration up a fault from a deep reservoir. Int. J. Greenh.
765 Gas Control 5(6), 1507–1516. https://doi.org/10.1016/j.ijggc.2011.08.008.

766 Harvey, O.R., Qafoku, N.P., Cantrell, K.J., Lee, G., Amonette, J.E., Brown, C.F., 2012.
767 Geochemical implications of gas leakage associated with geologic CO_2 storage. Crit Rev. Environ. Sci.
768 Technol. 47(1), 23–36. https://doi.org/10.1021/es3029457.

769 Holland, G., Gilfillan, S., 2013. Application of noble gases to the viability of CO_2 storage. In
770 : Burnard, P. (Eds), The Noble Gases as Geochemical Tracers. Advances in Isotope Geochemistry,
771 Springer, Berlin, Heidelberg 177–223. https://doi.org/10.1007/978-3-642-28836-4_8.

772 Ide, S.T., Friedmann, S.J., Herzog, H.J., 2006. CO_2 leakage through existing wells: current
773 technology and regulations. In 8th International Conference on Greenhouse Gas Control Technologies,
774 19–22.

775 IEAGHG, 2011. Potential Impacts on Groundwater Resources of CO_2 Storage. IEAGHG,
776 Cheltenham, UK.

777 IPCC, 2005. Intergovernmental Panel on Climage Change. Special Report on CO_2 Capture
778 and Storage, edited, pp. 208–210.

779 Ju, Y., Beaubien, S.E., Lee, S.S., Kaown, D., Hahm, D., Lee, S., Park, I.W., Park, K., Yun,
780 S.T., Lee, K.K., 2019. Application of natural and artificial tracers to constrain CO_2 leakage and
781 degassing in the K-COSEM site, South Korea. Int. J. of Greenh. Gas Control 86, 211–225.
782 https://doi.org/10.1016/j.ijggc.2019.05.002.

783 Ju, Y., Kaown, D., Lee, K.K., 2018a. A three-pronged approach for identifying source and

784 extent of nitrate contamination in groundwater. J. Soil Water Conserv. 73(5), 493–503.
785 https://doi.org/10.2489/jswc.73.5.493.

786 Ju, Y., Lee, S.S., Kaown, D., Lee, K.K., 2018b. Application of Inert Gas Tracers to Identify the
787 Physical Processes Governing the Mass Balance Problem of Leaking CO_2 in Shallow Groundwater
788 System. 14th Greenhouse Gas Control Technologies Conference; Melbourne; Australia; October 21–
789 26. https://papers.ssrn.com/sol3/papers.cfm?abstract_id=3365686.

790 Kilgallon, R., Gilfillan, S.M.V., Edlmann, K., McDermott, C.I., Naylor, M., Haszeldine, R.S.,
791 2018. Experimental determination of noble gases and SF_6, as tracers of CO_2 flow through porous
792 sandstone. Chem. Geol. 480, 93–104. https://doi.org/10.1016/j.chemgeo.2017.09.022.

793 Kim, I., Hahm, D., Rhee, T.S., Kim, T.W., Kim, C.S., Lee, S., 2016. The distribution of glacial
794 meltwater in the Amundsen Sea, Antarctica, revealed by dissolved helium and neon. J. Geophys. Res.:
795 Oceans 121(3), 1654–1666. https://doi.org/10.1002/2015JC011211.

796 Kipfer, R., Aeschbach-Hertig, W., Peeters, F., Stute, M., 2002. Noble gases in lakes and
797 ground waters. Rev. Mineral. Geochem. 47(1), 615–700. https://doi.org/10.2138/rmg.2002.47.14.

798 LaForce, T., Ennis-King, J., Boreham, C., Paterson, L., 2014. Residual CO_2 saturation estimate
799 using noble gas tracers in a single-well field test: the CO2CRC Otway project. Int. J. Greenh. Gas
800 Control 26, 9–21. https://doi.org/10.1016/j.ijggc.2014.04.009.

801 Lee, K.K., Lee, S.H., Yun, S.T., Jeen, S.W., 2016. Shallow groundwater system monitoring
802 on controlled CO_2 release sites: a review on field experimental methods and efforts for CO_2 leakage
803 detection. Geosci. J. 20(4), 569–583. https://doi.org/10.1007/s12303-015-0060-z.

804 Lee, S.S., Ju, Y., HA, S.W., Joun, W.T., Jun, S.C., Yun, S.T., Lee, K.K., 2018. Controlled CO_2
805 Injection into a Shallow Aquifer and Leakage Detection Monitoring by Two Different Leakage Events
806 at the K-Cosem Site, Korea. In 14th Greenhouse Gas Control Technologies Conference Melbourne;
807 Australia; October 21–26. https://papers.ssrn.com/sol3/papers.cfm?abstract_id=3366360.

Lee, S.S., Kim, H.H., Joun, W.T., Lee, K.K., 2017. Design and and Construction of Groundwater Monitoring Network at Shallow-depth CO_2 Injection and Leak Test Site, Korea. Energy Procedia 114, 3060–3069. https://doi.org/10.1016/j.egypro.2017.03.1434.

Lemieux, J.M., 2011. The potential impact of underground geological storage of carbon dioxide in deep saline aquifers on shallow groundwater resources. Hydrogeol J. 19(4), 757–778. https://doi.org/10.1007/s10040-011-0715-4.

Lions, J., Devau, N., De Lary, L., Dupraz, S., Parmentier, M., Gombert, P., Dictor, M.C., 2014. Potential impacts of leakage from CO_2 geological storage on geochemical processes controlling fresh groundwater quality: a review. Int. J. Greenh. Gas Control 22, 165–175. https://doi.org/10.1016/j.ijggc.2013.12.019.

Lollar, B.S., Ballentine, C.J., Onions, R.K., 1997. The fate of mantle-derived carbon in a continental sedimentary basin: integration of C/He relationships and stable isotope signatures. Geochim. Cosmochim. Acta 61(11), 2295–2307. https://doi.org/10.1016/S0016-7037(97)00083-5.

Lott, D.E., Jenkins, W.J., 1998. Advances in analysis and shipboard processing of tritium and helium samples. International WOCE Newsletter, 30, 27–30.

Lu, J., Cook, P.J., Hosseini, S.A., Yang, C., Romanak, K.D., Zhang, T., Freifeld, B.M., Smyth, R.C., Zeng, H., Hovorka, S.D., 2012. Complex fluid flow revealed by monitoring CO_2 injection in a fluvial formation. J. Geophys. Res. Solid Earth 117. https://doi.org/10.1029/2011JB008939.

Ma, L., Castro, M.C., Hall, C.M., 2009. Atmospheric noble gas signatures in deep Michigan Basin brines as indicators of a past thermal event. Earth Planet Sci. Lett. 277(1–2), 137–147. https://doi.org/10.1016/j.epsl.2008.10.015.

Mackintosh, S.J., Ballentine, C.J., 2012. Using $^{3}He/^{4}He$ isotope ratios to identify the source of deep reservoir contributions to shallow fluids and soil gas. Chem. Geol. 304–305, 142–150. https://doi.org/10.1016/j.chemgeo.2012.02.006.

Mazor, E., Bosch, A., 1987. Noble gases in formation fluids from deep sedimentary basins: a

review. Appl. Geochem. 2(5–6), 621–627. https://doi.org/10.1016/0883-2927(87)90014-X.

Myers, M., Stalker, L., Pejcic, B., Ross, A., 2013. Tracers–Past, present and future applications in CO_2 geosequestration. Appl. Geochem. 30, 125–135. https://doi.org/10.1016/j.apgeochem.2012.06.001.

Nimz, G.J., Hudson, G.B., 2005. The use of noble gas isotopes for monitoring leakage of geologically stored CO_2. In: Thomas, D., Benson, S. (Eds.), Carbon Dioxide Capture for Storage in Deep Geologic Formations vol. 2. Elsevier Press, Amsterdam 1113–1130.

Parkhurst, D.L., Appelo, C.A.J., 2013. Description of input and examples for PHREEQC version 3: a computer program for speciation, batch-reaction, one-dimensional transport, and inverse geochemical calculations (No. 6-A43). US Geological Survey. https://doi.org/10.3133/tm6A43.

Pinti, D.L., Marty, B., 1995. Noble gases in crude oils from the Paris Basin, France: Implications for the origin of fluids and constraints on oil-water-gas interactions. Geochim. Cosmochim. Acta 59(16), 3389–3404. https://doi.org/10.1016/0016-7037(95)00213-J.

Rillard, J., Loisy, C., Le Roux, O., Cerepi, A., Garcia, B., Noirez, S., Rouchon, V., Delaplaceb, P., Willequet, O., Bertrand, C., 2015. The DEMO-CO_2 project: A vadose zone CO_2 and tracer leakage field experiment. Int. J. Greenh. Gas Control 39, 302–317. https://doi.org/10.1016/j.ijggc.2015.04.012.

Risk, D., Lavoie, M., Nickerson, N., 2015. Using the Kerr investigations at Weyburn to screen geochemical tracers for near-surface detection and attribution of leakage at CCS/EOR sites. Int. J. Greenh. Gas Control 35, 13–17. https://doi.org/10.1016/j.ijggc.2015.01.019.

Sander, R., 2017. Henry's Law Constants. In: Linstrom, P.J., Mallard, W.G. (Eds.), NIST Chemistry WebBook, NIST Standard Reference Database Number 69. National Institute of Standards and Technology, Gaithersburg MD, 20899. https://doi.org/10.18434/T4D303.

Sathaye, K.J., Larson, T.E., Hesse, M.A., 2016. Noble gas fractionation during subsurface gas migration. Earth Planet Sci. Lett. 450, 1–9. https://doi.org/10.1016/j.epsl.2016.05.034.

Sechriest, R.E., 1960. Relationship between total alkalinity, conductivity, original pH, and buffer action of natural water. OHIO J. SCI. 60(5), 303.

Stalker, L., Boreham, C., Underschultz, J., Freifeld, B., Perkins, E., Schacht, U., Sharma, S., 2009. Geochemical monitoring at the CO2CRC Otway Project: tracer injection and reservoir fluid acquisition. Energy Procedia 1(1), 2119–2125. https://doi.org/10.1016/j.egypro.2009.01.276.

Stalker, L., Boreham, C., Underschultz, J., Freifeld, B., Perkins, E., Schacht, U., Sharma, S., 2015. Application of tracers to measure, monitor and verify breakthrough of sequestered CO_2 at the CO2CRC Otway Project, Victoria, Australia. Chem. Geol. 399, 2–19. https://doi.org/10.1016/j.chemgeo.2014.12.006.

Stanley, R.H., Jenkins, W.J., Lott, D.E., Doney, S.C., 2009. Noble gas constraints on air-sea gas exchange and bubble fluxes. J. Geophys. Res.: Oceans 114(C11). https://doi.org/10.1029/2009JC005396.

Vialle, S., Contraires, S., Zinzsner, B., Clavaud, J.B., Mahiouz, K., Zuddas, P., Zamora, M., 2014. Percolation of CO_2-rich fluids in a limestone sample: Evolution of hydraulic, electrical, chemical, and structural properties. J. Geophys. Res. Solid Earth 119(4), 2828–2847. https://doi.org/10.1002/2013JB010656.

Zheng, C., Bennett, G.D., 2002. Applied contaminant transport modeling. Wiley-Interscience, New York.

Zhou, Z., Ballentine, C.J., Kipfer, R., Schoell, M., Thibodeaux, S., 2005. Noble gas tracing of groundwater/coalbed methane interaction in the San Juan Basin, USA. Geochim. Cosmochim. Acta 69(23), 5413–5428. https://doi.org/10.1016/j.gca.2005.06.027.

Highlights

- Shallow aquifers are the last trapping zone for a CO_2 migrated from a storage site.
- CO_2 and noble gas tracers were co-injected into a shallow groundwater aquifer.
- ~~Noble gas~~The tracers showed a clear relationship to the~~with~~ CO_2 species ~~during CO_2~~after the injection ~~in shallow aquifer~~.
- ~~Most of~~ The released CO_2 was mostly retained in the ~~shallow~~ aquifer rather than lost ~~in~~to the vadose~~atmosphere~~.
- Physical mixing and solubility trapping controls ~~primarily determine~~ the mass retention of ~~migrated~~ released CO_2.
- ~~Shallow aquifer is the last trapping zone for mobile CO_2 that migrates from the deep CO_2 storage.~~

Application of noble gas tracers to identify the retention mechanisms of CO_2 migrated from a deep reservoir into shallow groundwater

YeoJin Ju[1], Stuart M. V. Gilfillan [2], Seong-Sun Lee[1], Dugin Kaown[1], Doshik Hahm[3], Sanghoon Lee[1], In-Woo Park[1], Seung-Wook Ha[1], Keyhong Park[4], Hyun-Kwon Do[5], Seong-Taek Yun[5], Kang-Kun Lee[1],*

[1]School of Earth and Environmental Sciences, Seoul National University, 1 Gwanak-ro, Gwanak-gu, Seoul, 08826, South Korea.

[2]School of GeoSciences, The University of Edinburgh, Grant Institute, James Hutton Road, Edinburgh EH9 3FE, UK.

[3]Department of Oceanography, Pusan National University, Busan, South Korea.

[4]Korea Polar Research Institute, Incheon, South Korea.

[5]Department of Earth and Environmental Sciences, Korea University, Seoul 02841, South Korea.

Email: jinee18@snu.ac.kr, stuart.gilfillan@ed.ac.uk, soon3311@snu.ac.kr, dugin1@snu.ac.kr, hahm@pusan.ac.kr, lshlsh2311@snu.ac.kr, inwoo0415@snu.ac.kr, hasabana@snu.ac.kr, keyhongpark@kopri.re.kr, iq1pc@korea.ac.kr, styun@korea.ac.kr.

*Corresponding author. Tel.: +82 2 873 3647. E-mail address: kklee@snu.ac.kr.

Abstract

Carbon Capture and Storage (CCS) is a valuable climate-mitigation technology, which offers the potential to cost-effectively reduce the emissions associated with the burning of fossil fuels. However, there is a potential risk of a small portion of the stored CO_2 unintentionally migrating from a storage site to a shallow groundwater aquifer which is the final retaining zone for any migrated CO_2 before it escapes to the atmosphere. Hence, it is imperative to identify the physical retention mechanisms of CO_2 within a shallow aquifer. In this study $1.70x10^2$ kg of CO_2 and noble gas tracers (He, Ar and Kr) were continuously injected into a groundwater aquifer over 28 days with the aim of identifying the mechanisms and amount of CO_2 retention. Among the tracers, Kr was found to be the earliest indicator of CO_2 migration. The other tracers – He and Ar – arrived later and exhibited diluted signals. The diluted signals were attributed to degassing of the plume mass (1.6% of CO_2) during the early stages of CO_2 migration. Diffusion accelerated the dilution of the lighter elements at the plume boundaries. Consequently, the clear relation of the noble gases with the CO_2 proved that degassing and mixing primarily control the mass retention of CO_2 in shallow groundwater, and the relative importance of these processes varies along the evolving path of migrating CO_2.

Keywords: CCS; monitoring; CO_2 leakage; noble gas tracing; artificial tracer; geochemical monitoring

1. Introduction

Carbon Capture and Storage (CCS) is a climate change mitigation technology that comprises the capture of CO_2 from an industrial point source, such as a power plant or refinery, transport of the captured CO_2 to a storage site followed by the injection of the captured CO_2 into deep geological strata for permanent disposal (IPCC, 2005). However, there is a potential risk that a small portion of the mobile CO_2 in a storage site could accidently migrate out of the subsurface reservoir and inadvertently reach shallower levels of the subsurface (Alcalde et al., 2018). This CO_2 could potentially migrate through geological conduits such as permeable faults and/or abandoned wells resulting in the deterioration of fresh water resources above the CO_2 reservoir (Harvey et al., 2012; IEAGHG, 2011; Lemieux, 2011; Lion et al., 2014) and leakage of a small portion of the CO_2 into the atmosphere (Ide et al., 2006; IPCC, 2005). Recently, the Weyburn-Midale (Canada) CO_2 monitoring and storage project faced allegations that leakage of CO_2 injected into the Weyburn-Midale oil field for Enhanced Oil Recovery (EOR) and storage was causing a deterioration of the groundwater quality on a farm located above the field (Beaubien et al., 2013; Gilfillan et al., 2017).

A variety of geochemical tools have been used to verify CO_2 storage security and track the fate of CO_2 injected for storage. These include CO_2 soil gas and groundwater concentrations, stable C and O isotopes within the CO_2, on-site monitoring parameters (pH, alkalinity, ORP, EC, temperature and DO), inert gas tracers, major and trace ions and radiocarbon (^{14}C) (Flude et al., 2016; Lee et al., 2016). Soil gas and dissolved CO_2 concentrations in groundwater can provide a direct tracer of CO_2 migration, allowing discrimination of different CO_2 origins and providing a means to establish the mass balance of CO_2 present in the groundwater system (Ballentine et al., 2001; Beaubien et al., 2014; Gilfillan et al., 2011; Lollar et al., 1997; Sathaye et al., 2016). Recent developments in on-site monitoring technologies now allow the continuous measurement of a number of parameters (e.g. alkalinity, T, EC, pH) which can be used to establish the overall distribution and temporal evolution of a small CO_2 plume within a shallow groundwater aquifer (Lee et al., 2016). Noble gases are characterized by their inert behavior, which makes them ideal tracers within a subsurface system. This inertness means that noble gases are

conservative tracers and do not partake in the chemical reactions that dilute the CO_2 leakage signals and hence are capable of providing a robust means to distinguish between natural and stored CO_2 (Risk et al., 2015).

Noble gas tracing techniques have been used to track both the fate and migration pathways of injected CO_2 in reservoirs. Within a typical porous CO_2 storage reservoir, CO_2 is retained by a combination of structural, residual and solubility trapping mechanisms (Alcalde et al., 2018; Holland and Gilfillan, 2013; IPCC, 2005). Recent experiments at the CO2CRC Otway Demonstration site for CO_2 storage in Australia have used Kr and Xe as conservative tracers to determine the degree of residual trapping within a porous saline formation, using a numerical mass balance approach (LaForce et al., 2014). The degree of solubility trapping has also been determined using noble gases, through identification of the degree of partitioning of the noble gases into groundwater present within the reservoir formations (Ballentine et al., 1991; Brennwald et al., 2005; Gilfillan et al., 2008, 2009; 2014; Pinti and Marty, 1995; Zhou et al., 2005).

Noble gas tracers are also suitable for monitoring the vertical migration of the reservoir CO_2, thanks to the compositional difference of natural noble gas tracers between storage reservoir and the near surface environment (Mackintosh and Ballentine, 2012). Gilfillan et al. (2011) applied noble gas tracing tools to constrain the nature of CO_2 leakage into shallow groundwater and surface water bodies. Further work by Gilfillan et al., (2017) used inherent tracers residing in the Weyburn-Midale injection and storage project reservoir to show that CO_2 migration from the deep reservoir into the shallow aquifer system had not occurred. This work found that the noble gas composition in the groundwater samples above the CO_2 injection and storage project did not vary over a typical background level of a shallow aquifer, of Air Saturated Water (ASW) with an excess air component of up to 45% (Gilfillan et al., 2017). Recent work by Flude et al. (2016) and Flude et al. (2017) evaluated the inherent tracing ability of noble gases focusing on the compositional difference of them between captured CO_2, the subsurface storage reservoir, air and ASW. Differences in the noble gas contents of these samples stemmed from the different CO_2 capturing processes and what controls the composition of noble gas tracer in a stored

fluid (e.g. gas stripping of reservoir water and/or interaction with radiogenic components).

The concept of inert tracers was extended to artificial enhancement studies, involving the addition of inert gas tracers such as SF_6 and noble gases to the injected CO_2 in CCS storage. This aimed to provide a much clearer distinction between the injected CO_2 and that naturally present in the subsurface and so improving the monitoring efficiency (Myers et al., 2013; Nimz and Hudson, 2005). For example, noble gases have been previously used as artificial tracers to indicate CO_2 leakage pathways in the vadose zone (Cohen et al., 2013; Rillard et al., 2015) and in the aquifer system (Lu et al., 2012; Nimz and Hudson, 2005; Stalker et al., 2009). In the CO_2-Vadose project, undertaken at a test CO_2 release site in France, the lighter noble gases (He and Ne) were found to have the fastest arrival time in monitoring wells due to their higher diffusion coefficient and low solubility within the soil water compared to the CO_2 and other tracers (Cohen et al., 2013). In contrast, the heavier noble gas tracers (Kr and Xe) exhibited the fastest arrival in the aquifer system due to their solubility in groundwater compared to other noble gases following the artificial injection into a deep reservoir (~2 km) (Stalker et al., 2015). In a recent test, a small amount of CO_2 (16.9 kg) spiked with noble gas was released into a shallow aquifer at Korea CO_2 Storage Environmental Management (K-COSEM) study site, in order to understand the behavior of the leaked plume in the shallow groundwater system. This study identified that the mass distribution of the leaked CO_2 is predominantly controlled by the solubility of the individual noble gases and mixing processes during the limited time of monitoring work (i.e. 4 months) (Ju et al., 2019).

The shallow groundwater is the final zone encountered by migrating CO_2 before it is lost into the vadose zone and atmosphere. Furthermore, this reservoir is directly linked into the human activity, hence, should be protected from a potential leakage of stored CO_2 (Lee et al., 2016). While noble gas tracers have proven useful to monitor leaked CO_2 plume in shallow aquifer systems (Flude et al., 2016; 2017), this has only been demonstrated on a few occasions, for example, in a natural CO_2 production site using inherent noble gases (Gilfillan et al., 2011), in a CO_2 injection test site using artificially enhanced noble gases (Ju et al., 2019) and to rule out CO_2 migration in a shallow aquifer above an

actual CO_2 storage reservoir using inherent noble gases (Gilfillan et al., 2017), as described above. In this study, we present the results of applying noble gases to a CO_2 injection test into a near-surface aquifer. This artificial CO_2 migration test aims to mimic a situation where a measurable amount of CO_2 ($1.70x10^2$ kg) has migrated from a deep CO_2 storage reservoir into a shallow groundwater aquifer. This study focuses on determining the amount of CO_2 retained in the groundwater and the mechanisms controlling the migration of the CO_2 plume using noble gas tracers. A mass balance model was constructed based on the partitioning coefficients of noble gas tracers in a gas-water system, to understand and to quantify the final retention of the injected CO_2 within the shallow aquifer system.

2. Materials and methods

2.1 Site description

The Korea CO_2 Storage Environmental Management (K-COSEM) Research Center has installed a controlled CO_2 release experiment at Eumseong gun (county) of South Korea (Figure 1). The geology at the field experimental site includes three different subsurface media, firstly consisting of a weathered soil layer composed of medium to coarse grained silty sand (0–30 m below ground surface (bgs)), followed by weathered biotite granite (30–70 m bgs), and finally consolidated biotite granite (starting at 70 m bgs) (Lee et al., 2017; Ju et al., 2018a). The water level was located at the 16.0–18.4 m bgs and the hydraulic conductivity of the aquifer was estimated from pumping tests, ranging from 1.7×10^{-5} cm/s for the consolidated bedrock to 2.0×10^{-4} cm/s for the weathered layer. Prior to the commencement of the experiment, the groundwater was flowing from the northwest toward the southeast following a hydraulic gradient of 0.003 (i.e., the regional flow in Figure 1a).

At the K-COSEM site, a total of 24 monitoring wells had been installed in the shallow aquifer (i.e. < 15 m below the water table) including the injection well (IW), partially screened (PS), boreholes (BH), borehole screened (BS) and saturated zone monitoring wells (SMWs) (Figure 1a). Each saturated zone monitoring well (SMW) contained several screened multi-depth monitoring wells for groundwater monitoring at different depths (Figure 1f). In this CO_2 injection study, the IW and six monitoring wells (PS-04, SMW1 to 4, BS-04, -09 and -10) were employed for the CO_2 injection experiment (Figure 1b).

The wells BS-04 and BS-10 located at both ends of the monitoring range were used to create an induced pressure gradient field by pumping out groundwater at a down-gradient location (BS-10) and successive injection in at an up-gradient location (BS-4) (Figure 1c). The SMWs are located along the created groundwater flow pathway, while PS-04 was up-gradient relative to the CO_2 injection point. The well BS-09 was intended to capture the preferential movement of the released CO_2 along a high connectivity zone between injection well and BS-09, identified in the work of Ju et al. (2019). Details on the study site and monitoring network can also be found in previous works (Lee et al., 2017; Lee et al., 2018; Ju et al., 2018b; Ju et al., 2019).

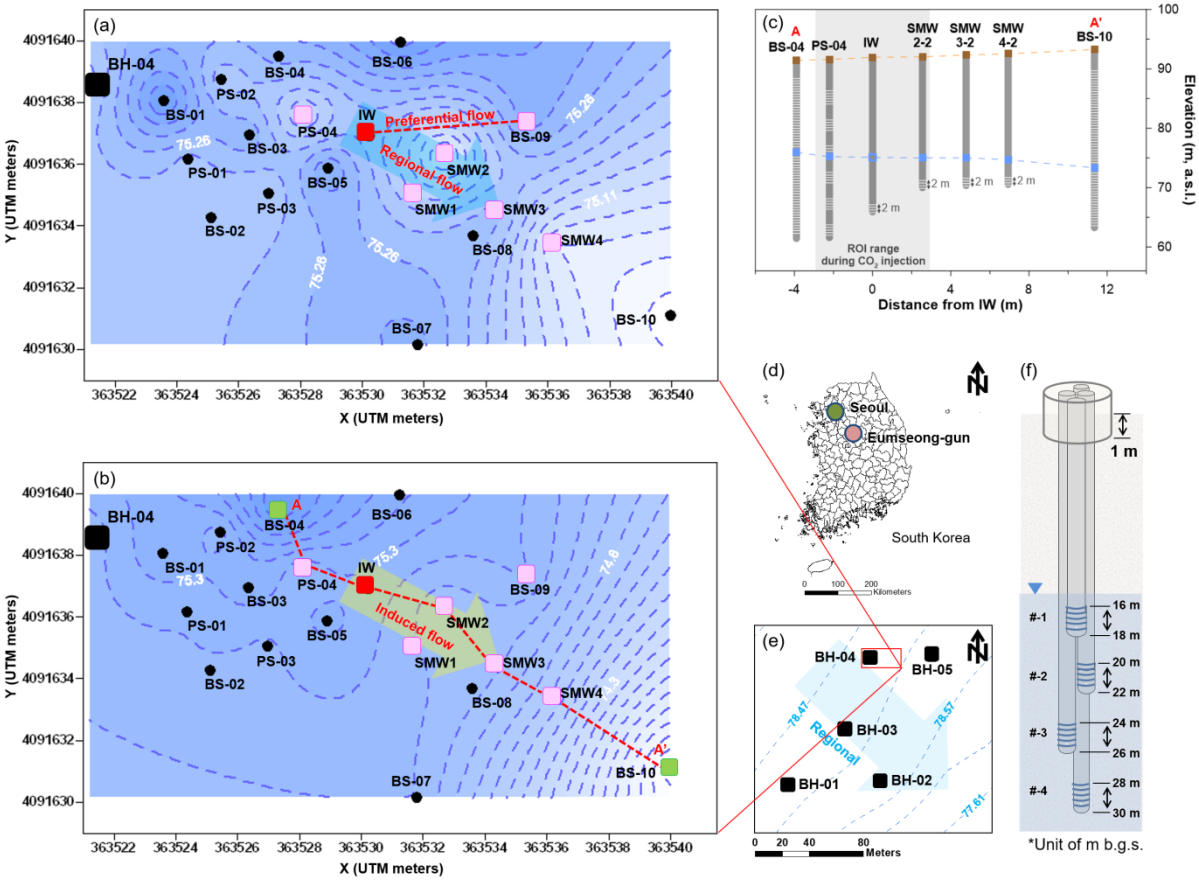

Figure 1. Maps of the study site. Figures on the left show (a) natural regional groundwater flow (shown as a blue-colored arrow) before enhanced groundwater circulation using the wells BS-04 and BS-10, where a preferential path exists in this field due to local hydrogeological heterogeneity (16 May 2016), (b) induced pressure gradient field (shown as a green-colored arrow) after the pumping out and pumping

in using the two wells (see green squares) (4 July 2016). Note that the induced flow was intended to speed up the plume migration along the groundwater flow (i.e., regional flow in [a]). Pink squares represent the wells used for monitoring; a red square represents the injection well (IW). Figures on the right show (c) a cross-section view along the induced pressure gradient (4 July 2016), (d) the location map of the study area, (e) the contours of groundwater levels obtained by kriging using 17 wells surrounding the study site (7 March 2015), and (f) the structure of each saturated zone monitoring well (SMW) containing a bundle of four screened pipes with different lengths.

2.2 Artificial injection

2.2.1 Induced pressure gradient field

The CO_2 injection was undertaken in the induced pressure gradient field to reinforce the groundwater flow, therefore, to speed up the CO_2 plume migration (Figure 2c). The hydraulic pressure gradient was achieved by enhancing groundwater circulation, consisting of water production and reinjection using the BS-04 and BS-10 wells located at both ends of the monitoring network (Figure 2c). A total of 24.0 m^3/d of groundwater was pumped from BS-10 and reinjected into BS-04 (Figure 2c). A period of 1 month was required to stabilize the pressure gradient (22 May 2017 to 27 June 2017). The pressure gradient was steeper near the injection site and production points (i.e. the BS-04 and BS-10), with the average gradient being 0.18 (Figure 2c). The circulation was maintained until 17 September 2017.

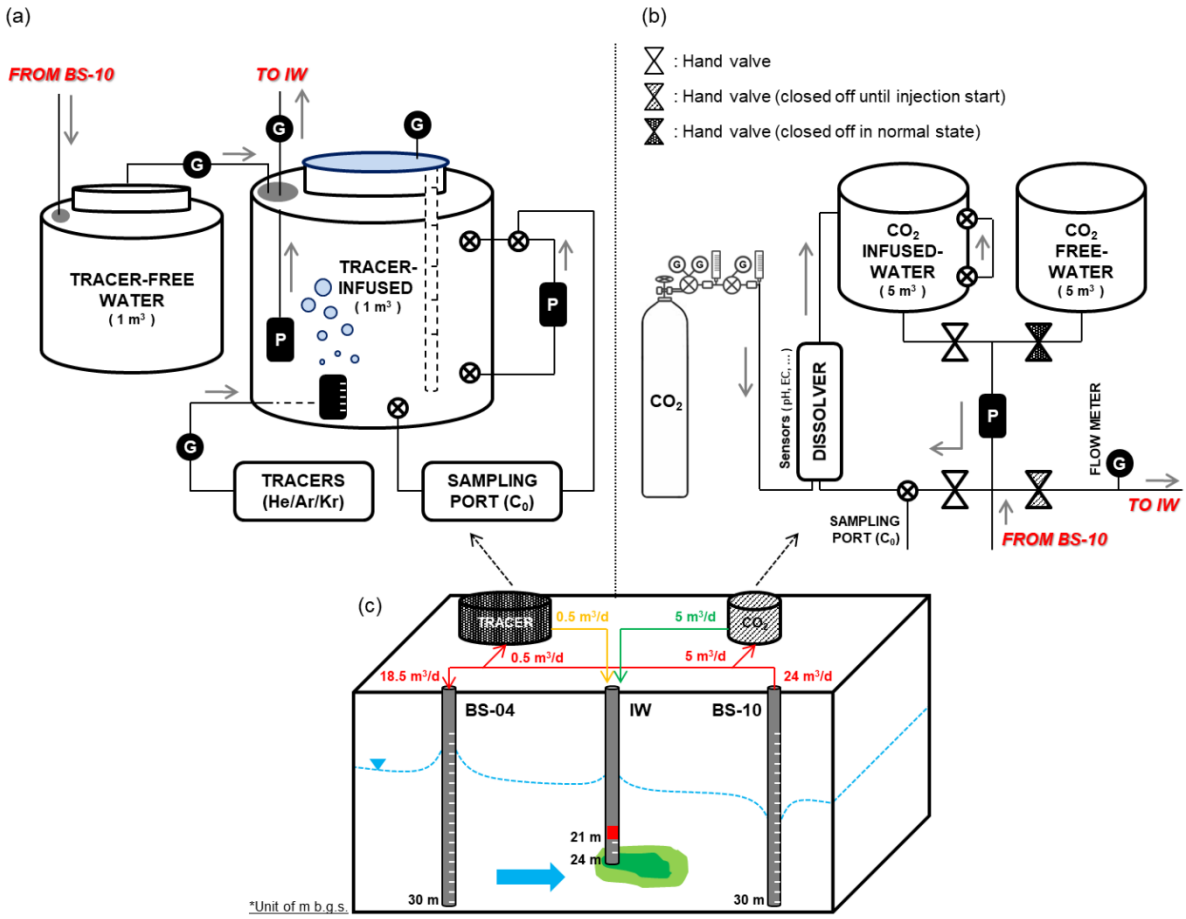

Figure 2. Injection systems for the artificial CO_2 release experiment. (a) tracer-infused groundwater was prepared in a 1 m^3 tank and (b) CO_2-infused groundwater was prepared in a 5 m^3 tank. (c) gas-charged groundwater was continuously released into the induced pressure gradient field through the IW.

2.2.2 Injection

To prepare the injection water, the water flux sent to BS-04 (24.0 m^3/d) was reduced to 18.5 m^3/d and 5.5 m^3/d of groundwater was sent into the injection tank (Figure 2c). 5.0 m^3/d of groundwater was sent into the CO_2 dissolver tank (Figure 2b) and 0.5 m^3/d of tracer–enhanced water was prepared in the other tank (Figure 2a). The CO_2-infused groundwater was prepared in the 5 m^3 tank equipped with the circulation pump, CO_2 dissolver, water sampling port and flow meter (Figure 2b). Injection was initiated when the CO_2 concentration reached the equilibrium state (termed C_0). To ensure that the equilibrium concentration was maintained, alkalinity, pH, EC, DO, ORP, temperature, salinity, TDS

was continuously monitored with real time measurement devices such as YSI (YSI Inc./Xylem Inc., USA), LTC Levelogger Junior (Solinist, Canada) and SH-300-DS (SOHA TECH, Inc., Korea) while circulating water within the tank using a pump (Figure 2b). These measurements showed that it took approximately 24 hours to achieve the equilibrium state. The noble gas infused groundwater was also prepared one day ahead of the injection test. Approximately 0.5 m^3/d of groundwater was pumped into the 1 m^3 of closed tank equipped with the circulation pump, tracer tank, water sampling port and flow meter (Figure 2a). The injected tracers were a mixture of He (0.2 vol. %), Ar (99.4 vol. %), and Kr (0.4 vol. %) and were injected through a flowmeter and diffuser (AS-10 3/8) into the 1 m^3 dissolver tank. The infused liquids were first injected into the subsurface on 27 June 2017 and continued to be injected for 27 days until 24 July 2017. Samples for initial concentration analyses (i.e. C_0) were collected during the injection event and through the sampling ports (Figures 2a and b). Injection took place at 4.5–7.5 m below the water table (corresponding to 21–24 m bgs) in an isolated zone below a packer (Figure 2c). The ambient surface weather conditions during the injection event were 20.4–26.9^{o}C without precipitation. The injection rate was controlled by a submersible and controllable quantitative pump (model MP1, Grundfos, Denmark) at a constant rate of 5.5 m^3/d (Figure 2c).

2.3 Real-time monitoring

Real-time monitoring data was collected from 17 May 2017 to 13 October 2017 (Figure 3). Over this period, hydraulic pressure (P), temperature (T) and electrical conductivity (EC) were measured in-situ using the LTC Levelogger Junior (Solinist, Canada) and the barometric state was monitored at the same time using the Barologger Edge (Solinist, Canada) at 10 minute intervals.

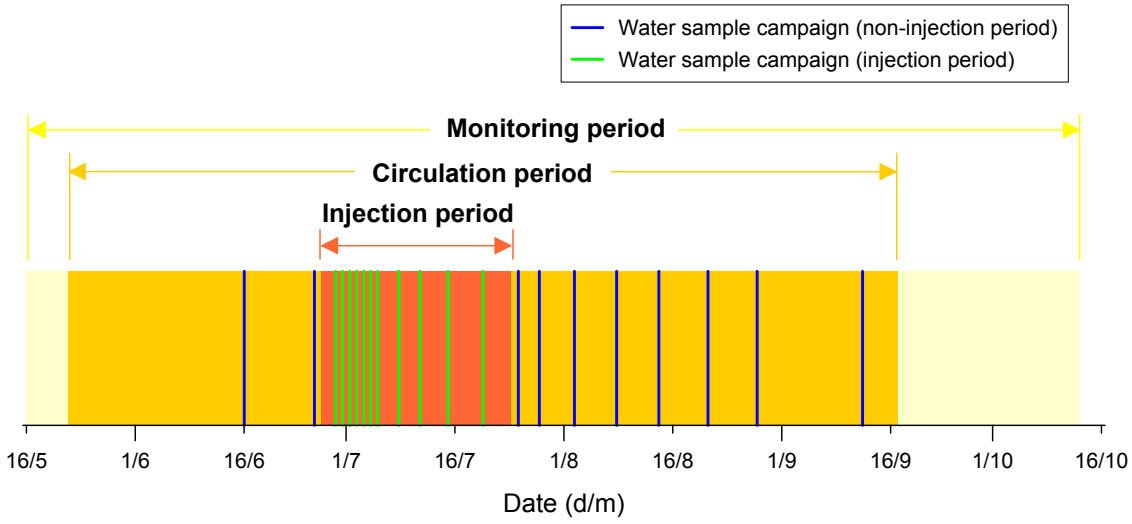

Figure 3. Schedule for water sample collection during the CO_2 injection test.

2.4 Water sampling campaign

2.4.1 Baseline survey period

Water samples were collected using a Waterra Inertial Pump with PowerPack PP-1 (Wattera, Canada) to obtain baseline data before the CO_2 injection. The local baseline of the pCO_2 was obtained on two occasions through water sampling between 16 June 2017 and 26 June 2017 (Figure 3). The baseline for the noble gas tracers was determined by a single water-sampling operation on 26 June 2017 (Figure 3). Alkalinity was determined in the field site by acid titration method with 0.05 N HNO_3. The pH and temperature were also measured in-situ using a portable water quality meter (YSI ProDSS, YSI Inc./Xylem Inc., USA). The noble gas samples were collected using a standard copper tube of 28 cm^3 and a pinch-off clamp set.

2.4.2 Injection and post-injection period

Data acquisition after the CO_2 injection was conducted in the same manner as the baseline data collection. Water samples were collected on 19 occasions following the injection event, over 76 days from 27 June 2017 to 12 September 2017 (Figure 3).

2.5 Laboratory analyses

2.5.1 Noble gas

The noble gas samples were analyzed in the noble gas analysis laboratory at the Korea Polar Research Institute (KOPRI) using an automated system as outlined in Stanley et al. (2009) and Kim et al. (2016). Gases were first extracted from a groundwater sample under high vacuum condition (~10^{-7} mbar) and stored in an aluminosilicate glass ampoule (Lott and Jenkins, 1998). Excessive water vapor, active gases, and condensable gases were then removed using cryogenic traps and a series of hot and cold Zr-Al alloy getters (St 101, SAES Getters S.p.A., Italy) before sample injection into the RGA200 mass spectrometer (Stanford Research Systems, California, USA) for analysis. The noble gases, He, Ne, Ar, and Kr were calibrated against air standards of 0.9 and 2.7 cm^3 STP, to cover the wide range of the tracer enhanced injection water. The discrepancy between duplicate samples was less than 5% (Ju et al., 2019).

2.6 Analytical methods

2.6.1 pCO_2 calculation

pCO_2 values for the sampled waters were calculated using the monitored parameters of alkalinity, pH, and temperature. Alkalinity, pH and temperature were measured in-situ. Using these data a robust calculation for pCO_2 value was made using the program PHREEQC Version 3 (Parkhurst and Appelo, 2013).

2.6.2 Mass balance model

At the early stage of the CO_2 injection, the CO_2 plume is unstable with a high partial pressure, resulting in a degree of CO_2 degassing. Hence, CO_2 bubbles rise freely from the brine with a proportion of the CO_2 remaining in the dissolved phase. During the degassing period, the free-phase CO_2 strips out the dissolved, relatively insoluble noble gases, especially the lighter elements (He and Ne), leaving the system relatively enriched in the heavier noble gases (Ar, Kr, Xe) (Ballentine et al., 2002; Holland and Gilfillan, 2013). Based on the degree of this enrichment, we can inversely constrain the mass balance of the CO_2 plume in terms of the degassing process (see the Appendix A mass balance model for detailed explanation).

3 Results

3.1 Prior to CO_2 injection

Pressure and temperature changes result in the degassing of insoluble substances from the groundwater system. At the K-COSEM test site, the groundwater level shows a clear decreasing trend due to large-scale water consumption from nearby industrial complexes (Figure 4) (Ju et al., 2019). However, prior to the experiment the hydrostatic pressure data showed a stable correlation with atmospheric pressure changes and no irregular turbulence (Supplementary Figure S1). Groundwater temperatures corresponded to normal seasonal values ranging between 12.7 to 13.6°C (Figure 4).

The induced pressure gradient commenced on the 22 May 2017 as a result of the onset of water circulation (Figure 3c). Perturbations were detected in the water level (WL), temperature (T), and electrical conductivity (EC) values during the initiation of water circulation (see the start points of dark grey zone in Figure 4). The pressure turbulence was most noticeable within the monitoring wells located inside the radius of influence (ROI) area both of the pumping (BS-10) and injection wells (BS-04). For example, PS-04, SMW 1 series and SMW 2 series wells showed an instant pressure increase after the circulation commenced, as they are located near the injection well (BS-04) (Figure 4d–j). In contrast, wells SMW 3-2 and 4-3 showed an abrupt decrease in pressure, as a result of their location near to well BS-10 where water was extracted (Figure 4k and l). Well BS-09 also displayed a modest increase in pressure 9 days after water circulation commenced (specifically on 31 May 2017) (Figure 4c). Temperature within all monitoring wells showed an overall increase after the water circulation regime started (see the start points of dark grey zone in Figure 4). This is most likely linked to the groundwater for injection having resided in the surface tank at temperatures warmer (i.e., 17.1 to 28.6^{o}C) than those of the subsurface groundwaters (i.e., 13.3^{o}C) for the day prior to re-injection into the subsurface. The EC showed the overall decreasing trend in the initial circulation period as the re-injected water (BS-10) has a relatively low EC background compared to the other wells, with the exception of well SMW 2-1 (Figure 4).

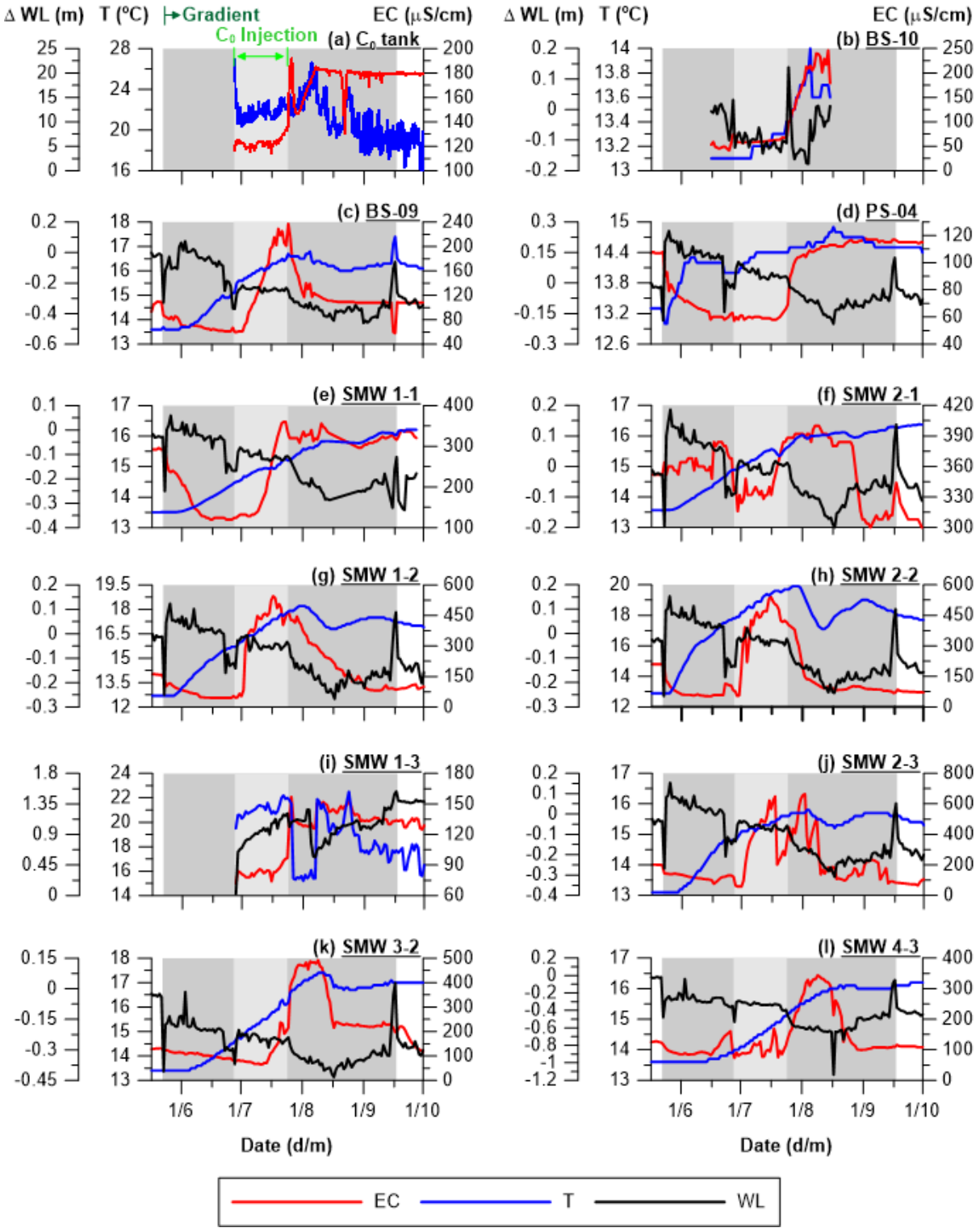

Figure 4. Water level (WL), temperature (T) and electrical conductivity (EC) data. Measurements were completed in the monitoring wells continuously using a LTC data logger. The groundwater circulation was initiated at 22 May 2017 (dark grey shaded zone) and the CO_2 injection started at 27 June 2017 and kept going till 24 July 2017 (light grey shaded zone).

As outlined previously, two water sampling campaigns were conducted during the circulation period and prior to CO_2 injection commenced, in order to establish the groundwater baseline composition (16 June 2017 and 26 June 2017) (Figure 3). The baseline alkalinity values were relatively low (27.5–64.1 mg/L), DO exhibited a wide variation (3.6–8.0), pH was weakly acidic (6.5–7.1) and pCO_2 was relatively low (0.0–0.01 atm) prior to CO_2 injection (Figure 5). All of the parameters were close to the baseline values of low carbonate levels in the biotite granite protolith (Ju et al., 2019).

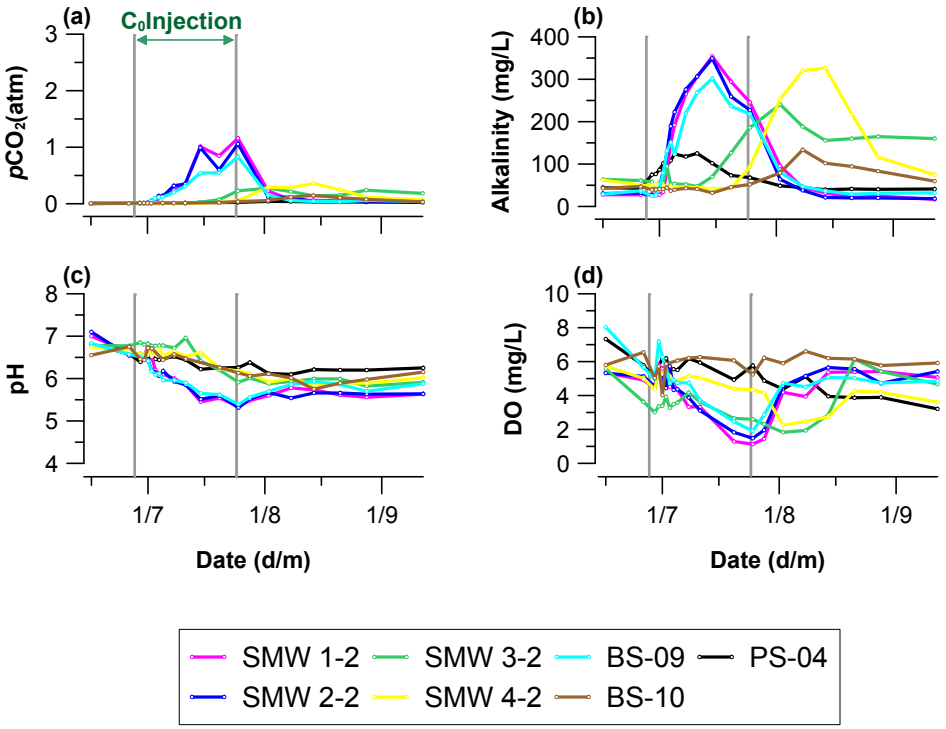

Figure 5. pCO_2, pH, alkalinity and DO values. The grey vertical lines represent the injection period.

During the water circulation period, pH exhibited an overall decreasing trend as the low-pH water was pumped out from the down-gradient well (BS-10) and reinjected into the up-gradient well (BS-04) (Figure 5c). DO also exhibited a decreasing trend as groundwater was re-equilibrated in the warm surface temperature (17.1–28.6°C) before being injected into the well BS-04 (Figure 4d). pCO_2 and alkalinity showed minor variation across the monitored region depending on the groundwater flow direction and the initial C parameter distributions (Figure 4a and b).

Mean He, Ar and Kr concentrations measured before the injection commenced were 5.43×10^{-8} cm^3 STP/g_{H2O}, 3.72×10^{-4} cm^3 STP/g_{H2O} and 9.80×10^{-8} cm^3 STP/g_{H2O}, respectively. These are close to the Air Saturated Water (ASW) value at the temperature condition (i.e. 13.3°C) of study site—such as 4.58×10^{-8} cm^3 STP/g_{H2O}, 3.58×10^{-4} cm^3 STP/g_{H2O} and 8.30×10^{-8} cm^3 STP/g_{H2O} for He, Ar and Kr values, respectively (Kipfer et al., 2002).

3.2 Injection fluid

The gas-infused groundwater was released into the IW from 27 June 2017 to 24 July 2017 (Figure 3). The CO_2–infused groundwater (C_0) collected from the 5 m^3 tank (Figure 2b) was initially below the saturation point (0.40 atm) for 11 days after the injection (29 June 2017 to 8 July 2017), and reached to the over-saturation state (> 2.3 atm) about 18 days after the injection on 15 July 2017 (Figure 5a). This CO_2 variation can be attributed to an accidentally reduced water flux going into the CO_2 tank, causing a decrease of the water level, resulting in altering of the C system balance in CO_2 tank. For the same reason, the pH and DO initially maintained 5.0 and 3.9 mg/L but showed a sudden decrease to 4.2 and 0.5 mg/L on the 15 July 2017. Water samples collected from the 1 m^3 tank (C_0) (Figure 2a) were analyzed for their He, Ar and Kr concentrations, and reported at 2.92×10^{-5} cm^3 STP/g_{H2O}, 2.26×10^{-2} cm^3 STP/g_{H2O} and 4.95×10^{-5} cm^3 STP/g_{H2O}, respectively. The noble gas concentrations lie between fully saturated and Air Saturated Water (ASW) levels, and thus they will remain dissolved in the groundwater system unless being exposed to low partial pressure conditions such as air bubbles or the vadose zone interface (i.e. water table) (Ju et al., 2019).

3.3 Post injection

3.3.1 P, T and EC

Pressure turbulence was observed in all monitoring wells prior to the initiation of CO_2 injection (Figure 4), which can be attributed to the change in water volume from 24.0 m^3/d to 18.5 m^3/d for preparing the gas-infused water of 5.5 m^3 (C_0) before CO_2 injection within the circulation system (see the section 2.2.2 Injection for detailed explanation). Minor changes in temperature were observed inside the Radius of Influence (ROI) zone of IW such as PS-04, BS-09, SMW 1 and SMW 2 (Figure 4c~j).

315 The temperature showed a gradual increase since the groundwater circulation initiated in which the
316 SMW 2-2 showed the highest increase of up to +7.0°C and followed by SMW1-2 (+5.5°C), SMW 3-2
317 (+4.0°C), BS-09 (+3.8°C) and the others (< +2.8°C) (Figure 4). The higher increase in the temperature
318 of BS-09 indicates a preferential flow gradient still exists in the study site even after the formation of
319 the induced pressure gradient (Figure 1a). In EC data, the most prominent signals were recorded at
320 SMW 1-2 (+464 µS/cm, +472%), SMW 2-2 (+447 µS/cm, +368%), SMW 2-3 (+531 µS/cm , +301%),
321 SMW 3-2 (+383 µS/cm, +250%) with the others showing a less pronounced change (< +129%). These
322 observations were consistent with temperature data, exhibiting the greatest change in the SMW #-2
323 wells. This indicated that the CO_2 plume moved horizontally from the injection depth of 21–24 m to the
324 screen depth of SMW #-2 (i.e., 20–22 m) (Figure 1c). The response in EC is clearly different to that of
325 temperature as a notable increase in EC was only observed after CO_2 injection occurred. This is because
326 EC is the function of geochemical interaction between the CO_2 water and the rock materials (Vialle et
327 al., 2014). In the groundwater flow regime, the SMW series wells, BS-09 and BS-10 are located ahead
328 of the migration direction of the IW, which is illustrated by the clearly increasing EC trend (Figure 1b).
329 Alternatively, well PS-04 is located upgradient from the CO_2 injection point, resulting in a gradual
330 lowering of the EC trend after the CO_2 injection was initiated as there is no communication between
331 this well and the CO_2 rich-water (Figure 1b).

332 **3.3.2 *p*CO_2, pH, alkalinity and DO**

333 As expected, the chemical elements exhibited strong signals correlating with the CO_2 plume
334 arrival. The parameters are presented as breakthrough curves (BTCs) (Figure 5). Note that for the
335 SMWs, the parameters represent the data from the injection depth (i.e., SMW #-2) only, as this
336 generated the largest signals among all depths. The *p*CO_2 produced the strongest signal at SMW 1-2
337 (+1.15 atm, +25,385%) which was followed by SMW 2-2 (+1.05 atm, +18,067%), BS-09 (+0.82 atm,
338 +12,631%), SWM 4-2 (+0.35 atm, +3,746%) and the other wells (< +2,923%) (Figure 5a). The
339 pronounced response of *p*CO_2 compared to other parameters is attributed to its low baseline
340 concentration (0.0–0.01 atm) (Risk et al., 2015). Alkalinity also showed significant increases with the
341 arrival of the injected CO_2, particularly in wells SMW 1-2 (+326.4 mg/L, +1,189%), SMW 2-2 (+318.0

342 mg/L, +1,017%), BS-09 (+269.2 mg/L, +821%), SMW 4-2 (+270.0 mg/L, +478%) with other wells
343 showing smaller, but measureable changes (< +286%) (Figure 5b). Alkalinity gradually increases with
344 the chemical interactions between the CO_2 plume and the aquifer materials similar to the EC. The small
345 differences in response to CO_2 injection between EC and alkalinity can be attributed to the geochemical
346 variation of the study site resulting in different CO_2 related buffering capacities (Sechriest, 1960).

347 The pH also decreased noticeably, changing by -1.5 units at SMW 2-2, which was followed by
348 -1.5 units at SMW 1-2, -1.4 units at SMW 2-3, -1.3 units at BS-09 and > -0.96 units at the others (Figure
349 5c). The DO showed relatively modest change by up to -4.0 mg/L (-78%) at SMW 1-2 which was
350 followed by BS-09 (-4.9 mg/L, -72%), SMW 2-2 (-3.7 mg/L, -72%), SMW 3-2 (-2.8 mg/L, -60%) and
351 the others (< -58%) (Figure 5d). In this experimental setting, the DO evolves with the three-component
352 groundwater mixing between low-DO water volumes (re-injection water at BS-04 and injection water
353 at IW) and high-DO water volume (local groundwater) (Figure 2).

354 **3.3.3 Noble gas tracers**

355 The measured concentrations of He, Ar and Kr tracers are presented in BTCs (Figure 6). The
356 concentration was normalized to the injection amount (C_0) after the background portion (i.e.
357 atmospheric origin) was subtracted from both monitored (C) and initial concentration (C_0), to simply
358 define the CO_2 arrival as a positive signal. Note that for the SMWs, the parameters present the data
359 from the injection depth (i.e., SMW #-2) only, as this exhibited the largest signals of all depths. As a
360 result, the tracers successfully produced the strong positive signals with the CO_2 plume arrival in the
361 BTCs (Figure 6). The tracer concentrations exhibited variable arrival times and concentrations due to
362 the CO_2 plume following different flow paths within the heterogeneous groundwater system at the site,
363 similar to the findings of Kilgallon et al. (2018), Lee et al. (2017), Lu et al. (2012) and Stalker et al.
364 (2015). Most importantly, Kr showed the earliest arrivals through all monitoring wells compared to the
365 He and Ar tracer. This was attributed to the Kr taking a less distributed pathway through the subsurface
366 than the other tracers, and a result of the dilution of CO_2 plume along the concentration gradient (see
367 the discussion section 4.1.2 Diffusion process controlling the efficiency of noble gas tracing).

The tracers associated with the CO_2 plume were firstly detected in SMW 2-2 (+4 d) followed by BS-09 (+4 d), SMW 1-2 (+5 d), SMW 3-2 (+18 d) and SMW 4-2 (+23 d) (Figure 6a, c, d, e and f). The strongest signal was recorded at SMW 2-2 (+1,430% for He, +322% for Ar and +6,904% for Kr) suggesting the majority of the CO_2 plume moved along the induced groundwater pressure gradient (Figure 6). A portion of the tracers also moved toward BS-09 and produced a strong signal in spite of being a greater distance away from the injection point (5.2 m) than that of SWM 1-1 and SMW 2-2 (2.6 m). This can be attributed to the preferential flow pathway present in the study site (Figure 1a) (Ju et al., 2019; Lu et al., 2012). Well PS-04 did not record the presence of any tracers during the injection period due to its location behind the IW in the groundwater flow direction (Figure 1b). It is worth noting that SMW 4-2 exhibited a higher concentration of Kr once the tracers arrived than SWM 3-2 (Figure 6), implying that a low conductivity zone hinders well SMW 3-2 from capturing the full CO_2 plume. This result was consistent with the observations made in alkalinity and pCO_2 (Figure 5).

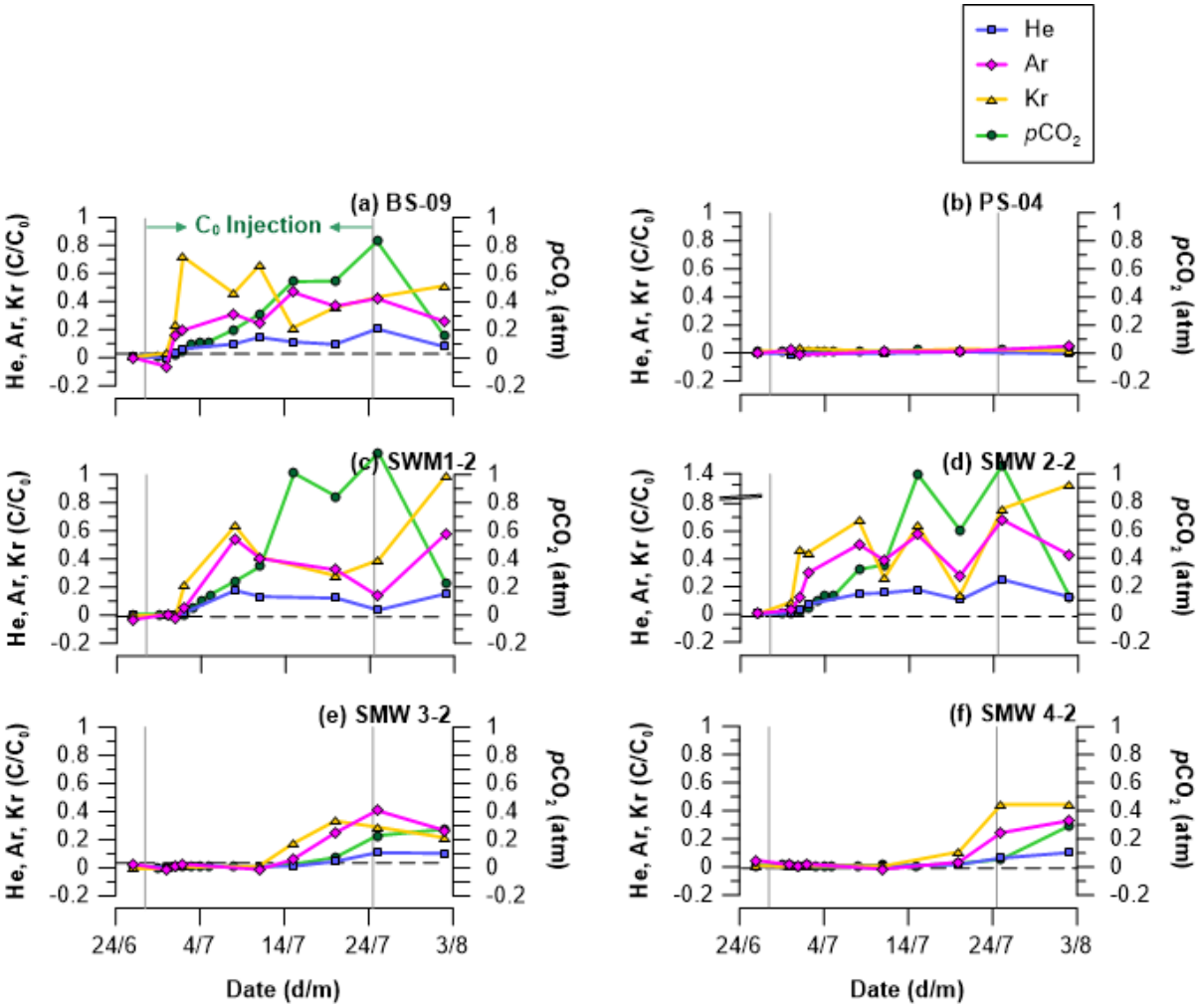

Figure 6. Gas tracer concentration during the experiment. Noble gas was presented as C/C_0 (see the text for details) with pCO_2. The grey vertical lines show the start and end of the injection period. The Air Saturated Water (ASW, black dotted horizontal line) was calculated according to Kipfer et al. (2002) to indicate the local background level of noble gas tracers.

As the injection water gradually approached the monitoring network, the observation wells captured the temporal evolution of the CO_2 plume. In the early stage of BTCs, Kr showed the fastest arrival time compared to the other tracers for all monitoring wells (Figure 6). This was followed by an increase in Ar and He concentrations, with both parameters soon reaching their peak concentration within a few days (Figure 6). In the final stage of BTCs, the plume tail is recorded in all of the monitoring wells through the decrease of noble gas concentrations after injection at the IW ceased. However, it can be observed that the concentration increased in the last stage of the BTCs for monitoring wells adjacent to IW (Figure 6c and d). This can be attributed to the circulation injection system of this

393 experiment. In the final stage of the injection period (4 days before the end of injection), the tracer-
394 charged plume had reached BS-10 (Figure 4b). As water was still being produced for the reinjection at
395 the IW, a portion of the CO_2 plume was returned back into the injection tank containing the artificial
396 noble gas tracers. Note that heavier components such as Ar and Kr acted as an early warning tracer for
397 CO_2 arrival in every monitoring well during the monitoring period. This was attributed to physical
398 mechanisms affecting the distribution of the dissolved gases (see the section 4.1.2 Diffusion process
399 controlling the efficiency of noble gas tracing).

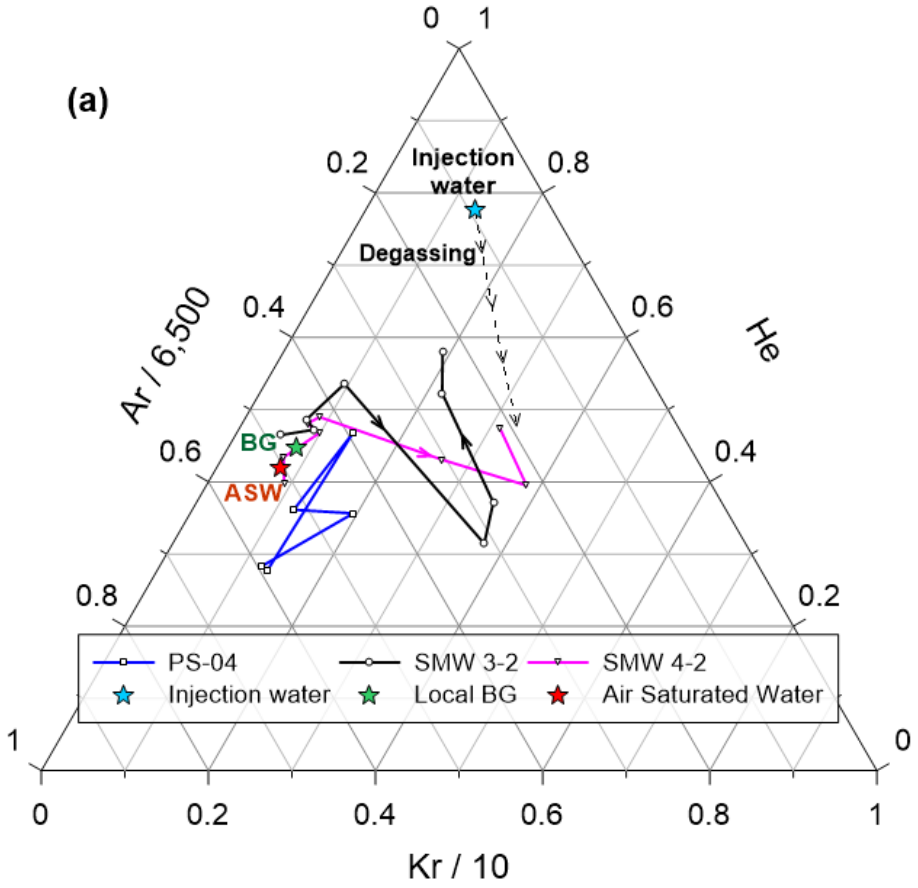
(a)
Injection water
Degassing
BG
ASW
Ar / 6,500
He
Kr / 10
PS-04
SMW 3-2
SMW 4-2
Injection water
Local BG
Air Saturated Water

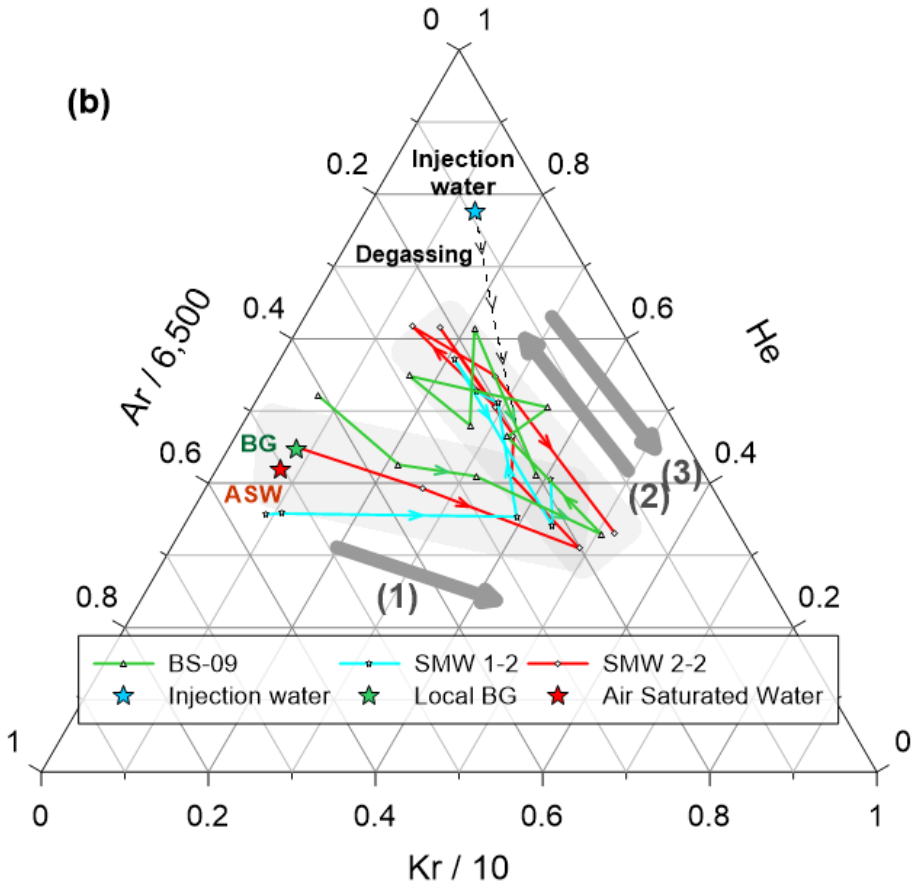
(b)
Injection water
Degassing
BG
ASW
(1)
(2)
(3)
Ar / 6,500
He
Kr / 10
BS-09
SMW 1-2
SMW 2-2
Injection water
Local BG
Air Saturated Water

400

401 **Figure 7.** Noble gas ternary diagram showing the two groups of wells categorized by their response.
402 (a) monitoring wells which showed no concentration change from background level (i.e., PS-04) or
403 only an early-stage evolution (i.e., SMW 3-2 and SMW 4-2). (b) monitoring wells that showed a three-
404 step evolution as located close to the injection point (i.e., SMW 1-2 and SMW 2-2) and located in a
405 preferential migration path (i.e., BS-09). The early-stage CO_2 plume is characterized by high Kr
406 concentration (Arrow 1), the plume then gradually increases in He and Ar concentrations (Arrow 2). In
407 the final stage, it becomes rich in Kr again, following the cessation of injection (Arrow 3). The peak
408 composition was different from that of injection water due to initial degassing loss.

409 The consistent temporal evolution of the recorded noble gas concentrations within the six
410 monitoring wells is depicted in the ternary diagram of Figure 7. The local BG (i.e., green star) represents
411 the average of background level of individual monitoring wells. Prior to the CO_2 plume arrival, each
412 monitoring well plots near to the Air Saturated Water (ASW) level. The initial arrival of the CO_2 plume
413 was marked by a significant increase in Kr in all monitoring wells (see the arrow 1 in Figure 7) which
414 corresponds to the early stage evolution in the BTCs (Figure 6). Note that PS-04 did not exhibit a
415 response after injection. Following the arrival of the Kr tracer, the He and Ar concentrations within the
416 monitoring wells increase as the plume center approached, converging at a single point (Figure 7).
417 However, the concentrations of noble gas tracers at the peak concentrations were lower than those at
418 the time of injection. They were 73.6–88.3% (He), 26.2–55.5% (Ar), and 0–65.5% (Kr) of the initial
419 concentrations. The lower concentrations can be attributed to the degassing loss of the injection fluid
420 (Sathaye et al., 2016), explained in more detail in the section 4.1.1. This degassing process controls the
421 overall retention amount of the injected CO_2. The composition of the plume tail captured in the
422 monitoring wells was similar to the composition of the plume front, characterized by a high Kr
423 concentration (Figure 7).

424 **3.4 Following injection**

425 CO_2 injection ceased after 28 days (27 June 2017 to 24 July 2017) (Figure 3). This corresponds
426 to the point where the monitoring parameters start to change at the BS-10 (Figure 4b and 5). In this

moment, the slight increase of EC was also observable in the CO_2 tank as CO_2 water re-entered the injection tank (Figure 4a). Additionally, PS-04 also showed a minor increase in EC at the termination period due to the re-circulation of CO_2 injected water (Figure 4d). From this point (24 July 2017), the groundwater circulation system was modified to avoid the re-enhancement of the CO_2 plume. Another local groundwater from BH-03 was prepared and from then onwards substituted the circulation portion going to the BS-04 (Figure 1e and 2c).

3.5 Following groundwater circulation

The groundwater circulation ended on 17 September 2017, 56 days after CO_2 injection stopped and 118 days after groundwater circulation commencement (Figure 3). The pressure turbulence was observable in all monitoring wells (Figure 4) and also EC turbulence was detected in some of the monitoring wells (Figure 4c, f and k), but the groundwater quickly recovered to its previous state (Figure 4).

4 Discussion

4.1 Mass retention mechanisms

4.1.1 Degassing process controlling the overall retention amount of released CO_2

If an inert tracer is continuously released into the groundwater system, the concentration will gradually increase in monitoring wells and eventually become similar to the composition of injection fluid. In this study, as the tracer-charged water was continuously released into the groundwater system, the monitored concentration was expected to resemble the injection fluid's concentration by the final stage. However, a notable difference in CO_2 and noble gas concentrations was observed between the injection fluid and the plateau points (Figure 7). This phenomenon indicates that tracer mass was not conserved in the groundwater system and suffered from mass-reducing processes. As the noble gas tracer is biochemically inert in the groundwater system, the decrease is likely to be the result of physical processes (Holland and Gilfillan, 2013). For instance, a similar noble gas deficit has been observed in a natural CO_2-rich system, where CO_2 and CH_4 bubbles also stripped out the insoluble gases from the groundwater system (Gilfillan et al., 2008, 2017; Brennwald et al., 2005; Zhou et al., 2005) and in

artificial CO_2 injection sites (Nimz and Hudson, 2005; Stalker et al., 2015). Hence, this deficit could be explained by the degassing of unstable CO_2-rich plume.

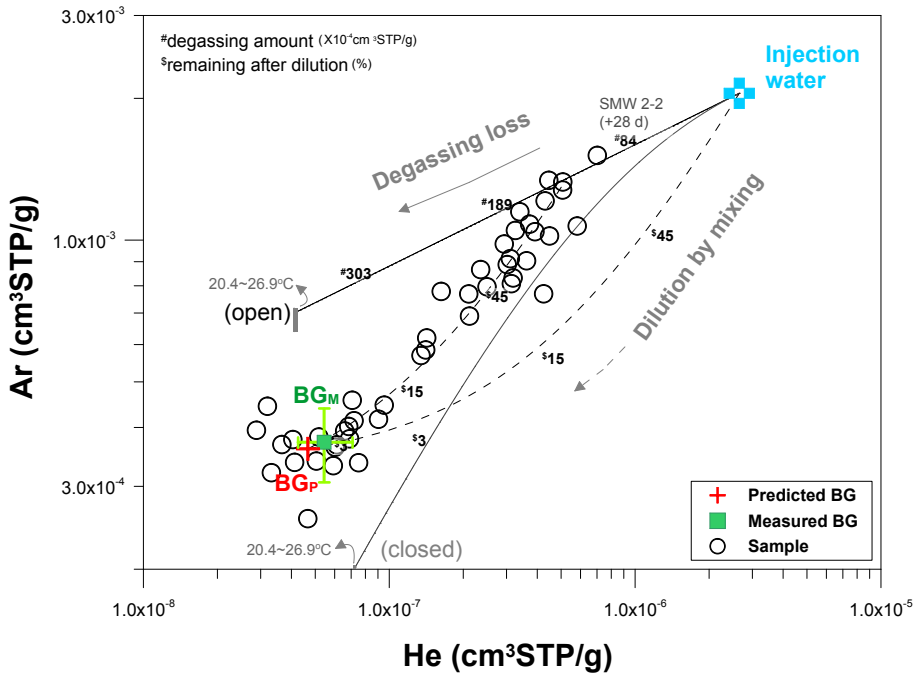

Figure 8. Mass balance of the CO_2 plume depicted with He and Ar tracer. The plume was expected to follow the mixing line between the injection water (blue cross symbol) and the measured background concentration (BG_M, green square symbol). Degassing loss of CO_2 from the dissolved CO_2 plume, would result in a new mixing line starting from the SMW 2-2 (+28 days) toward the background concentration (BG_P, red cross symbol). The BG_P was estimated based on the optimization process of the degassing model (see the Appendix B Model optimization for detailed explanation). The shaded zone on the degassing models indicates the uncertainty arising from the injection water temperature (20.4–26.9°C).

A diagram was constructed using noble gas tracers to determine the major processes influencing the CO_2 plume migration (Figure 8). In Figure 8, the concentrations of He and Ar at the well SMW 2-2 (on 25 July 2017) decreased gradually to their background concentration (BG_p), indicating mixing of the plume with the local groundwater. The mass distribution of observed samples was the function of two distinct processes over the testing period: mass reduction of the CO_2 plume occurred through the degassing process (black line), followed by the dilution of the plume by the local

groundwater (black dotted line). The observed data clearly indicated the mixing process was preceded by the degassing process.

Table 1 Mass balance of the leaked CO_2 plume in shallow aquifer system.

Open system	Injection		After degassing loss			Solubility †
	Amount (kg)	partial pressure (atm)	ΔAmount (kg)	Δpartial pressure (atm)	Remaining (%)	(mM/atm)
He	7.04×10^{-5}	3.07×10^{0}	5.64×10^{0}	2.46×10^{0}	19.9	0.386
Ar	5.43×10^{0}	6.11×10^{0}	1.85×10^{0}	2.08×10^{0}	66.0	1.50
Kr	2.50×10^{0}	7.41×10^{0}	5.13×10^{0}	1.52×10^{0}	79.5	2.71
$CO_{2\,p.}$ ‡	1.70×10^{2}	6.62×10^{0}	2.72×10^{0}	1.07×10^{0}	98.4	38.7

†NIST chemistry webbook of Sander (2017) at temperature of 21.8°C.

‡The predicted value from model optimization (see the Appendix B Model optimization for detailed explanation).

Elemental fractionation of noble gases is controlled by their differing solubilities and the ambient reservoir conditions (Figure 8) (Ballentine et al., 2002; Ma et al., 2009). In a closed system, the dissolved air remains in the groundwater, and equilibrium is achieved between the bubbles and the surrounding groundwater. In an open system, the air bubbles are mobile after the phase transition and escape from the aquifer system continuously until the end of the degassing process. In Figure 8, the mixing line (black dotted line) intersects a degassing line (black line) explaining the loss of air bubbles by 1.40×10^{-2} cm^3/g_{H2O} through the degassing process in an open system. The analytical technique for this calculation is shown in Appendix A Mass balance model. In the experiment, CO_2 degassing was detected just above the water table at the IW reconfirming the initial loss happened into the vadose zone (Supplementary Figure S2).

Unlike noble gases, CO_2 is involved in diverse chemical and biological processes in the groundwater. To identify the major controls on the CO_2 distribution, the pCO_2 was plotted against measured noble gas tracer concentrations in Figure 9. As expected, the total mass of CO_2 in the plume was decreased by degassing and mixing processes. Our data designate a clear mixing line stretching

from SMW 1-2 (25 July 2017) to BGp, indicating that mixing process mainly controlled the mass distribution of CO_2 in the plume after the initial degassing event. The minor variations from the mixing trend mostly fall in the ranges of the initial composition of injected CO_2-infused water (Figure 9). The solubility-controlled process is shown as the black arrow stretching from the blue-cross symbol to red-cross symbol (Figure 9). The abrupt change in He/Ar ratio stands in strong contrast to the minimal change observed in the pCO_2 during the degassing event (ca. 1.6% overall loss of CO_2). Losses of noble gases (20.5% for Kr, 34.0% for Ar, and 80.1% for He) are much greater than for CO_2 (Table 1).

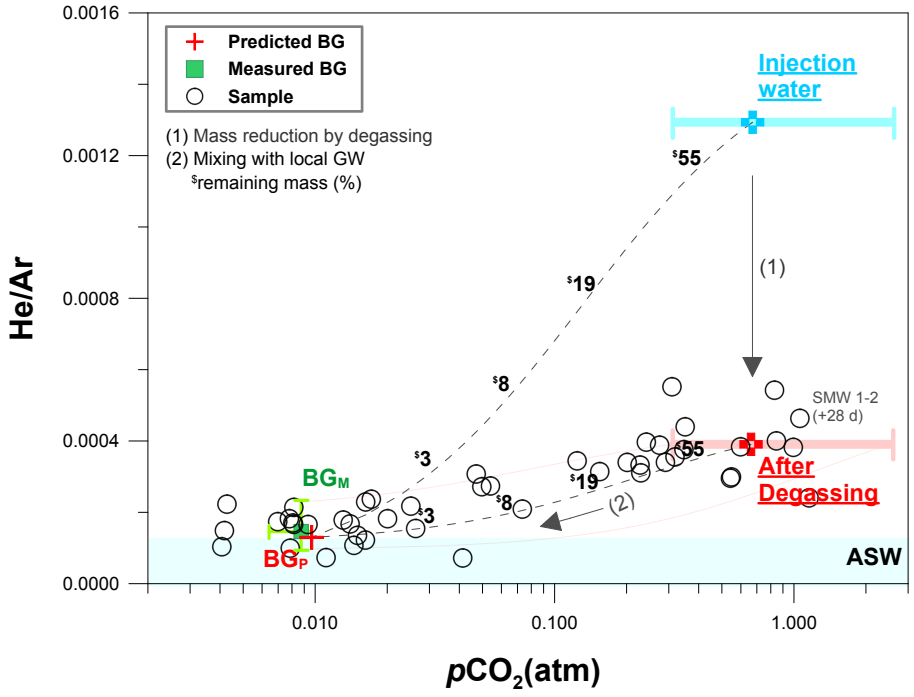

Figure 9. Plot of pCO_2 against He/Ar showing the concentration changes of CO_2 and noble gas tracers during CO_2 plume evolution. The BG_M (green square symbol) is the measured background level, and the BG_P (red cross symbol) is an estimated value from the optimization process of the degassing model (see the Appendix B Model optimization for detailed explanation). The CO_2 plume firstly reduces total mass by the degassing process (Arrow 1) and then gradually gets diluted by mixing with local groundwater (Arrow 2).

4.1.2 Diffusion process controlling the efficiency of noble gas tracing

The different noble gas species cover a wide mass range and thus may provide a chance to

506 constrain the mass-dependent processes occurring in the groundwater system. A comparison was made
507 to scrutinize the behavioral difference for noble gases, as observed from the He/Ar (Figure. 8) and
508 He/Kr (Figure 10) relationships. The mixing line in Figure 10, represented by a black dotted line
509 stretching from the degassing line to BGp, corresponds to the mixing line estimated in Figure 8.
510 However, it is noteworthy that the He and Kr pair did not exhibit a singular trend with many variations
511 scattering from the estimated mixing line. It is also noteworthy that samples from the plume's center
512 tend to converge on the estimated mixing line, while the samples from both the plume's front and tail
513 display a large scatter pattern over the estimated line (Figure 10). Such discordance was also observable
514 in the pCO_2 versus He/Kr diagram (Figure 11) in which many samples, especially those from the
515 plume's front and tail had significantly lower He/Kr ratios (around 0.10) than the ratio describing the
516 estimated mixing line (0.24). This difference indicates that another mass-dependent process was
517 affecting the tracer distribution in addition to the solubility-controlled process.

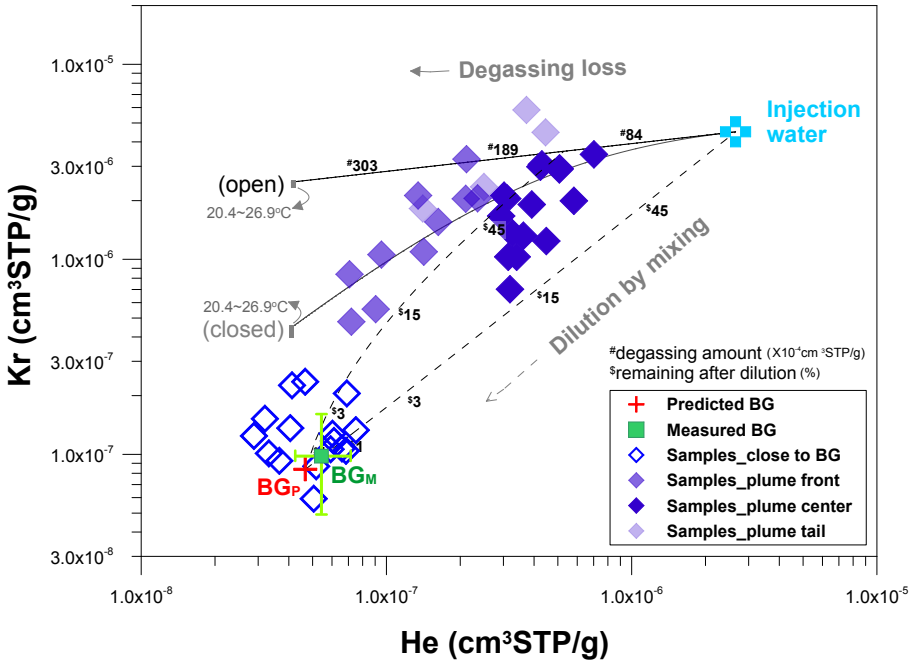

518

519 **Figure 10.** Mass balance of the CO_2 plume depicted with He and Kr tracers. To see the plume evolution
520 in detail, the samples were sorted by the breakthrough positions. Note that many samples, especially on
521 the plume front and tail, are scattered over the estimated mixing line, contrary to the He–Ar pair mixing
522 trend in Figure 8.

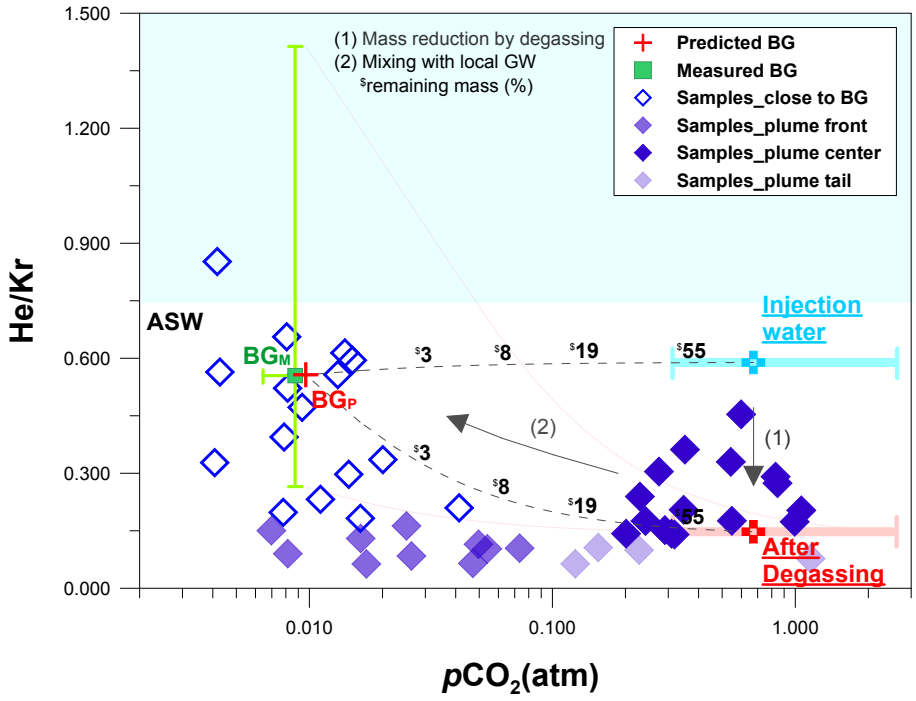

523

524 **Figure 11.** Diagrams showing the concentration changes of CO_2 and noble gas tracers during CO_2
525 plume evolution. To see the plume evolution in detail, the samples were sorted by the breakthrough
526 positions. Note that, many samples, especially on the plume's front and tail, are scattered from the
527 estimated mixing line, as compared to the observations in the pCO_2 versus He/Ar relationship in Figure
528 9.

529 To further examine the temporal progression of the CO_2 plume, ternary plots of pCO_2 He, and
530 Ar or Kr were composed according to the locations of samples in the plume (i.e., front, center, and tail)
531 (Figure 12). In the He/Ar/pCO_2 diagram, the samples have a small variation near BG_P in the initial
532 period, while as the plume center approached the monitoring points, it showed an upward shift toward
533 the degassing point in the Figure 12a. In the He/Kr/pCO_2 diagram, the samples show a much wider
534 variation during the initial stage of the CO_2 plume arrival than the observed change in the He/Ar/pCO_2
535 diagram (Figure 12b). This difference indicated that another physical process was involved in the mass
536 distribution at the CO_2 plume's front. Note that the initial composition of the plume was characterized
537 by the high concentration of Kr as it appeared firstly in the observation wells (see also Figure 7).

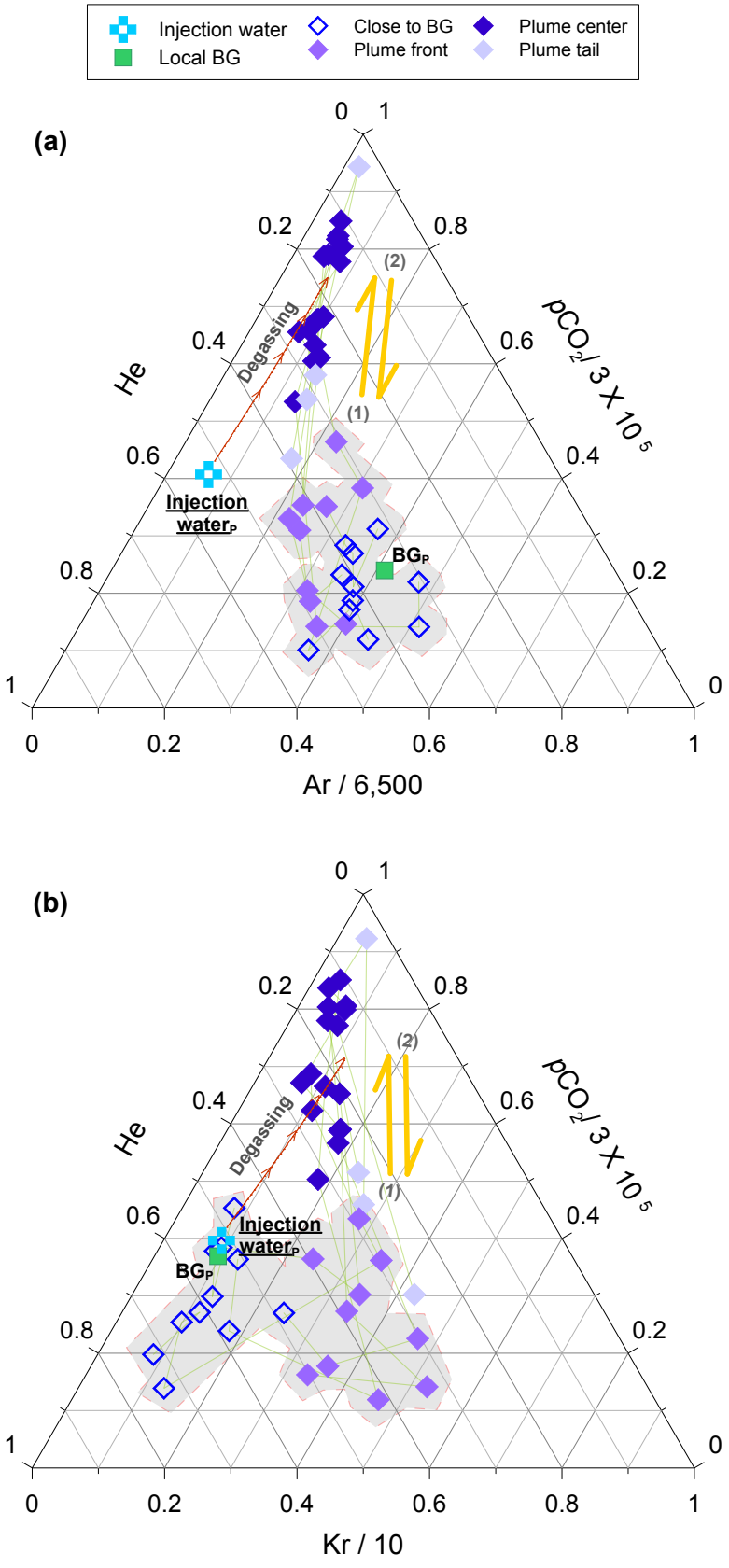
Injection water
Local BG
Close to BG
Plume front
Plume center
Plume tail
(a)
He
pCO2 / 3 X 10 5
Ar / 6,500
Degassing
(1)
(2)
Injection waterP
BGP
(b)
He
pCO2 / 3 X 10 5
Kr / 10
Degassing
(1)
(2)
Injection waterP
BGP

Figure 12. Ternary diagram showing the compositions of pCO_2, He, and Ar (a) or Kr (b) tracers. To scrutinize the plume evolution, the samples were sorted according to the breakthrough positions. In the initial period of plume evolution, the relative compositional change among pCO_2, He and Kr (b) showed a much wider variation near the background levels (BG_P, green square symbol) than that observed among pCO_2, He and Ar (a), which attributed to the diffusion process (see the text for details). This diffusion-dominant movement was followed by the upward shift toward the degassing point (see Arrow 1), as also shown by the intersection point in Figure 8. In the final stage, the samples return to the composition similar to the plume front (see Arrow 2), after cessation of injection.

In open water, diffusion is capable of elemental fractionation depending on the molecular mass (Zheng and Bennett, 2002). According to Fick's law, the mass distribution of a solute in a groundwater system is restricted by molecular diffusion along the concentration gradient. In our experimental design, the artificial injection formed a CO_2- and tracer-rich plume in the groundwater system, setting a steep concentration gradient at the plume boundary. Consequently, the plume boundary was actively subjected to the diffusion process facing with the local groundwater of low concentration level of noble gases. As the diffusion rate is inversely proportional to the elemental mass of the solute, the tracer composition at the plume boundary was regulated by the mass-dependent fractionation. This phenomenon also has been observed in a coal bed methane field, where the free CO_2 and CH_4 gases stripped off the insoluble noble gases from groundwater and this action set the concentration gradient at interfaces with the un-degassed local groundwater, at which diffusion process resulting in a mass dependent fractionation of noble gas tracers (Zhou et al., 2005). Overall, the fact that the diffusion allocates the mass distribution at plume boundary (i.e., plume's front and tail) suggests that the early detection of the migrated CO_2 plume is dependent on this process. This further implies that the early-stage degassing loss is of primary importance in terms of the noble gas tracing efficiency because the degassing process is associated with the overall plume composition including the feature of the concentration gradient at plume front.

5 Conclusions

A portion of CO_2 stored within the deep subsurface may unintentionally migrate upward to reach overlying shallow aquifers. Whilst noble gas tracers have proved to be useful in monitoring CO_2 leakage, they have been rarely adopted for monitoring purposes in the shallow aquifer system. This study utilized the noble gas tracers to indicate the CO_2 leakage and also to elucidate the mass balance of the leaked plume after injection of 1.70×10^2 kg of CO_2 into a shallow aquifer system. The CO_2- and tracer-enhanced groundwater was released into the induced gradient field and subsequent monitoring works have been conducted. The noble gas tracers produced a strong signal of the migrated CO_2, with Kr consistently exhibiting the first arrival time, ahead of the plume and the other noble gas tracers throughout all of the monitoring points.

The mass distribution of the CO_2 plume was controlled by three different physical processes; solubility-controlled (degassing), physical groundwater mixing and diffusion. The degassing process reduced the overall mass of the CO_2 plume and caused noble gas tracers to be mass-dependently fractionated, which occurred at the initial stage of CO_2 leakage before plume migration. The diffusion process was also involved during the plume migration, but only influenced the noble gas distributions in the leaked plume and did not act as a primary control for the CO_2 distribution within the monitoring period. This phenomenon, however, can accelerate the dilution of artificial tracers at the plume front, especially for the lighter elements, suggesting this process has an important control on the monitoring efficiency of the artificial tracers in terms of early detection of CO_2 leakage. Most importantly, as the noble gas tracers display more apparent changes according to the retention mechanisms than CO_2 itself, they can provide a robust system for precisely monitoring both the fate and pathway taken by the migrating CO_2.

Noble gas tracers were used to constrain the physical retention mechanisms of the injected CO_2 within a shallow aquifer. Our findings indicate that around the injection point, CO_2 degassing dominantly occurs from the dissolved plume due to the high gas pressure, suggesting a near-surface monitoring network is necessary for capturing the active “vertical” movement of degassed budget in this area. This can be accomplished by performing a continuous monitoring of CO_2 at the vadose zone,

for example by a soil flux measure, soil gas sampling and borehole head space sampling around a potential leak point. The monitoring regime can be performed cost-effectively with limiting a "degassing boundary" around a suspected leak point. In this study, only a few meters away from the leak point (>2.6 m), the degassing behavior was greatly diminished as a gas pressure of CO_2 plume reduced significantly. From this point, the CO_2 plume was stabilized as a dissolved phase and dominantly diluted by mixing with a local groundwater along a flow direction. Therefore, from this stage, sparse monitoring of saturated zone is recommended for tracing down a horizontal migration of a dissolved CO_2 plume, rather than an intensive gas monitoring for a degassed component. Hence, the key aspect to establish an effective monitoring network is how well constrained the "CO_2 degassing boundary" around a potential leak point is, and how well the groundwater flow regime is understood.

Monitoring of degassed CO_2 might not be easily achieved in a real CCS field using direct measurements. In this study, the degassing boundary was just a few meters from the leak point (< 2.6 m), whilst a strong artificial gradient (~0.18) was enforced for the plume migration. This suggests that a degassing boundary would be even narrower in a natural gradient system, making a direct detection of this extremely difficult. Furthermore, heterogeneity in the vadose zone can put an additional uncertainty in monitoring of the vertical flux, as gaseous CO_2 can take various pathways in the vadose zone depending on the soil permeability distribution (Cohen et al., 2013). Hence, identification of a point source of CO_2 leakage using a direct measurement technique in the vadose zone would be very difficult, unless an intensive monitoring is undertaken around the exact point source. However, noble gas monitoring of groundwater is able to record the migration of a CO_2 plume from the leak point along the groundwater flow pathway, as highlighted in this study. Our findings are similar to previous work (Mackintosh and Ballentine, 2012) that showed monitoring of noble gases in groundwater is an order of magnitude more sensitive for detecting migrated gases than vadose zone gas monitoring. Therefore, we recommend that monitoring of noble gases in groundwaters should be used in addition to direct vadose zone methods, in order to increase the sensitivity of the monitoring regime and improve the protection of the shallow groundwater aquifer above a storage site.

Acknowledgements

This research was supported by a Korea Environmental Industry & Technology Institute (KEITI) grant entitled “R&D Project on Environmental Management of Geologic CO2 Storage” (Project Number: 2018001810002), by a Korea Polar Research Institute grant (PE19060) and by a National Research Foundation of Korea (NRF) grant funded by the Korean government (MSIT) (No. 0409-20190119). We thank all the members of the K-COSEM team and, appreciate Intae Kim and Minjung Kim for their efforts and support on noble gas analysis. Also, we appreciate the help of Dr. Stan E. Beaubien in interpreting the noble gas data. Finally, the authors would like to thank two anonymous reviewers for their detailed comments and observations which greatly improved the present paper.

Appendix A. Mass balance model

At least, two noble gases of different solubility are necessary to determine the degassed mass as outlined in Ju et al. (2019). The closed system is a one-step phase-partitioning process, and therefore, the degassed amount can be determined just by repeatedly adjusting the gas/liquid ratio until the result ($(\frac{A}{B})_{(l)}$) fits into the measured data:

$$(\frac{A}{B})_{(g)} = (\frac{A}{B})_{(l)} \times \alpha$$

$$\alpha = \frac{\frac{r_A}{\emptyset_A}K_A}{\frac{r_B}{\emptyset_B}K_B}$$

Here:

$(\frac{A}{B})_{(g)}$ = A and B ratio in exsolved bubbles, where A and B are different noble gases

$(\frac{A}{B})_{(l)}$ = the composition of A and B remaining in the dissolved phase

α = partitioning coefficient for gas/liquid system

K_A, K_B = Henry's constant for A and B, from Sander et al., (2017)

r_A, r_B = dissolved-phase activity coefficients for A and B and

$\emptyset_A$, $\emptyset_B$ = gas-phase fugacity coefficients for A and B.

In open system, the CO_2 bubble ($V_{(g)}$) is continuously lost into vadose zone carrying the noble gas tracers with it from the groundwater system until the plume is stabilized. An iteration calculation can be undertaken to account for the continuous loss and which terminates when the resultant mass ($m^{i}_{(l)}$) fits the observed noble gas data:

$$m_A{}^{i}_{(l)} = m_A^{i-1}{}_{(l)} - m_A^{i-1}{}_{(g)}$$

$$m_B{}^{i}_{(l)} = m_B^{i-1}{}_{(l)} - m_B^{i-1}{}_{(g)}$$

Here:

i = Iteration step

$m^{i-1}{}_{(l)}$ = mass in dissolved phase before $i-1^{th}$ degassing loss (g)

$m^{i}{}_{(l)}$ = mass in dissolved phase after $i-1^{th}$ degassing loss (g)

$m^{i-1}{}_{(g)}$ = degassed mass during $i-1^{th}$ degassing process (g)

and degassed mass was determined from the degassed volume, such that:

$$m^{i-1}{}_{(g)} = C(V_{(g)} \times p^{i-1})$$

$$C = M/R \cdot T$$

$$p^{i-1} = \gamma\, K\, x^{i-1}/\Phi$$

$$x^{i-1} = 18\,[NG]^{i-1}\,(\rho_{(l)}\, V_{(l)})^{-1}$$

Here:

$V_{(g)}$ = degassed volume during $i-1^{th}$ degassing process (cc)

C = conversion factor from volume to mass

M = molar mass ($\mathrm{g/mol}$)

R = gas constant ($8.314\ \mathrm{cc \cdot atm/K/mol}$)

T = temperature (K)

p^{i-1} = partial pressure of removed noble gas during $i-1^{th}$ degassing process

K = Henry's constant in units of pressure (atm)

γ = liquid-phase activity coefficient

Φ = gas-phase fugacity coefficient

667 x^{i-1} = molar fraction of noble gas in dissolved phase at $i-1^{th}$ degassing moment ($mol_{NG}/mol_{(l)}$)

668 $[NG]^{i-1}$ = number of moles in dissolved phase at $i-1^{th}$ degassing moment (mol)

669 $\rho_{(l)}$ = density of dissolved phase (g/cm^3)

670 $V_{(l)}$ = volume of dissolved phase (cm^3)

671 For an open system, an iterative model was used with a fixed $V_{(g)}$ value which should be small enough
672 to finally achieve convergence with the measured noble gas composition. The noble gas concentration
673 in the groundwater was gradually decreased in iterative steps. In the final stage ($i = n$), $\frac{m_A{}^n_{(l)}}{m_B{}^n_{(l)}}$ was
674 matched against the monitored composition, and then the total degassed volume was calculated by
675 multiplication of the bubble size ($V_{(g)}$) and the number of iteration steps (i) in the open system model.

676 **Appendix B. Model optimization**

677 Model optimization can be achieved in a similar manner to that used by Ballentine (1997) and
678 Castro et al. (2009). The optimization aims to replicate the monitored noble gas data into a calculated
679 mixing line with the smallest misfit to the observed data. As the monitored concentration is defined by
680 mixing between two end-members, therefore, to achieve the minimum misfit, the end-members
681 constituting the predicted mixing line were repeatedly updated. There are two end-members for the
682 mixing line such as: 1) the noble gas concentration after the degassing event; and 2) the noble gas
683 concentration of the background concentration (Supplementary Figure S3). The first end-member is the
684 function of the initial amount and total degassed budget ($V_{(g)}$) of a species as discussed in the previous
685 section. The second end-member is the function of excess air intrusion level (A) to the Air Saturated
686 Water (ASW) (Mazor and Bosch, 1987; Kipfer et al., 2002). Hence, this optimization process allows
687 quantification of the degassing amount and the background level of leaked plume within the
688 groundwater system. The optimization process is given by:

689

690 $$\chi^2 = \sum_{i=1}^{N}\left[\left(\frac{NG1_i^m - NG1_i^p}{\sigma_{NG_{1,i}}}\right)^2 + \left(\frac{NG2_i^m - NG2_i^p}{\sigma_{NG_{2,i}}}\right)^2\right]$$

691 Here:

692 $i = i^{\text{th}}$ sample

693 N = the number of sample

694 σ = error of the observed data

695 $NG1^m$= measured value of noble gas sample

696 $NG1^p$= predicted value of noble gas sample from the arbitrary mixing line

697 This optimization process was conducted using a code compatible with the Matlab program.

698

699 **References**

700 Alcalde, J., Flude, S., Wilkinson, M., Johnson, G., Edlmann, K., Bond, C.E., Scott, V.,
701 Gilfillan, S.M.V., Ogaya, X., Haszeldine, R.S., 2018. Estimating geological CO_2 storage security to
702 deliver on climate mitigation. Nat. Commun. 9(1), 2201. https://doi.org/10.1038/s41467-018-04423-1.

703 Ballentine, C.J., 1997. Resolving the mantle He/Ne and crustal $^{21}Ne/^{22}Ne$ in well gases. Earth
704 Planet Sci. Lett. 152(1-4), 233–249. https://doi.org/10.1016/S0012-821X(97)00142-8.

705 Ballentine, C.J., Burgess, R., Marty, B., 2002. Tracing fluid origin, transport and interaction
706 in the crust. Rev. Mineral. Geochem. 47(1), 539–614.

707 Ballentine, C.J., O'nions, R.K., Oxburgh, E.R., Horvath, F., Deak, J., 1991. Rare gas
708 constraints on hydrocarbon accumulation, crustal degassing and groundwater flow in the Pannonian
709 Basin. Earth Planet Sci. Lett. 105(1-3), 229–246. https://doi.org/10.1016/0012-821X(91)90133-3.

710 Ballentine, C.J., Schoell, M., Coleman, D., Cain, B.A., 2001. 300-Myr-old magmatic CO_2 in
711 natural gas reservoirs of the west Texas Permian basin. Nature 409(6818), 327.
712 https://doi.org/10.1038/35053046.

713 Beaubien, S.E., Bigi, S., Lombardi, S., Sacco, P., and Tartarello, M.C., 2014. Groundwater
714 changes caused by flow through naturally occurring gas (±water) leakage points. 4th EAGE CO_2
715 Geological Storage Workshop 2014; Stavanger; Norway; April 22–24, 2014.

716 Beaubien, S.E., Jones, D.G., Gal, F., Barkwith, A.K.A.P., Braibant, G., Baubron, J.C., Ciotoli,
717 G., Graziani, S., Lister, T.R., Lombardi, S., Michel, K., Quattrocchi, F., Michel, K., 2013. Monitoring
718 of near-surface gas geochemistry at the Weyburn, Canada, CO_2-EOR site, 2001–2011. Int. J. Greenh.
719 Gas Control 16, 236–262. https://doi.org/10.1016/j.ijggc.2013.01.013.

720 Brennwald, M.S., Kipfer, R., Imboden, D.M., 2005. Release of gas bubbles from lake sediment
721 traced by noble gas isotopes in the sediment pore water. Earth Planet Sci. Lett. 235(1–2), 31–44.
722 https://doi.org/10.1016/j.epsl.2005.03.004.

723 Castro, M.C., Ma, L., Hall, C.M., 2009. A primordial, solar He–Ne signature in crustal fluids
724 of a stable continental region. Earth Planet Sci. Lett. 279(3–4), 174–184.
725 https://doi.org/10.1016/j.epsl.2008.12.042.

726 Cohen, G., Loisy, C., Laveuf, C., Le Roux, O., Delaplace, P., Magnier, C., Rouchon, V., Garcia,
727 B., Cerepi, A., 2013. The CO_2-Vadose project: Experimental study and modelling of CO_2 induced
728 leakage and tracers associated in the carbonate vadose zone. Int. J. Greenh. Gas Control 14, 128–140.
729 https://doi.org/10.1016/j.ijggc.2013.01.008.

730 Flude, S., Györe, D., Stuart, F.M., Zurakowska, M., Boyce, A.J., Haszeldine, R.S.,
731 Chalaturnyk, R., Gilfillan, S.M.V., 2017. The inherent tracer fingerprint of captured CO_2. Int. J. Greenh.
732 Gas Control 65, 40–54. https://doi.org/10.1016/j.ijggc.2017.08.010.

733 Flude, S., Johnson, G., Gilfillan, S.M., Haszeldine, R.S., 2016. Inherent tracers for carbon
734 capture and storage in sedimentary formations: composition and applications. Environ. Sci. Technol.
735 50(15), 7939–7955. https://doi.org/10.1021/acs.est.6b01548.

736 Gilfillan, S.M.V., Ballentine, C.J., Holland, G., Blagburn, D., Sherwood Lollar, B., Scott, S.,
737 Schoell, M., Cassidy, M., 2008. The noble gas geochemistry of natural CO_2 gas reservoirs from the
738 Colorado Plateau and Rocky Mountain provinces, USA. Geochim. Cosmochim. Acta 72, 1174–1198.
739 https://doi.org/10.1016/j.gca.2007.10.009.

740 Gilfillan, S.M.V., Haszeldine, S., Stuart, F., Gyore, D., Kilgallon, R., Wilkinson, M., 2014.
741 The application of noble gases and carbon stable isotopes in tracing the fate, migration and storage of
742 CO_2. Energy Procedia 63, 4123–4133. https://doi.org/10.1016/j.egypro.2014.11.443.

743 Gilfillan, S.M.V., Lollar, B.S., Holland, G., Blagburn, D., Stevens, S., Schoell, M., Cassidy,
744 M., Ding, Z., Zhou, Z., Lacrampe-Couloume, G., Ballentine, C.J., 2009. Solubility trapping in
745 formation water as dominant CO_2 sink in natural gas fields. Nature 458(7238), 614.
746 https://doi.org/10.1016/j.gca.2007.10.009.

747 Gilfillan, S.M.V., Sherk, G.W., Poreda, R.J., Haszeldine, R.S., 2017. Using noble gas

748 fingerprints at the Kerr Farm to assess CO_2 leakage allegations linked to the Weyburn-Midale CO_2
749 monitoring and storage project. Int. J. Greenh. Gas Control 63, 215–225.
750 https://doi.org/10.1016/j.ijggc.2017.05.015.

751 Gilfillan, S.M.V., Wilkinson, M., Haszeldine, R.S., Shipton, Z.K., Nelson, S.T., Poreda, R.J.,
752 2011. He and Ne as tracers of natural CO_2 migration up a fault from a deep reservoir. Int. J. Greenh.
753 Gas Control 5(6), 1507–1516. https://doi.org/10.1016/j.ijggc.2011.08.008.

754 Harvey, O.R., Qafoku, N.P., Cantrell, K.J., Lee, G., Amonette, J.E., Brown, C.F., 2012.
755 Geochemical implications of gas leakage associated with geologic CO_2 storage. Crit Rev. Environ. Sci.
756 Technol. 47(1), 23–36. https://doi.org/10.1021/es3029457.

757 Holland, G., Gilfillan, S., 2013. Application of noble gases to the viability of CO_2 storage. In
758 : Burnard, P. (Eds), The Noble Gases as Geochemical Tracers. Advances in Isotope Geochemistry,
759 Springer, Berlin, Heidelberg 177–223. https://doi.org/10.1007/978-3-642-28836-4_8.

760 Ide, S.T., Friedmann, S.J., Herzog, H.J., 2006. CO_2 leakage through existing wells: current
761 technology and regulations. In 8th International Conference on Greenhouse Gas Control Technologies,
762 19–22.

763 IEAGHG, 2011. Potential Impacts on Groundwater Resources of CO_2 Storage. IEAGHG,
764 Cheltenham, UK.

765 IPCC, 2005. Intergovernmental Panel on Climage Change. Special Report on CO_2 Capture
766 and Storage, edited, pp. 208–210.

767 Ju, Y., Beaubien, S.E., Lee, S.S., Kaown, D., Hahm, D., Lee, S., Park, I.W., Park, K., Yun,
768 S.T., Lee, K.K., 2019. Application of natural and artificial tracers to constrain CO_2 leakage and
769 degassing in the K-COSEM site, South Korea. Int. J. of Greenh. Gas Control 86, 211–225.
770 https://doi.org/10.1016/j.ijggc.2019.05.002.

771 Ju, Y., Kaown, D., Lee, K.K., 2018a. A three-pronged approach for identifying source and

extent of nitrate contamination in groundwater. J. Soil Water Conserv. 73(5), 493–503. https://doi.org/10.2489/jswc.73.5.493.

Ju, Y., Lee, S.S., Kaown, D., Lee, K.K., 2018b. Application of Inert Gas Tracers to Identify the Physical Processes Governing the Mass Balance Problem of Leaking CO_2 in Shallow Groundwater System. 14th Greenhouse Gas Control Technologies Conference; Melbourne; Australia; October 21–26. https://papers.ssrn.com/sol3/papers.cfm?abstract_id=3365686.

Kilgallon, R., Gilfillan, S.M.V., Edlmann, K., McDermott, C.I., Naylor, M., Haszeldine, R.S., 2018. Experimental determination of noble gases and SF_6, as tracers of CO_2 flow through porous sandstone. Chem. Geol. 480, 93–104. https://doi.org/10.1016/j.chemgeo.2017.09.022.

Kim, I., Hahm, D., Rhee, T.S., Kim, T.W., Kim, C.S., Lee, S., 2016. The distribution of glacial meltwater in the Amundsen Sea, Antarctica, revealed by dissolved helium and neon. J. Geophys. Res.: Oceans 121(3), 1654–1666. https://doi.org/10.1002/2015JC011211.

Kipfer, R., Aeschbach-Hertig, W., Peeters, F., Stute, M., 2002. Noble gases in lakes and ground waters. Rev. Mineral. Geochem. 47(1), 615–700. https://doi.org/10.2138/rmg.2002.47.14.

LaForce, T., Ennis-King, J., Boreham, C., Paterson, L., 2014. Residual CO_2 saturation estimate using noble gas tracers in a single-well field test: the CO2CRC Otway project. Int. J. Greenh. Gas Control 26, 9–21. https://doi.org/10.1016/j.ijggc.2014.04.009.

Lee, K.K., Lee, S.H., Yun, S.T., Jeen, S.W., 2016. Shallow groundwater system monitoring on controlled CO_2 release sites: a review on field experimental methods and efforts for CO_2 leakage detection. Geosci. J. 20(4), 569–583. https://doi.org/10.1007/s12303-015-0060-z.

Lee, S.S., Ju, Y., HA, S.W., Joun, W.T., Jun, S.C., Yun, S.T., Lee, K.K., 2018. Controlled CO_2 Injection into a Shallow Aquifer and Leakage Detection Monitoring by Two Different Leakage Events at the K-Cosem Site, Korea. In 14th Greenhouse Gas Control Technologies Conference Melbourne; Australia; October 21–26. https://papers.ssrn.com/sol3/papers.cfm?abstract_id=3366360.

796 Lee, S.S., Kim, H.H., Joun, W.T., Lee, K.K., 2017. Design and and Construction of
797 Groundwater Monitoring Network at Shallow-depth CO_2 Injection and Leak Test Site, Korea. Energy
798 Procedia 114, 3060–3069. https://doi.org/10.1016/j.egypro.2017.03.1434.

799 Lemieux, J.M., 2011. The potential impact of underground geological storage of carbon
800 dioxide in deep saline aquifers on shallow groundwater resources. Hydrogeol J. 19(4), 757–778.
801 https://doi.org/10.1007/s10040-011-0715-4.

802 Lions, J., Devau, N., De Lary, L., Dupraz, S., Parmentier, M., Gombert, P., Dictor, M.C., 2014.
803 Potential impacts of leakage from CO_2 geological storage on geochemical processes controlling fresh
804 groundwater quality: a review. Int. J. Greenh. Gas Control 22, 165–175.
805 https://doi.org/10.1016/j.ijggc.2013.12.019.

806 Lollar, B.S., Ballentine, C.J., Onions, R.K., 1997. The fate of mantle-derived carbon in a
807 continental sedimentary basin: integration of C/He relationships and stable isotope signatures. Geochim.
808 Cosmochim. Acta 61(11), 2295–2307. https://doi.org/10.1016/S0016-7037(97)00083-5.

809 Lott, D.E., Jenkins, W.J., 1998. Advances in analysis and shipboard processing of tritium and
810 helium samples. International WOCE Newsletter, 30, 27–30.

811 Lu, J., Cook, P.J., Hosseini, S.A., Yang, C., Romanak, K.D., Zhang, T., Freifeld, B.M., Smyth,
812 R.C., Zeng, H., Hovorka, S.D., 2012. Complex fluid flow revealed by monitoring CO_2 injection in a
813 fluvial formation. J. Geophys. Res. Solid Earth 117. https://doi.org/10.1029/2011JB008939.

814 Ma, L., Castro, M.C., Hall, C.M., 2009. Atmospheric noble gas signatures in deep Michigan
815 Basin brines as indicators of a past thermal event. Earth Planet Sci. Lett. 277(1–2), 137–147.
816 https://doi.org/10.1016/j.epsl.2008.10.015.

817 Mackintosh, S.J., Ballentine, C.J., 2012. Using $^{3}He/^{4}He$ isotope ratios to identify the source of
818 deep reservoir contributions to shallow fluids and soil gas. Chem. Geol. 304–305, 142–150.
819 https://doi.org/10.1016/j.chemgeo.2012.02.006.

820 Mazor, E., Bosch, A., 1987. Noble gases in formation fluids from deep sedimentary basins: a

821 review. Appl. Geochem. 2(5–6), 621–627. https://doi.org/10.1016/0883-2927(87)90014-X.

822 Myers, M., Stalker, L., Pejcic, B., Ross, A., 2013. Tracers–Past, present and future applications
823 in CO_2 geosequestration. Appl. Geochem. 30, 125–135.
824 https://doi.org/10.1016/j.apgeochem.2012.06.001.

825 Nimz, G.J., Hudson, G.B., 2005. The use of noble gas isotopes for monitoring leakage of
826 geologically stored CO_2. In: Thomas, D., Benson, S. (Eds.), Carbon Dioxide Capture for Storage in
827 Deep Geologic Formations vol. 2. Elsevier Press, Amsterdam 1113–1130.

828 Parkhurst, D.L., Appelo, C.A.J., 2013. Description of input and examples for PHREEQC
829 version 3: a computer program for speciation, batch-reaction, one-dimensional transport, and inverse
830 geochemical calculations (No. 6-A43). US Geological Survey. https://doi.org/10.3133/tm6A43.

831 Pinti, D.L., Marty, B., 1995. Noble gases in crude oils from the Paris Basin, France:
832 Implications for the origin of fluids and constraints on oil-water-gas interactions. Geochim. Cosmochim.
833 Acta 59(16), 3389–3404. https://doi.org/10.1016/0016-7037(95)00213-J.

834 Rillard, J., Loisy, C., Le Roux, O., Cerepi, A., Garcia, B., Noirez, S., Rouchon, V., Delaplaceb,
835 P., Willequet, O., Bertrand, C., 2015. The DEMO-CO_2 project: A vadose zone CO_2 and tracer leakage
836 field experiment. Int. J. Greenh. Gas Control 39, 302–317. https://doi.org/10.1016/j.ijggc.2015.04.012.

837 Risk, D., Lavoie, M., Nickerson, N., 2015. Using the Kerr investigations at Weyburn to screen
838 geochemical tracers for near-surface detection and attribution of leakage at CCS/EOR sites. Int. J.
839 Greenh. Gas Control 35, 13–17. https://doi.org/10.1016/j.ijggc.2015.01.019.

840 Sander, R., 2017. Henry's Law Constants. In: Linstrom, P.J., Mallard, W.G. (Eds.), NIST
841 Chemistry WebBook, NIST Standard Reference Database Number 69. National Institute of Standards
842 and Technology, Gaithersburg MD, 20899. https://doi.org/10.18434/T4D303.

843 Sathaye, K.J., Larson, T.E., Hesse, M.A., 2016. Noble gas fractionation during subsurface gas
844 migration. Earth Planet Sci. Lett. 450, 1–9. https://doi.org/10.1016/j.epsl.2016.05.034.

Sechriest, R.E., 1960. Relationship between total alkalinity, conductivity, original pH, and buffer action of natural water. OHIO J. SCI. 60(5), 303.

Stalker, L., Boreham, C., Underschultz, J., Freifeld, B., Perkins, E., Schacht, U., Sharma, S., 2009. Geochemical monitoring at the CO2CRC Otway Project: tracer injection and reservoir fluid acquisition. Energy Procedia 1(1), 2119–2125. https://doi.org/10.1016/j.egypro.2009.01.276.

Stalker, L., Boreham, C., Underschultz, J., Freifeld, B., Perkins, E., Schacht, U., Sharma, S., 2015. Application of tracers to measure, monitor and verify breakthrough of sequestered CO_2 at the CO2CRC Otway Project, Victoria, Australia. Chem. Geol. 399, 2–19. https://doi.org/10.1016/j.chemgeo.2014.12.006.

Stanley, R.H., Jenkins, W.J., Lott, D.E., Doney, S.C., 2009. Noble gas constraints on air-sea gas exchange and bubble fluxes. J. Geophys. Res.: Oceans 114(C11). https://doi.org/10.1029/2009JC005396.

Vialle, S., Contraires, S., Zinzsner, B., Clavaud, J.B., Mahiouz, K., Zuddas, P., Zamora, M., 2014. Percolation of CO_2-rich fluids in a limestone sample: Evolution of hydraulic, electrical, chemical, and structural properties. J. Geophys. Res. Solid Earth 119(4), 2828–2847. https://doi.org/10.1002/2013JB010656.

Zheng, C., Bennett, G.D., 2002. Applied contaminant transport modeling. Wiley-Interscience, New York.

Zhou, Z., Ballentine, C.J., Kipfer, R., Schoell, M., Thibodeaux, S., 2005. Noble gas tracing of groundwater/coalbed methane interaction in the San Juan Basin, USA. Geochim. Cosmochim. Acta 69(23), 5413–5428. https://doi.org/10.1016/j.gca.2005.06.027.

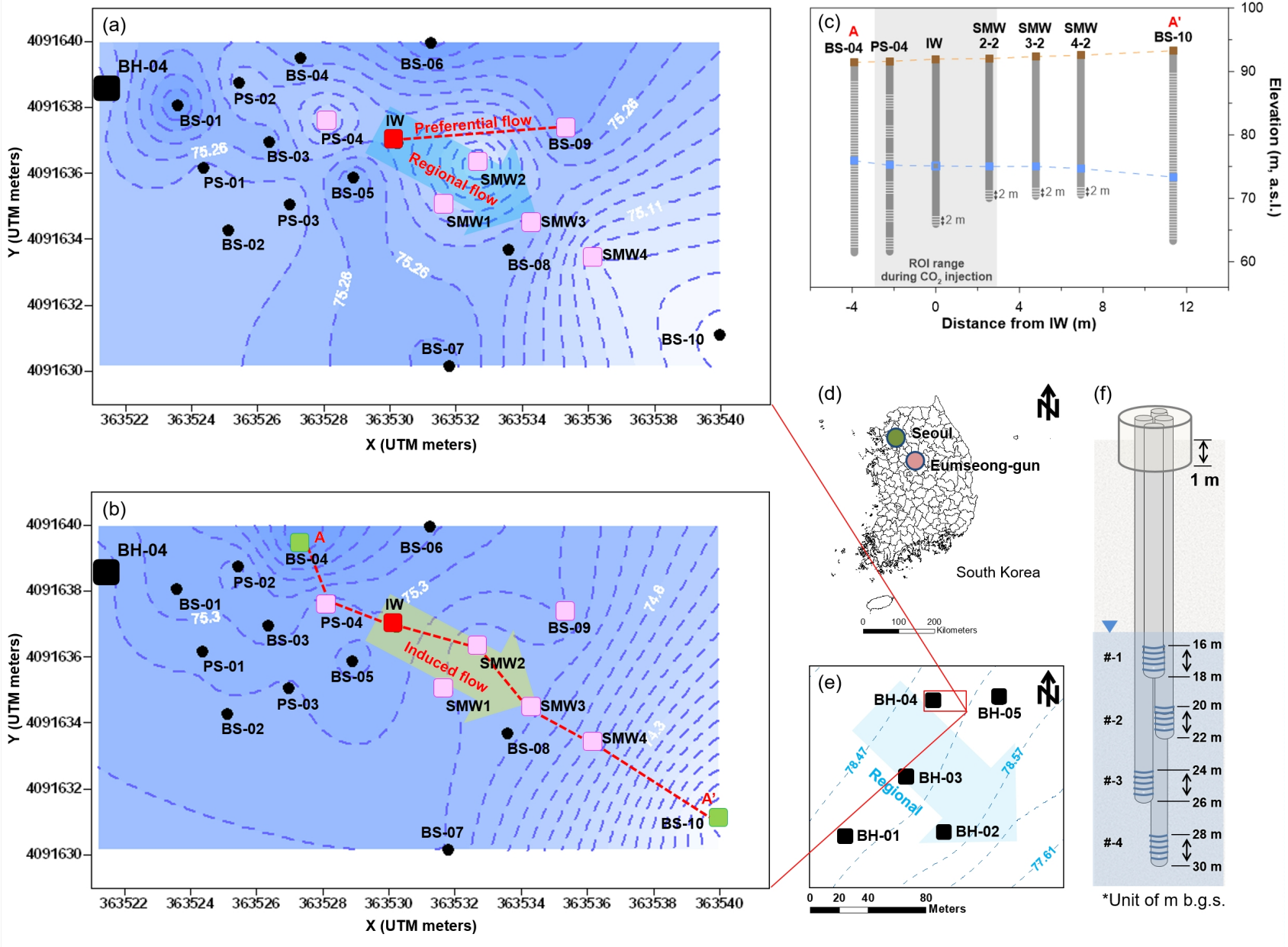
(a)
BH-04
BS-04
BS-06
PS-02
BS-01
IW
Preferential flow
PS-04
BS-09
BS-03
Regional flow
SMW2
PS-01
BS-05
SMW1
SMW3
PS-03
BS-02
SMW4
BS-08
BS-07
BS-10
75.26
75.28
75.11
Y (UTM meters)
X (UTM meters)
4091640
4091638
4091636
4091634
4091632
4091630
363522
363524
363526
363528
363530
363532
363534
363536
363538
363540
(b)
A
A'
Induced flow
75.3
74.8
(c)
SMW 2-2
SMW 3-2
SMW 4-2
2 m
ROI range during CO2 injection
Distance from IW (m)
Elevation (m, a.s.l.)
100
90
80
70
60
-4
0
4
8
12
(d)
Seoul
Eumseong-gun
South Korea
Kilometers
(e)
BH-05
BH-03
BH-01
BH-02
Regional
78.47
78.57
77.61
Meters
(f)
1 m
#-1
#-2
#-3
#-4
16 m
18 m
20 m
22 m
24 m
26 m
28 m
30 m
*Unit of m b.g.s.

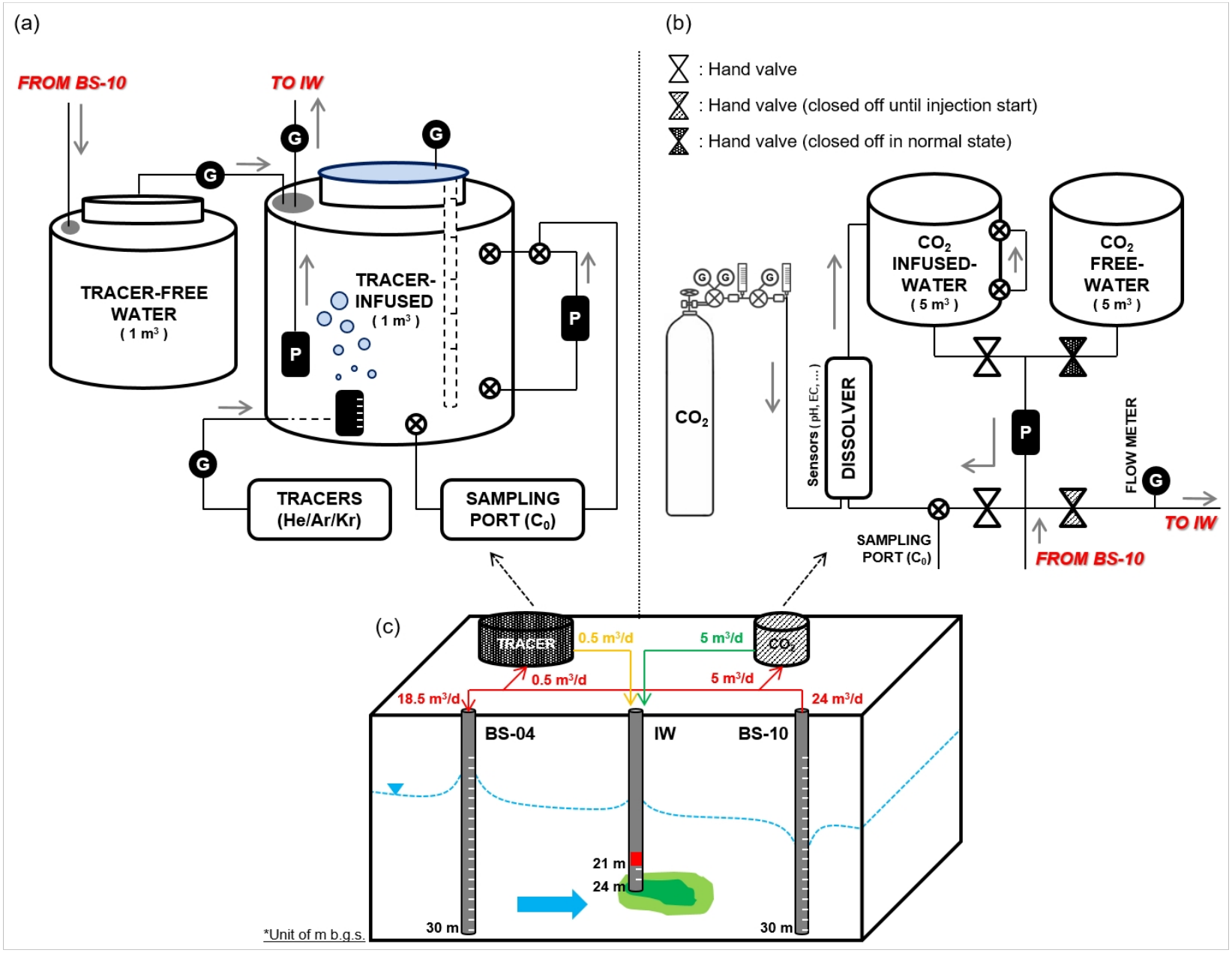
(a)
FROM BS-10
TO IW
G
P
TRACER-FREE WATER
(1 m³)
TRACER-INFUSED
(1 m³)
TRACERS (He/Ar/Kr)
SAMPLING PORT (C_0)
(b)
: Hand valve
: Hand valve (closed off until injection start)
: Hand valve (closed off in normal state)
CO_2
CO_2 INFUSED-WATER (5 m³)
CO_2 FREE-WATER (5 m³)
Sensors (pH, EC, ...)
DISSOLVER
FLOW METER
TO IW
FROM BS-10
SAMPLING PORT (C_0)
(c)
TRACER
CO_2
0.5 m³/d
5 m³/d
18.5 m³/d
24 m³/d
BS-04
IW
BS-10
21 m
24 m
30 m
*Unit of m b.g.s.

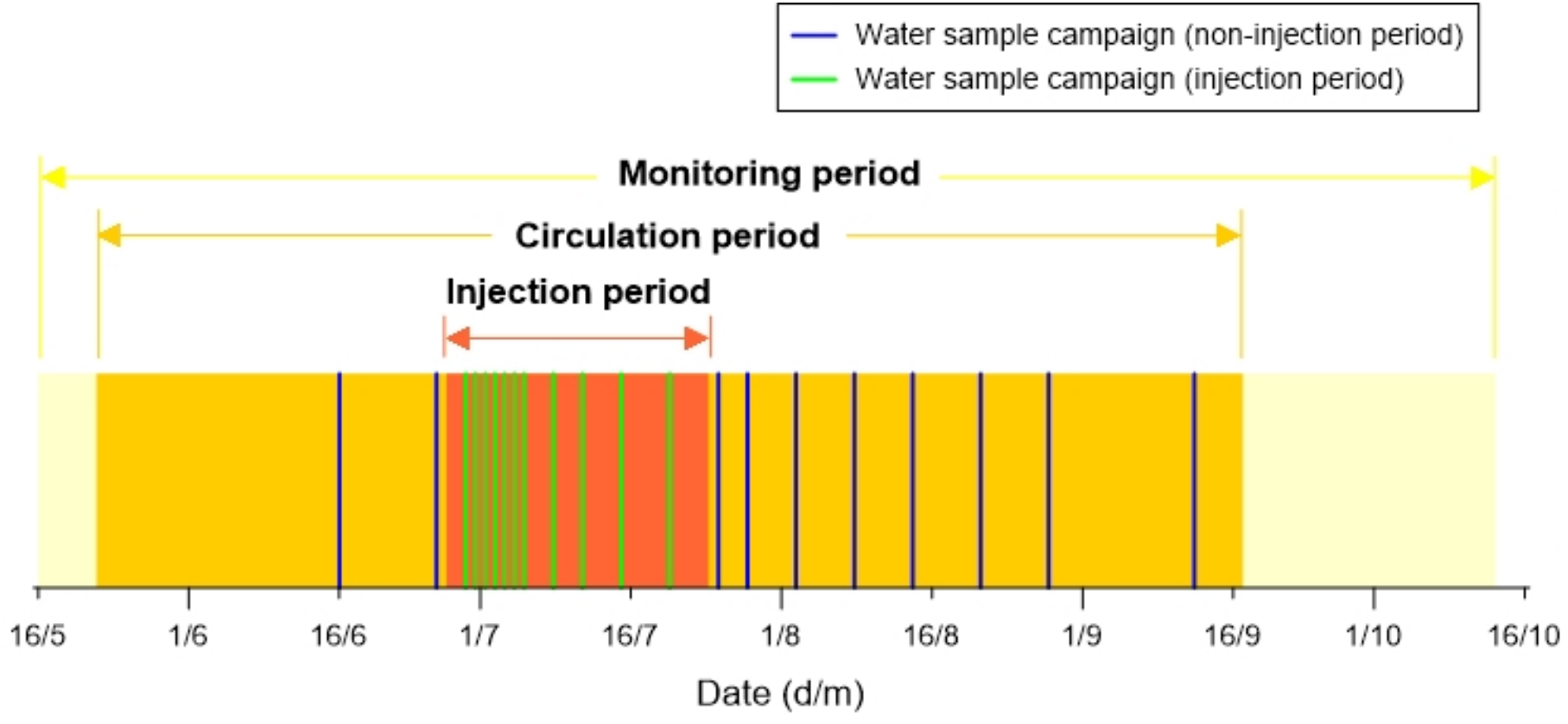
Water sample campaign (non-injection period)
Water sample campaign (injection period)
Monitoring period
Circulation period
Injection period
16/5
1/6
16/6
1/7
16/7
1/8
16/8
1/9
16/9
1/10
16/10
Date (d/m)

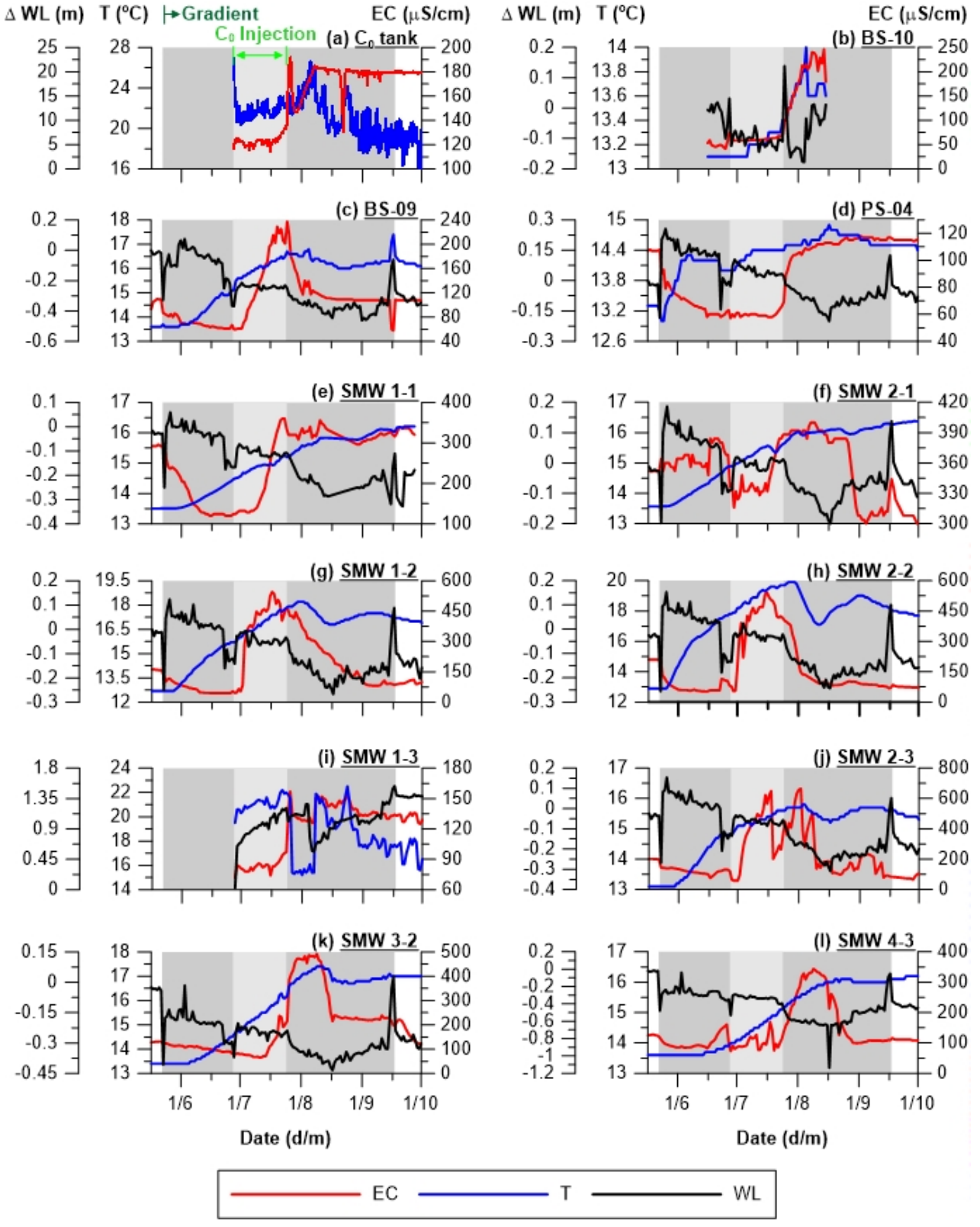
Δ WL (m)
T (°C)
Gradient
EC (μS/cm)
C0 Injection
(a) C0 tank
(b) BS-10
(c) BS-09
(d) PS-04
(e) SMW 1-1
(f) SMW 2-1
(g) SMW 1-2
(h) SMW 2-2
(i) SMW 1-3
(j) SMW 2-3
(k) SMW 3-2
(l) SMW 4-3
1/6
1/7
1/8
1/9
1/10
Date (d/m)
EC
T
WL

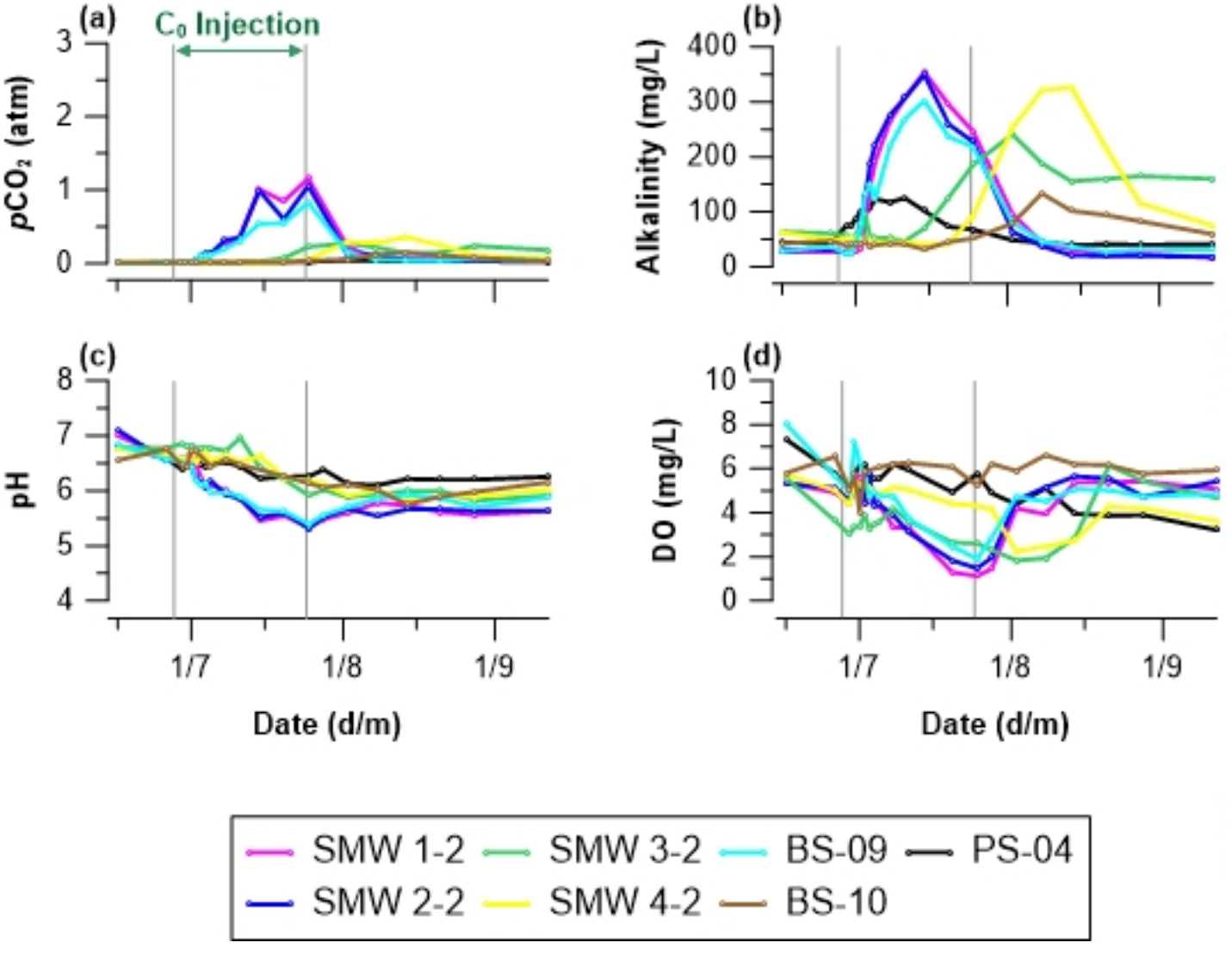
(a)
C₀ Injection
pCO₂ (atm)
3
2
1
0
(b)
Alkalinity (mg/L)
400
300
200
100
0
(c)
pH
8
7
6
5
4
(d)
DO (mg/L)
10
8
6
4
2
0
1/7
1/8
1/9
Date (d/m)
1/7
1/8
1/9
Date (d/m)
SMW 1-2
SMW 2-2
SMW 3-2
SMW 4-2
BS-09
BS-10
PS-04

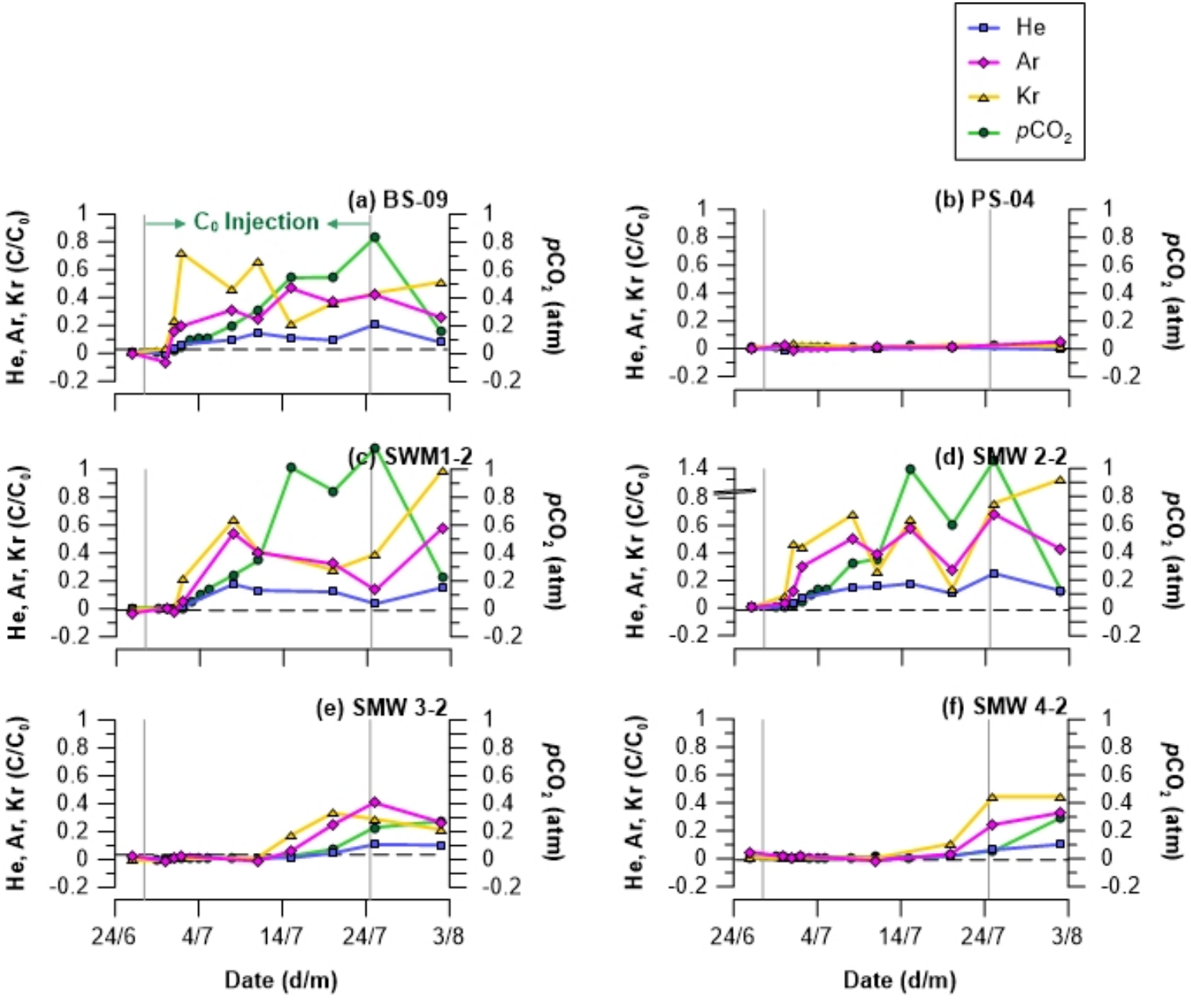
He
Ar
Kr
pCO2
(a) BS-09
C0 Injection
(b) PS-04
(c) SWM1-2
(d) SMW 2-2
(e) SMW 3-2
(f) SMW 4-2
He, Ar, Kr (C/C0)
pCO2 (atm)
24/6
4/7
14/7
24/7
3/8
Date (d/m)

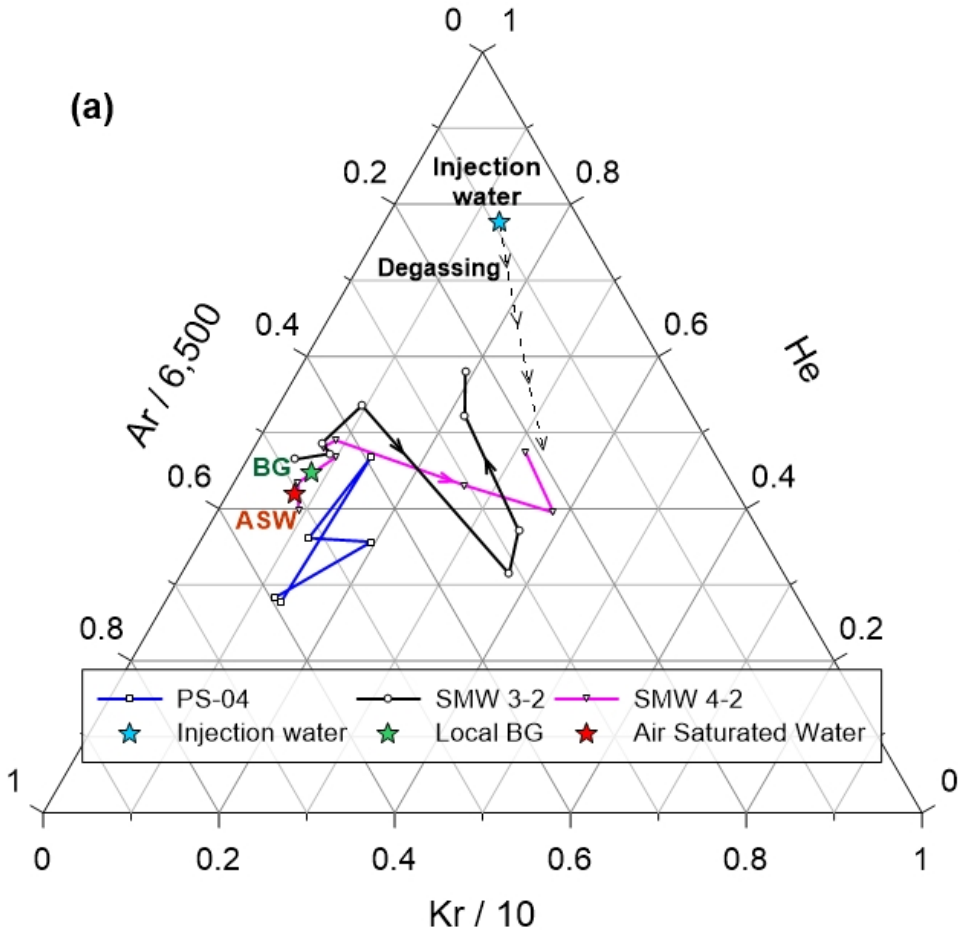
(a)
Injection water
Degassing
BG
ASW
Ar / 6,500
He
Kr / 10
PS-04
SMW 3-2
SMW 4-2
Injection water
Local BG
Air Saturated Water

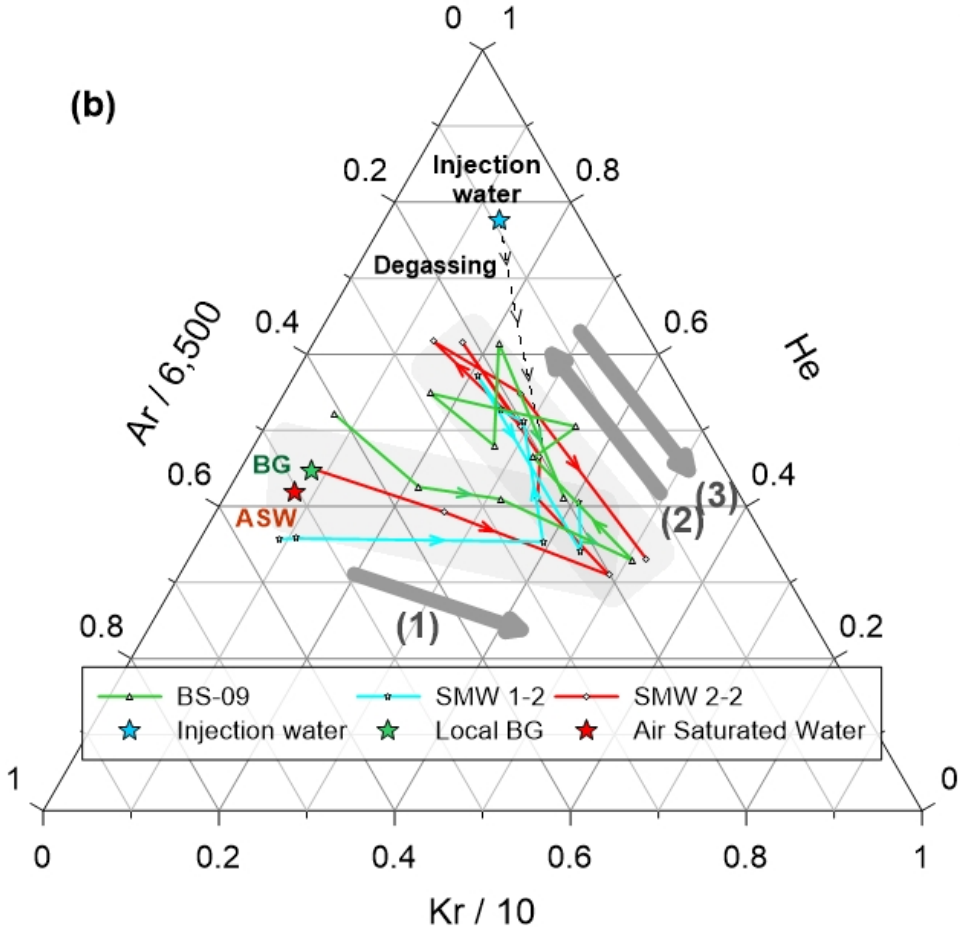
(b)
Injection water
Degassing
BG
ASW
(1)
(2)
(3)
Ar / 6,500
He
Kr / 10
BS-09
SMW 1-2
SMW 2-2
Injection water
Local BG
Air Saturated Water

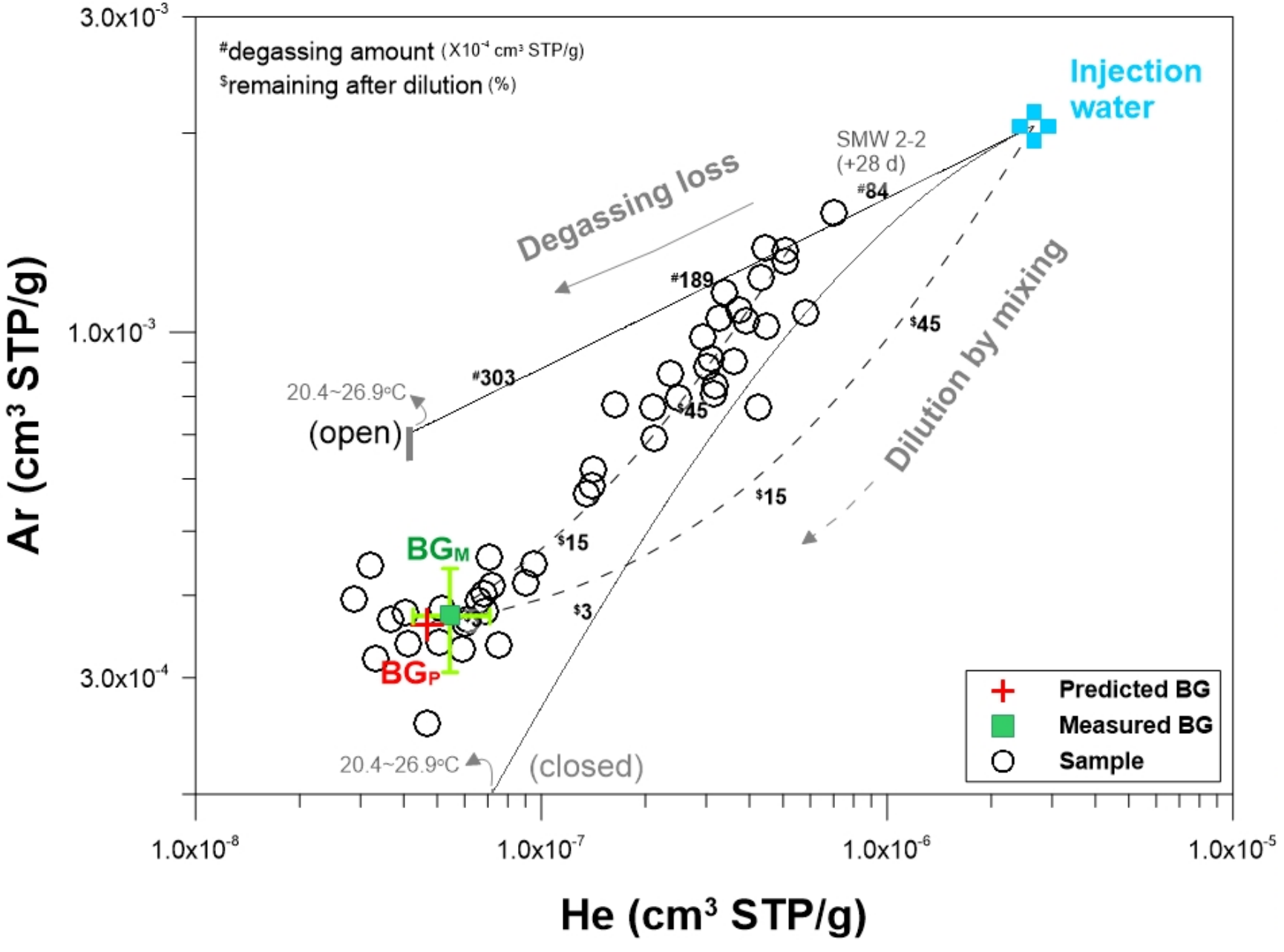
#degassing amount (X10⁻⁴ cm³ STP/g)
$remaining after dilution (%)
Injection water
SMW 2-2 (+28 d)
#84
#189
#303
Degassing loss
Dilution by mixing
$45
$15
$3
20.4~26.9°C
(open)
20.4~26.9°C
(closed)
BGM
BGP
Predicted BG
Measured BG
Sample
3.0x10-3
1.0x10-3
3.0x10-4
1.0x10-8
1.0x10-7
1.0x10-6
1.0x10-5
Ar (cm³ STP/g)
He (cm³ STP/g)

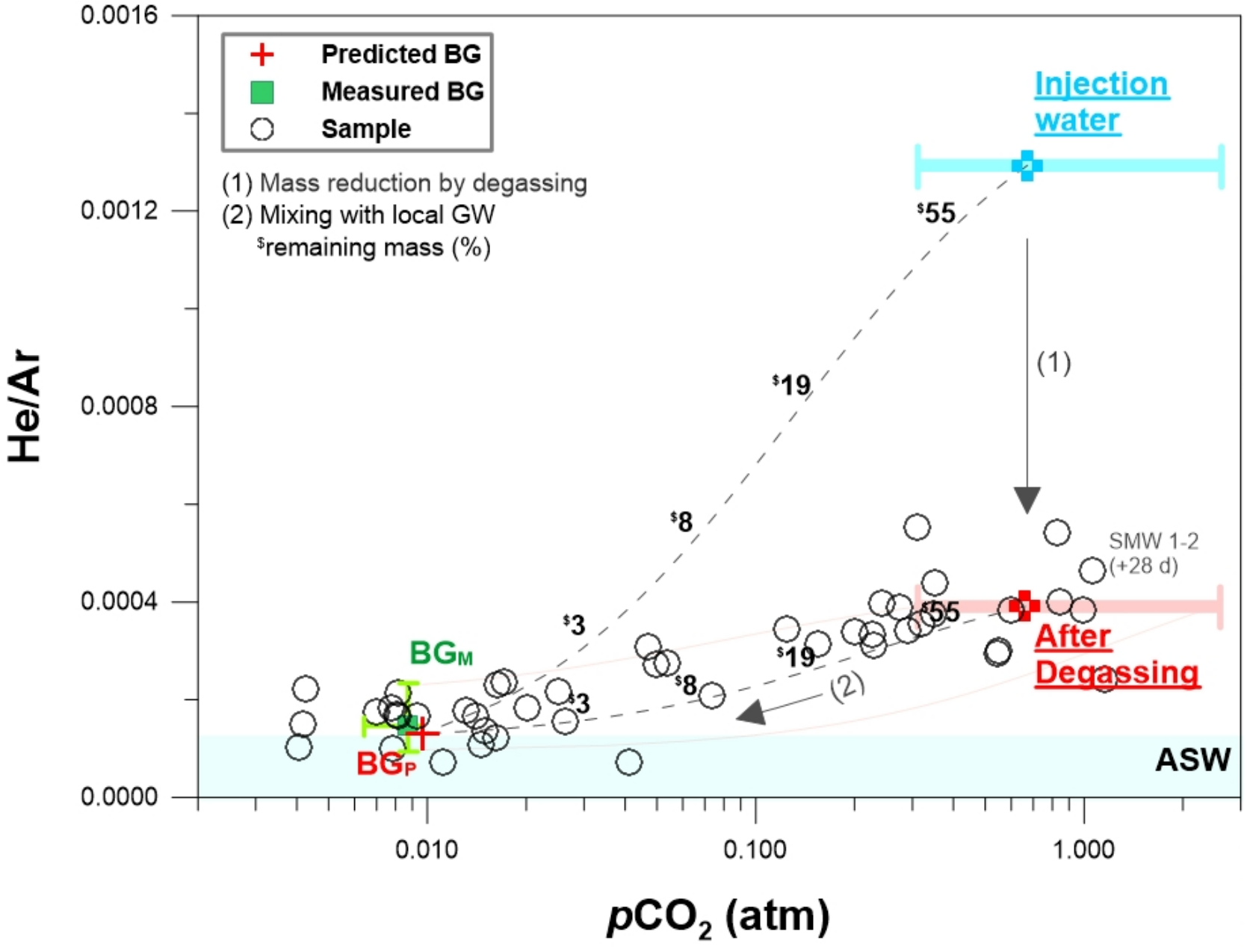
Predicted BG
Measured BG
Sample
(1) Mass reduction by degassing
(2) Mixing with local GW
$remaining mass (%)
Injection water
$55
$19
$8
$3
(1)
(2)
SMW 1-2 (+28 d)
After Degassing
BGM
BGP
ASW
0.0016
0.0012
0.0008
0.0004
0.0000
0.010
0.100
1.000
He/Ar
pCO2 (atm)

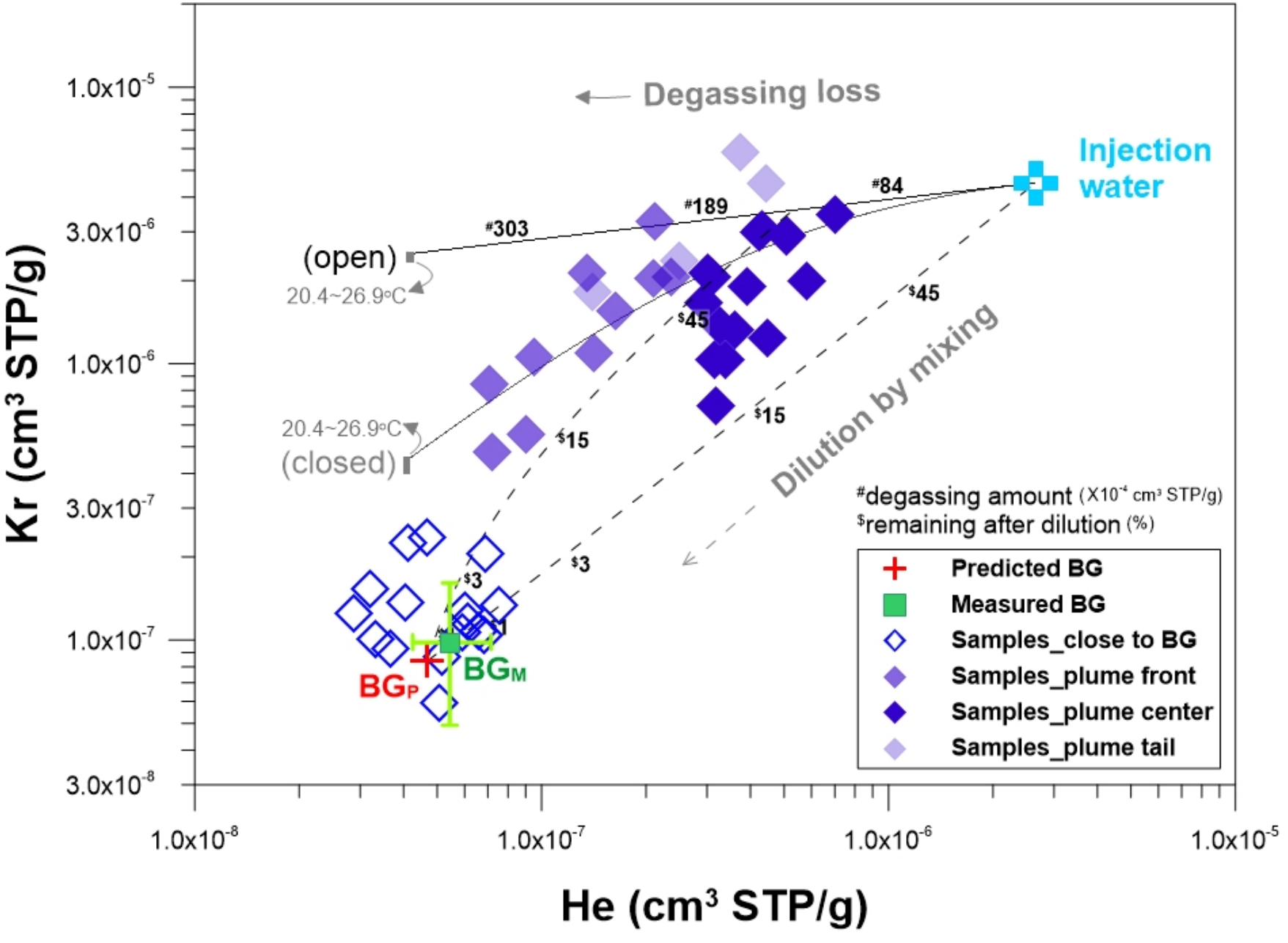
Degassing loss
Injection water
#84
#189
#303
(open)
20.4~26.9°C
20.4~26.9°C
(closed)
$45
$45
$15
$15
$3
$3
Dilution by mixing
#degassing amount (X10⁻⁴ cm³ STP/g)
$remaining after dilution (%)
Predicted BG
Measured BG
Samples_close to BG
Samples_plume front
Samples_plume center
Samples_plume tail
BGP
BGM
1.0x10-5
3.0x10-6
1.0x10-6
3.0x10-7
1.0x10-7
3.0x10-8
1.0x10-8
1.0x10-7
1.0x10-6
1.0x10-5
Kr (cm³ STP/g)
He (cm³ STP/g)

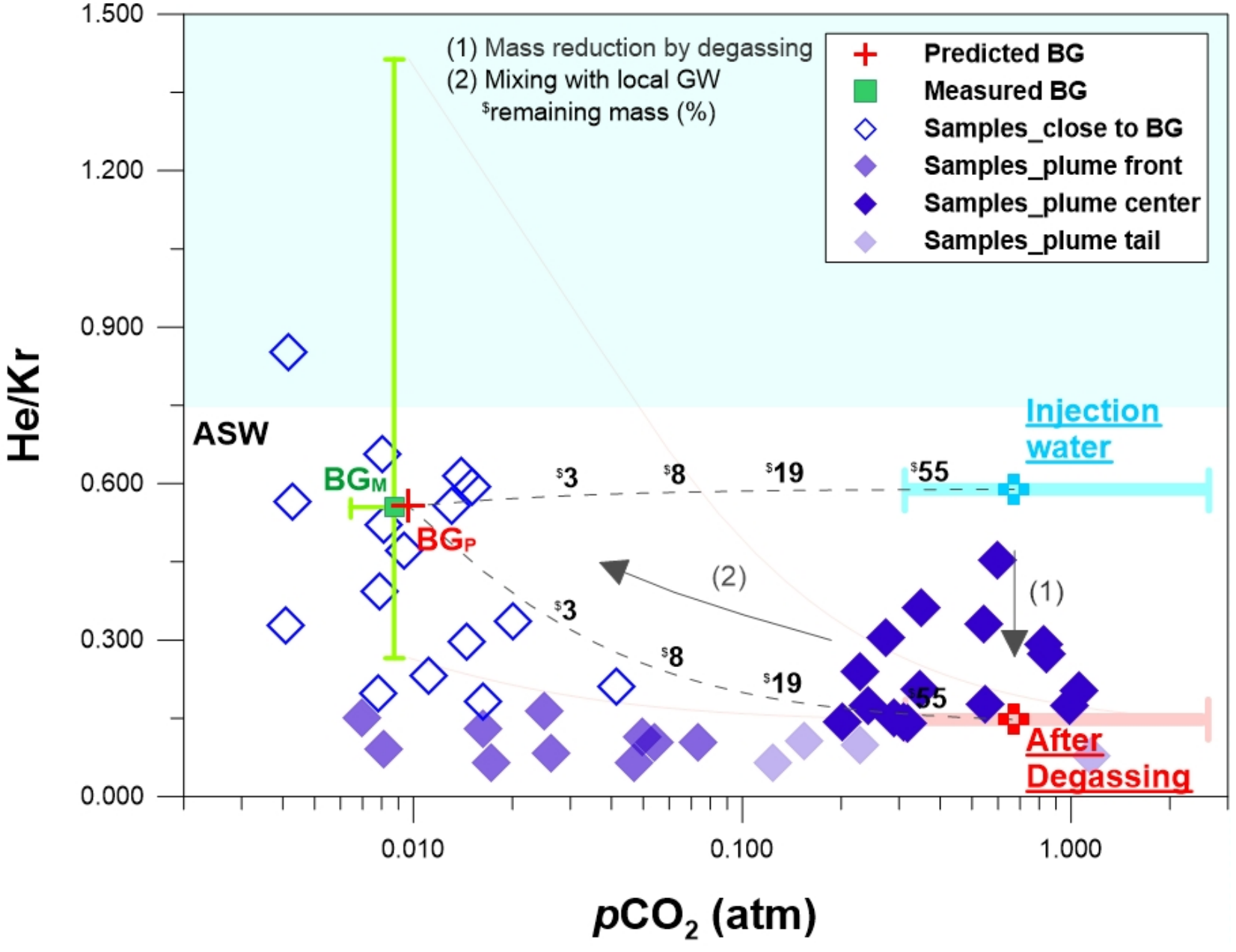
(1) Mass reduction by degassing
(2) Mixing with local GW
$remaining mass (%)
Predicted BG
Measured BG
Samples_close to BG
Samples_plume front
Samples_plume center
Samples_plume tail
ASW
Injection water
After Degassing
BGM
BGP
$3
$8
$19
$55
(1)
(2)
He/Kr
pCO2 (atm)
1.500
1.200
0.900
0.600
0.300
0.000
0.010
0.100
1.000

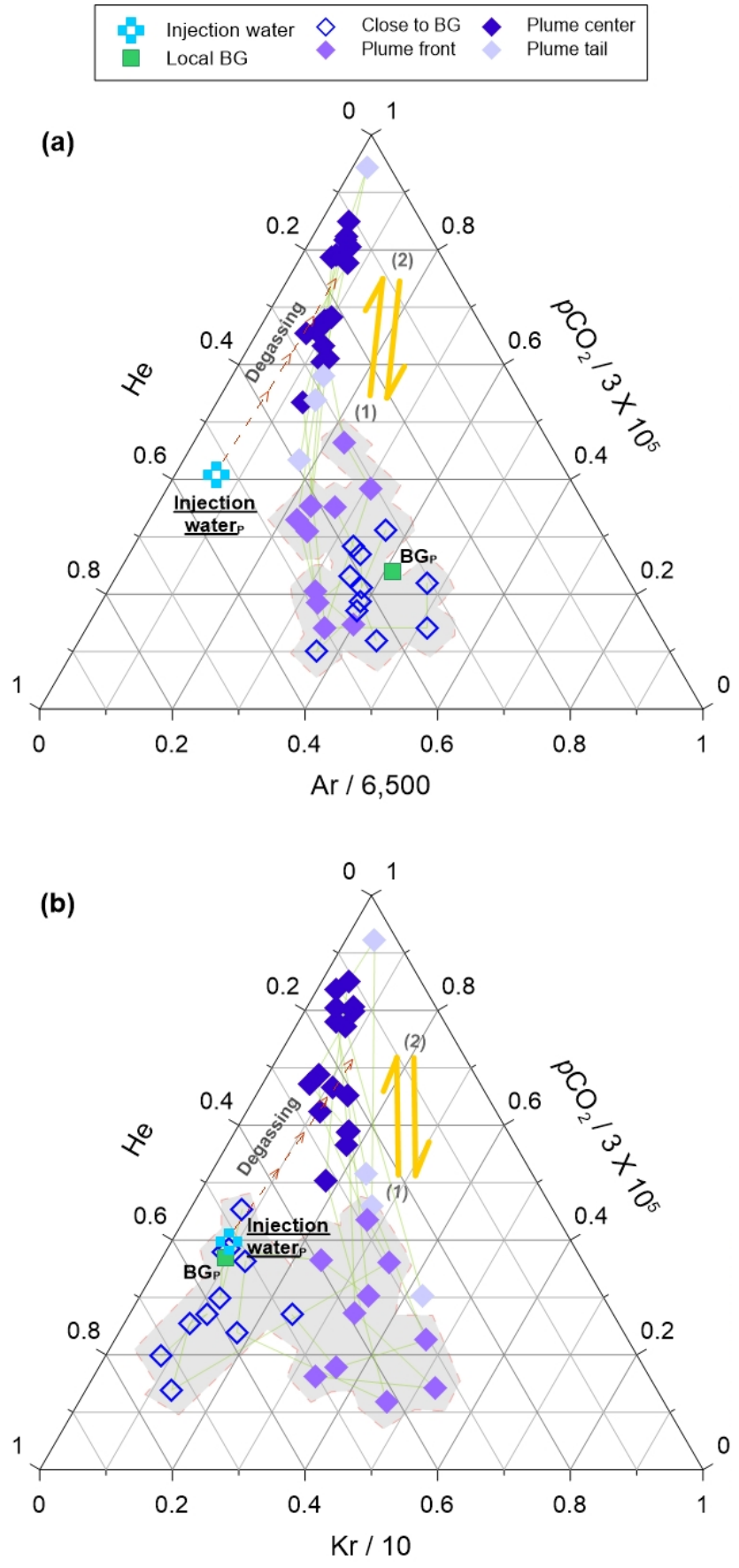
Injection water
Local BG
Close to BG
Plume front
Plume center
Plume tail
(a)
He
pCO2 / 3 X 10^5
Ar / 6,500
Degassing
(1)
(2)
Injection water_P
BG_P
(b)
He
pCO2 / 3 X 10^5
Kr / 10
Degassing
(1)
(2)
Injection water_P
BG_P

Declaration of interests

 The authors declare that they have no known competing financial interests or personal relationships that could have appeared to influence the work reported in this paper.

☐The authors declare the following financial interests/personal relationships which may be considered as potential competing interests:

YeoJin Ju: Conceptualization, Methodology, Data Curation, Investigation, Writing - Original Draft

Stuart M. V. Gilfillan: Writing - Review & Editing

Seong-Sun Lee: Project administration, Investigation

Dugin Kaown: Data Curation

Doshik Hahm: Resources, Data Curation, Writing - Review & Editing

Sanghoon Lee: Data Curation

In-Woo Park: Data Curation

Seung-Wook Ha: Investigation

Keyhong Park: Resources, Data Curation

Hyun-Kwon Do: Investigation

Seong-Taek Yun: Funding acquisition, Project administration, Writing - Review & Editing

Kang-Kun Lee: Funding acquisition, Supervision, Writing - Review & Editing

Supplementary Material

Application of noble gas tracers to identify the retention mechanisms of CO_2 migrated from a deep reservoir into shallow groundwater

YeoJin Ju[1], Stuart M. V. Gilfillan[2], Seong-Sun Lee[1], Dugin Kaown[1], Doshik Hahm[3], Sanghoon Lee[1], In-Woo Park[1], Seung-Wook Ha[1], Keyhong Park[4], Hyun-Kwon Do[5], Seong-Taek Yun[5], Kang-Kun Lee[1],*

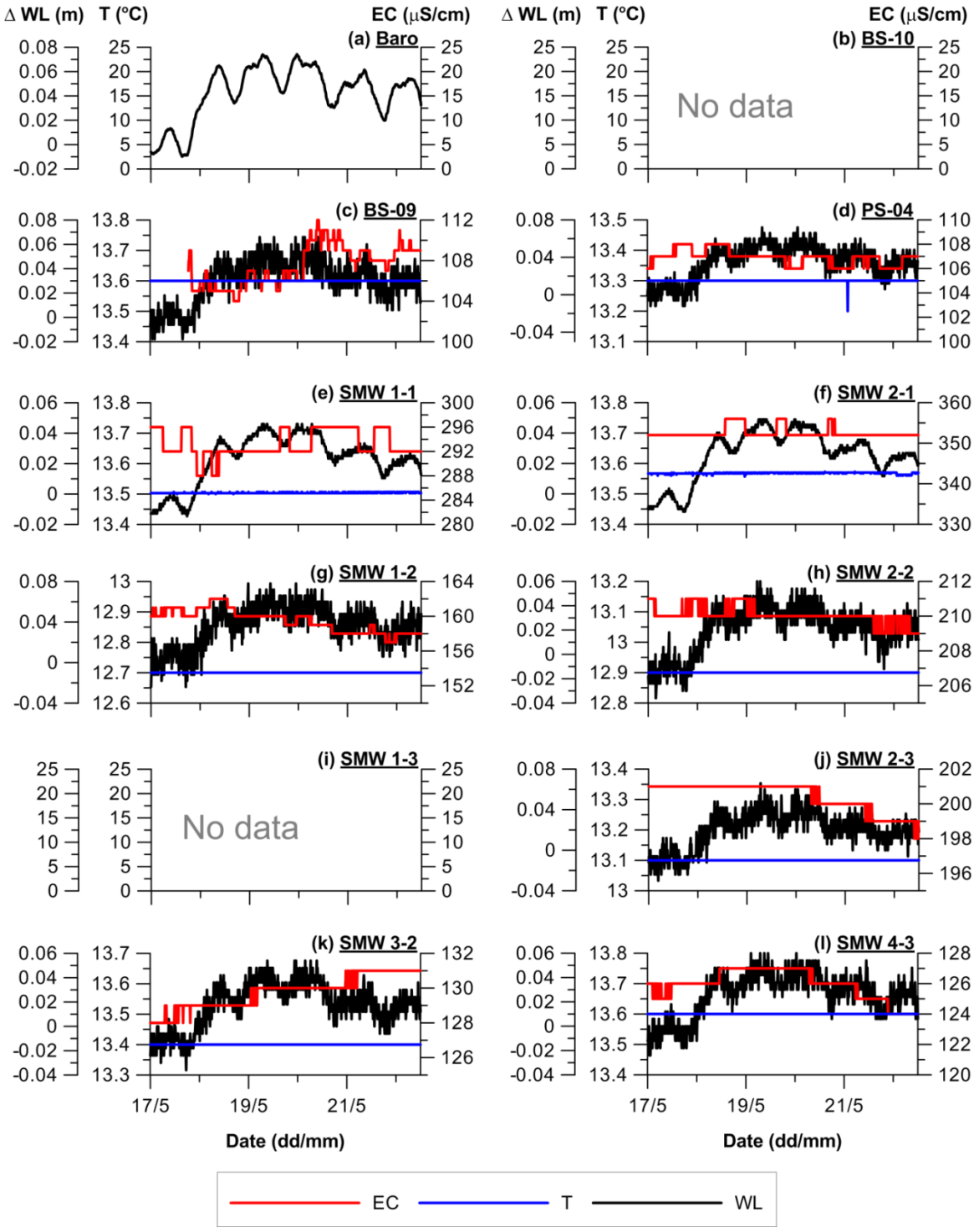

Supplementary Figure S1. Water level (WL), temperature (T) and electrical conductivity (EC) data. Measurement was completed in the monitoring wells continuously using LTC data logger before groundwater circulation (from 16 May 2017 to 22 May 2017). Note that the WL was corresponding to the atmospheric pressure chance before experiment initiation and, T and EC were consistent throughout this period.

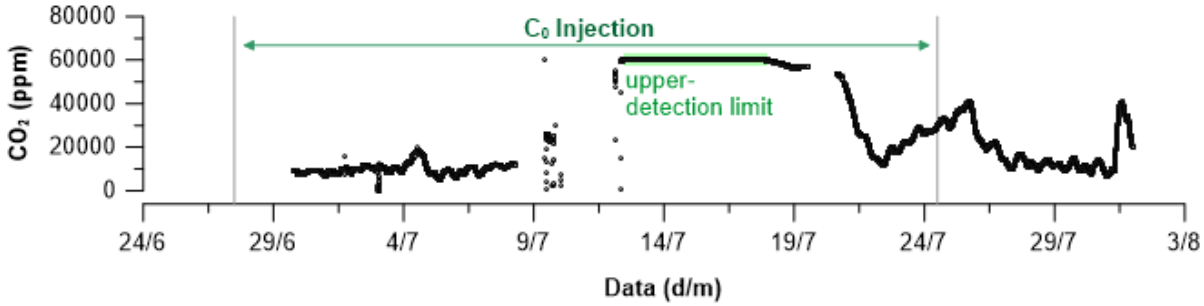

Supplementary Figure S2. CO_2 concentration monitored above the injection material inside the IW. The concentration was significantly elevated and reached to the maximum limit of the equipment suggesting the CO_2 leakage through the isolation materials occurred during injection period.

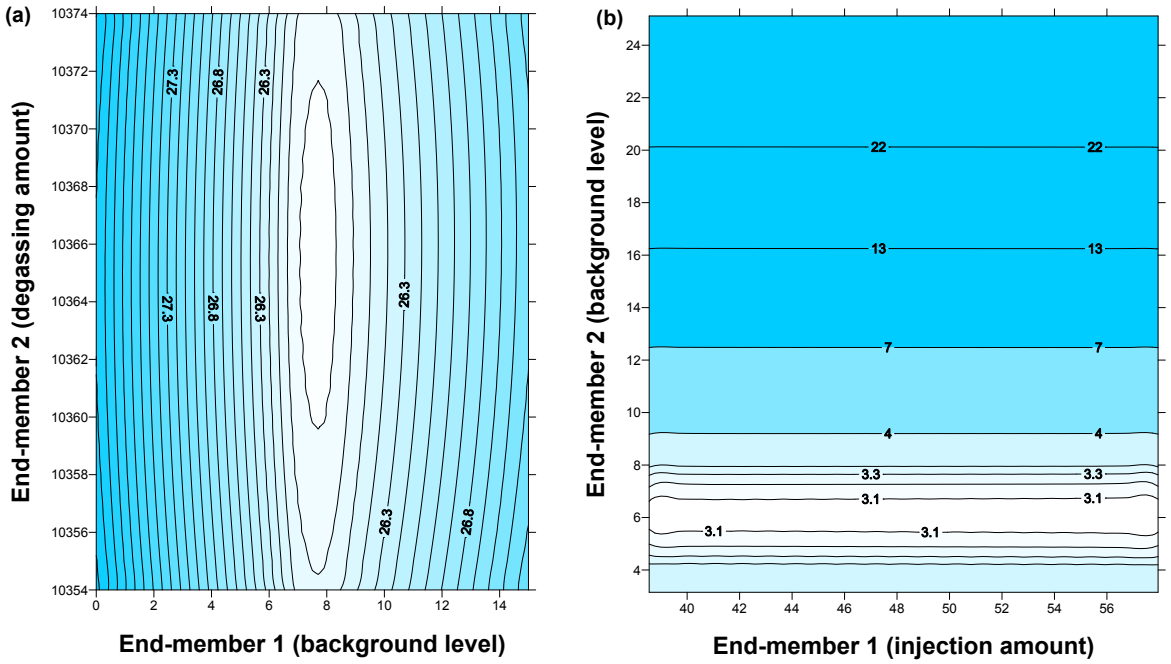

Supplementary Figure S3. Model optimization by χ^2 minimization method. In the left figure (a), the degassing amount (i.e. y-axis) and background level of noble gases (i.e. x-axis) were decided at the smallest χ^2 (i.e. center of the white-colored zone). In the right figure (b), the background level of CO_2 (i.e. y-axis) and injection amount of CO_2 (i.e. BG_P, x-axis) were decided at the smallest χ^2 (i.e. center of the white-colored zone).